SIMULATION AND MULTI-OBJECTIVE OPTIMIZATION OF COLD-END SEPARATION PROCESS OF AN ETHYLENE PLANT

SHRUTI PANDEY

NATIONAL UNIVERSITY OF SINGAPORE

2013

SIMULATION AND MULTI-OBJECTIVE OPTIMIZATION OF COLD-END SEPARATION PROCESS OF AN ETHYLENE PLANT	**SHRUTI PANDEY**	**2013**

SIMULATION AND MULTI-OBJECTIVE OPTIMIZATION OF COLD-END SEPARATION PROCESS OF AN ETHYLENE PLANT

SHRUTI PANDEY

(*B.Tech. NIT Jaipur, India*)

A THESIS SUBMITTED
FOR THE DEGREE OF MASTER OF ENGINEERING

DEPARTMENT OF CHEMICAL AND BIOMOLECULAR ENGINEERING
NATIONAL UNIVERSITY OF SINGAPORE

2013

DECLARATION

I hereby declare that this thesis is my original work and it has been written by me in its entirety. I have duly acknowledged all the sources of information which have been used in the thesis.

This thesis has also not been submitted for any degree in any university previously.

Shruti Pandey

10-January-2014

(*This page is left blank intentionally*)

Acknowledgements

It has been an honor to be a part of pCOM group, led by Professor G. P. Rangaiah. He has been extremely supportive and patient throughout the two years of my tenure at National University of Singapore. As a research graduate, my experience in the Master of Engineering programme has been a steep learning curve under his guidance. I have been given a disciplined and organized training during my research-work. He ensured weekly interaction and reasonable target-setting which gave way to a smoother transition into an efficient researcher. He also taught me the art of scientific arguments with genuine source of referencing which was very important to establish the credibility of my work. I have gradually improved my writing skills, thanks to his suggestions over my articles. Last but not the least, one quality that I have developed from his subset of professional ethics and vow to maintain for life is punctuality.

It was all the more a great pleasure to learn from my coursework modules by Prof. Karimi, A/Prof. Laksh, A/Prof. Mark Saeys, A/Prof. Saif A. Khan, A/Prof. Rajagopalan Srinivasan, and A/Prof. D. Y. Lee. I would like to acknowledge the NUS administration, including ChBE Department staff and Registrar's office for functioning in one of the quickest and most efficient manner. It was a delight to experience faster processing of applications and smarter access to information through NUS website, Library, and many other facilities. Latest infrastructure and innovative events around the campus had a very positive impact on me and it gave me enthusiasm to work hard as well as smart.

I was a part of lot of extra-curricular activities like Senior Director for Public Relations at Graduate Students' Society (GSS), Student Assistant at Students' Service Centre (SSC), Technical Writer at Office of Estate and Development (NUS), MarketZoom team with students from NUS Business and Laboratory Assistant for module CN3421E. The experience of meeting people from different parts of the world has widened my horizon about life. I wish to thank all my friends, whom I met through these activities and will surely miss them.

I would like to give a special mention to Miss Tan Phaik Lee from SSC who has been such a motivation during my part-time employment at SSC.

My daily life in lab E5-B-02 and around the department would not have been so much fun and happening without the great people here. I would start by thanking Dr. Shivom Sharma who has always been there to take me out of any technical glitch in my work and has been really kind and helpful. Vaibhav and Naviyn have been the best lab-mates one could ever have with their great sense of humor and readiness to help. Wendou enlightened us a lot about life in China and made it so much more familiar to us. Krishna has been a great source of motivation for me as he would always encourage going deeper into the concepts and understanding the basics well. Bhargav, Arghya, Sumit, KMG, Ashwini, Maninder, Ammu, Hari, and Manoj have been nice (read: mischievous) colleagues. Xu Chen was kind enough to translate a paper from Chinese journal into English for me. Sadegh and Naresh also helped me through optimization related issues. Rajnish and Akshay, my seniors from undergraduate and Bharat lived up to my expectation for being the dearest friends at NUS.

I would like to thank my Mom, Dad, my sister Avantika, my fiancée Sulabh and his family, and all my relatives and friends in India for understanding my busy schedule and still continuing to shower their love and care. Last but not the least; I would like to thank God, as I thank Him every day, for being my back in all the tough times and making me a stronger human being, with every passing day.

Table of Contents

SUMMARY

Ethylene is the largest volume petrochemical produced in the world. It is an important building block for many chemicals like polyethylene, ethylene dichloride, ethylene oxide and ethyl benzene. Capacity of ethylene production worldwide touched 155.9 million tons per annum (MTA) in 2012 and it is likely to increase [1]. It is generally produced from ethane, propane and naphtha by thermal cracking. Ethylene separation from cracking products is one of the most energy-intensive processes and involves separation of close boiling-point hydrocarbons like ethylene/ethane and propylene/propane using expensive cryogenic distillation. Hence, it is imperative to employ available techniques for the reduction of energy consumption in ethylene plants. This can be done by either optimizing the plant operating conditions or retrofitting to economical separation systems like hybrid membrane-distillation system.

The primary objective of this study is to perform operation optimization of cold-end separation process of a conventional ethylene plant. The process simulated in Aspen Hysys and validated with typical design data. Then, using this simulation model, multi-objective optimization (MOO) of the cold-end separation is studied using the elitist non-dominated sorting genetic algorithm. The major objectives were: minimizing utility cost, maximizing utility credit, and maximizing production rate of ethylene (or propylene). It is shown that the plant can be operated at different optimal conditions, each of which involves some trade-off among the objectives of interest.

In the second part of this study, the techno-economic viability of retrofitting a membrane to the existing cold-end separation process of an ethylene is carried out. Optimization of four distillation columns, namely, deethanizer, depropanizer, ethylene and propylene fractionator with membrane separation was carried out for two objectives: minimizing capital cost of membrane separation and maximizing utility cost savings for the hybrid system. It is concluded that the hybrid systems significantly reduce the utility cost of depropanizer, and propylene fractionator and comparatively less reduction is observed for deethanizer. Ethylene fractionator, which generates energy credit from the reboiler duty, is not suitable for membrane retrofitting.

LIST OF TABLES

LIST OF FIGURES

LIST OF SYMBOLS

Alphabetical Symbols

A_m	Area per unit membrane
A_c	Heat exchanger area for cooler
atm	Atmospheric pressure
C	Total Module Cost of Equipment
D_A	Diffusion coefficient
F_{bm}	Bare module factor
F_m	Material factor for the equipment
F_P	Pressure factor for the equipment
ℓ	Thickness of the membrane
N	Total number of units
n_A	Flux of component A through the membrane
P	Pressure
P_A	Permeance of fast-permeating component A
$P_{A,l}$	Permeability of fast-permeating component A
p_F	Feed Pressure
p_P	Permeate Pressure
Px_1	Partial pressure of component x in feed
Px_2	Partial pressure of component x in permeate
Per_x	Permeability (Flux) for component x
ppm	Parts per Million
psig	Pound per square inch gauge
Q_x	Permeate molar flow for component x
S	Power Input required by the Equipment
S_A	Solubility coefficient
T	Temperature

T_b	Boiling Temperature
T_c	Critical Temperature
U	Heat-transfer Coefficient
UC	Utility Cost
x_F	Feed Mole Fraction
x_R	Retentate Mole Fraction
y_P	Permeate Mole Fraction
y_i	Permeate Mole Fraction at the retentate end of the membrane

Greek Symbols

$\alpha_{LK\text{-}HK}$	Relative volatility of light-heavy key components
α_{AB}	Selectivity of A shown by the membrane as compared to slow-permeating component B
β_{AB}	Front factor of the upper bound
Δp_A	Trans-membrane partial pressure of component A
λ_{AB}	Slope of the upper bound
σ	Lennard–Jones diameter
μ	Feed liquid viscosity

ABBREVIATIONS

BTU	British Thermal Units
CAPEX	Capital Cost
CEPCI	Chemical Engineering Plant Cost Index
CGCC	Column Grand Composite Curve
CMS	Carbon Molecular Sieve
CNT	Carbon Nanotubes
CTO	Coal To Olefins
DB	Debutanizer
DE	Deethanizer
DEA	Di-ethanolamine
DM	Demethanizer
DMC	Dimethyl carbonate
DP	Depropanizer
DS	Distillate Stripper
EC	Energy Credit
EF	Ethylene Fractionator
EP	Ethylene Production
FTM	Facilitated Transport Membrane
GJ	Giga Joules
HIDiC	Heat Integrated Distillation Column
HMD	Hybrid Membrane-Distillation
IC	Internal Combustion
LMTD	Log Mean Temperature Difference
LNG	Liquefied Natural Gas
LPS	Low Pressure Steam
MAPDH	Methyl Acetylene Propadiene Hydrogenation

MEA	Mono-ethanolamine
MILP	Mixed Integer Linear Programming
MINLP	Mixed Integer Non Linear Programming
MMM	Mixed Matrix Membrane
MMT	Million Metric Tons
MOF	Metal Organic Frameworks
MOO	Multi Objective Optimization
MTA	Million Tons per Annum
MTBE	Methyl Tert Butyl ether
MTO	Methanol To Olefins
NLP	Non Linear Programming
NS	Net Savings
NSGA	Non-dominated Sorting Genetic Algorithm
OPEX	Operating Cost
PCE	Purchased Cost of an Equipment
PF	Propylene Fractionator
PNMTC	Practical Near Minimum Thermodynamic Condition
PP	Propylene Production
PR	Peng-Robinson
PTFE	Polytetrafluoroethylene
SD	Secondary Deethanizer
SIHIDiC	Simple Ideal Heat Integrated Distillation Column
SQP	Sequential Quadratic Programming
SRK	Soave Redlich Kwong
TC	Target Component
VB	Visual Basic
VLE	Vapour-Liquid Equilibrium

Chapter 1

INTRODUCTION

1.1 Overview

Ethylene is the largest-volume organic petrochemical produced in the world. The majority of it is used in the production of ethylene oxide, ethylene dichloride, ethyl-benzene, linear alcohols, vinyl acetate, and a variety of homo- and co-polymers (plastics ranging from plastic food wrap to impact-absorbing dashboards in cars). These chemicals are used to make consumer and industrial products like plastics, textiles, coatings, packaging, rubber, construction materials etc. Increasing modernization and urbanization in developing countries in Asia have created new markets for the consumption of these products, thereby accelerating the demand for ethylene in these regions. To meet this demand, the capacity of ethylene production worldwide touched 155.9 million tons per annum (MTA) in 2012 and it is likely to increase due to newly-ventures shale gas production [1].

Ethylene plants are complex, large-scale, flexible factories that can process a wide variety of hydrocarbon feed-stocks (ethane, propane, butane, naphtha, gasoil, LPG) via a cracking process. The desired products and type of feed-stock used are influenced by market demands and ethylene units integrated in petrochemical plants. Many types of co-products can be generated with different equipment. Main products are polymer-grade ethylene and propylene. Ethane, ethylene, propane and propene can be obtained by hydrogenating C_2 and C_3 acetylenes. Aromatics can be recovered from hydro-treated pyrolysis gasoline. Butadiene, butylenes, isobutylene or mixtures can be obtained from C_4 stream. Isoprene, piperylene and cyclopentadiene can be obtained from C_5 stream. Ethane is recycled as cracking feed-stock, or used as a fuel. Fuel oil can be used as fuel or to produce coke and carbon black. Hydrogen and methane can be used as fuel, or sold. Naphthalene can be obtained for selling purposes. Propane is fed to the steam crackers, used as fuel or sold. Propene is available in various grades like chemical grade. Raw pyrolysis gasoline can be hydro-treated and sold as gasoline or is used in aromatics production as feed. Tar is can be used as fuel, for road-making

purposes, or used as a feedstock for making coke and resins. Sulfur can be recovered and sold [2].

1.2 Industrial trends

An environment of mixed global demand is growing for ethylene, with markets expanding in developing regions and slowdown in developed regions. After contraction in 2008, it was forecasted to be approximately 135 million metric tons (MMT) in 2013, which was higher than the previous demand peak of nearly 130 MMT in 2012. In the next five years, it is forecast to grow at more than 4%/yr, reaching nearly 160 MMT tons by 2017 [3].

The ethylene industry witnesses a frequent rise and fall in margins, which determine whether existing plants have to be revamped or new grass-root plant need to be built, respectively. A number of reasons are responsible for a revamp like health, safety and environmental requirements, expansion of capacity and process improvements. However, ethylene process is extremely sensitive to minor changes, and no major adjustments should be made in the operations of the unit when the plant has reached steady state. Hence, a very strong objective and direction is required by the process engineer before embarking into a revamp exercise [4].

Five years ago, when the ethylene capacities were on the verge of shutdown, US ethylene industry is now experiencing a complete turnaround. High ethylene margins due to low regional ethane prices are generating profits for producers, despite a global oversupply situation. The ethane-based producers are in more profitable position than their naphtha counterparts. A report has reasoned the low prices of ethane as a result of ample supplies of natural gas liquids from shale development [3].

Now that US ethylene industry is nearing its maximum capacity utilization, there is a tremendous amount of capital investment underway, including new infrastructure needed for feedstock supply, ethylene and ethylene-derivative capacity, and new logistics investments to support higher levels of ethylene-derivative exports. This will create more supply than demand in the domestic market, and it is expected to be diverted to Asian markets like China and

India, where demand is greatest and the scenario is completely favorable for producers in Middle East, other parts of Asia and North America [3].

1) FEPCO, a subsidiary of Rosneft, is developing the Russia Far East olefins project. Processing capacity of the petrochemical complex is planned at 3.4 million tpy of hydrocarbon feedstock, predominantly naphtha. The capacity of ethylene and propylene production unit is planned at 2 million tpy. The complex is expected to be started up in 2017 [5].
2) Dow Chemical will build a world-scale ethylene plant at its chemical hub in Freeport, Texas, to utilize cheaper feed-stocks available from increasing US shale gas supplies. [6].
3) China is trying to capitalize on the huge domestic supply of coal by using coal-to-olefins (CTO) processes for meeting the local demand of several chemical feed-stocks like especially ethylene and propylene An IHS study assessed CTO processes which include the gasification of bituminous coal by GE Texaco or Shell gasifiers to produce synthetic gas, followed by methanol synthesis and methanol-to-olefins (MTO) production [7]. KBR has recently got a license to design an olefins-recovery unit in Yulin, Shaanxi Province, China. [8].
4) SK Global is working with Sinopec for starting a petrochemical plant in Wuhan, central China, with an annual capacity of 2.5 million tons of petrochemicals [9].
5) ExxonMobil plant in Singapore has recently started production of ethylene using the second steam cracker with the finest world-class technology. [10].

These above-mentioned developments in ethylene capacity additions and production are important because ethylene is the “bell weather” product for assessing the health of the petrochemical industry as it is by far the largest market of the basic petrochemical building blocks, including olefins, aromatics, chlor-alkali and syngas chemicals [3].

1.3 Olefin/Paraffin Separation

Olefin/paraffin separation is often categorized as one of the difficult separations in petrochemical industry. This is due to the small differences in physical properties such as boiling points between olefins and paraffins with same number of carbon atoms. Currently, highly energy intensive low temperature (cryogenic) distillation is used for carrying out such separations at the industrial level. These require one or two-column configurations containing 150 – 200 trays at temperatures around 200 K and pressures around 18 bar for obtaining high product purities, necessary for further polymerization reactions. Such low temperatures and high pressures are due to the similar boiling points of light olefins and their corresponding paraffins. Around 3% of total US Energy is consumed by nearly 40,000 distillation columns in refineries and petrochemical plants, separating organic liquid mixtures [11].

1.4 Operation Optimization

There are many challenges faced by the olefin producers due to rise in crude oil prices as well as global warming concerns, some of which are yield improvement, product maximization and energy intensity reduction in the product recovery section. With advanced control and optimization technology, annual production can be increased and energy consumption can be decreased, resulting in substantial economic benefits in millions of dollars.

An olefin plant contains a separation train of distillation columns integrated with compression network and refrigeration system, apart from flash drums, heat exchangers, pumps and acetylene reactors. The olefin/paraffin separation is associated with various operating characteristics which can be broadly divided into two categories. The universal characteristics include 1) no product blending, 2) stringent product quality requirements, 3) slow dynamics from gate to gate, 4) gradual furnace and converter coking, 5) frequent furnace decoking and switching and 6) converter decoking. The site-specifics cover 1) feed quality variations, 2) product demand changes, 3) sensitivity to ambient conditions and 4) periodic switching (for example, dryers). The main operating degrees of freedom for ethylene plant-wide control and optimization

include feed selection, furnace feed rates, cracking severity, dilution steam, cracked gas compressor and refrigeration compressor suction pressures, typical column variables (reflux, reboiler, and pressure), and converter temperature and H_2 ratio. Advanced control and optimization goals include stabilizing operation, minimizing product quality giveaway, maximizing selectivity and yield, minimizing converter over-hydrogenation and minimizing ethylene loss to methane and ethane recycle [12]. With such multi-dimensional characterization and energy-intensive nature of the process, fine-tuning of various variables is necessary to minimize utility costs while maximizing production rates. This makes ethylene process an ideal candidate for steady-state multi-objective operation optimization.

1.5 Process Retrofitting

Various technologies have been developed to replace the traditional low-temperature distillation like extractive distillation, physical adsorption using molecular sieves, chemisorption using complexing metals like copper and silver ions, absorption (physical and chemical), and membrane separation. Since the last three decades, research has gathered momentum in the area of membrane applications for olefin/paraffin separation. However, due to harsh industrial operating conditions like high pressure and high feed flowrates, these systems could not be scaled-up and fully replace the conventional distillation. Nevertheless, membranes have proved to provide a cost-effective method of separation through various experiments of gas permeation and pervaporation for different hydrocarbon mixtures at laboratory scale. This has gradually led to the concept of hybrid membrane-distillation systems which aim at reducing the overall energy consumption of a distillation by virtue of separation characteristics of the associated membrane. Although, there is an absence of suitable membrane materials at industrial scale, certain polyimide membranes have showed promising results towards the hydrocarbon separation. Hence, a hybrid process combining a membrane unit and a distillation column is of high interest for petrochemical engineers from retrofitting point of view.

1.6 Motivation and Scope of Work

Being an energy-intensive process on a large-scale, cold-end separation of an ethylene process is a matter of great interest, particularly from the multi-objective optimization perspective. The resulting Pareto fronts can be useful for selecting the right operating conditions for the process, depending upon the preferences of the user. A small percentage reduction in energy consumption can lead to savings in thousands of dollars annually. Moreover, advanced, energy efficient technologies like hybrid-membrane distillation systems must be studied for their commercial demonstration and economic feasibility. Most of these technologies claim huge energy savings at the laboratory scale but fail to commercialize due to several operation hazards like high feed pressure and high feed flowrates. Hence, a techno-economic evaluation can reveal whether retrofitting of an ethylene separation process with hybrid-membrane distillation system in different columns is a viable option or not.

In this study, operation optimization of a conventional ethylene separation process has been conducted with for multiple objectives simultaneously. Retrofitting opportunities in this process are also explored using hybrid-membrane distillation systems. Specific objectives of this study are:

- To simulate a conventional cold-end separation of ethylene process using Aspen Hysys and to validate it on industrial design data.
- To perform multi-objective optimization of conventional cold-end separation of ethylene process using NSGA-II.
- To investigate potential of hybrid membrane-distillation system for deethanizer, depropanizer, ethylene and propylene fractionators in ethylene process.
- To perform multi-objective optimization of retrofitted hybrid membrane-distillation systems using NSGA-II.
- To carry out techno-economic evaluation of the process of both conventional and retrofitted processes.

1.7 Outline of the Thesis

Chapter 1 is the introduction to the thesis topic; it provides an overview of ethylene industry, operation optimization and process retrofitting, motivation, scope of work and outline of the thesis chapters.

Chapter 2 contains process description of cold-end separation of ethylene plant, a review of literature related to ethylene process, including analysis, optimization, and new developments and retrofitting. Second part of this chapter covers the history of membranes in olefin/paraffin separation, effect of various membrane parameters, techniques for improving membrane performance and hybrid-membrane distillation systems.

Simulation and optimization of conventional cold-end separation of ethylene process are presented in Chapter 3. It covers the step-by-step method of process simulation using Hysys and also multi-objective optimization using NSGA-II. Results of Pareto fronts obtained for various set of objectives are presented and discussed in the later part of Chapter 3.

In Chapter 4, retrofitting of conventional process with hybrid-membrane distillation systems is discussed; it includes discussion on recent hybrid membrane-distillation applications, techno-economic evaluation of the retrofitted systems and assumptions related to membrane simulation. Multi-objective optimization of hybrid-membrane distillation systems is also discussed.

Conclusions from the study and recommendations for further work are given in Chapter 5.

Chapter 2

LITERATURE REVIEW

This review is broadly partitioned in two sections. The first section titled "Cold-End Separation of Ethylene Process" presents the process details of cold-end separation of ethylene process and discusses the related literature on process optimization and developments. The second section titled "Membranes for Olefin/Paraffin Separation" highlights the membranes application in olefin/paraffin separation along with a detailed review on hybrid membrane-distillation systems in recent past.

2.1 Cold-End Separation of Ethylene Process

The ethylene process has been a subject of research for long now. A lot of studies have been carried out on analyzing this process, optimizing the current process flow-sheet and suggesting modifications. Since the present research is on the cold-end part of ethylene plant, most of the review in this section is on the separation section of the process. The first section of literature review is divided into three sub-sections.

1. **Process Description**: This sub-section describes the process of a conventional ethylene plant.
2. **Analysis & Optimization**: This sub-section reviews efforts to analyze various structural and operational parameters of the ethylene process and to optimize the process flow-sheet using different algorithms and objective functions.
3. **New Developments & Retrofitting:** This sub-section highlights various improvements in the ethylene process which contributes to cost reduction as well as energy savings.

2.1.1 Process Description

For a long time, ethylene and propylene have been primarily produced using steam cracking of naphtha. Even though the process chemistry and overall flow sheet remains relatively unchanged, process efficiency is increased by improving the configurations of the pyrolysis module and the product recovery sections. The sequence for hydrocarbon separation is flexible, depending on

size of the plant, relative amounts of ethylene and its co-products, impurities, product slate, desired product purity and other factors. Typically, ethylene separation and refining consist of a number of unit operations. They first recover the pyrolysis gasoline and fuel oil fractions in the effluent gas at above ambient temperature and then fractionate the remaining gaseous effluent at sub-ambient temperatures and elevated pressures into desired light fractions.

In a conventional ethylene plant, hydrocarbons along with superheated steam at radiant-coil inlet temperature of about 600°C are sent to tubular heaters for pyrolysis [13]. Cracked gases leave the radiant coil of an ethylene furnace at 750–900°C. Thereafter, the effluent is quickly cooled in exchangers by generating steam. Quench oil is directly sprayed into the cracker effluent, to reduce the temperature quickly, in order to minimize further cracking into undesired products. This is followed by a gasoline fractionator to separate fuel oil and lighter components from the heavies. The top products of this column are sent to a quench tower which acts as a partial condenser to condense the fuel oil fraction at 185°C. The quench water drum separates the water phase from the gasoline phase, and the latter is returned to the gasoline fractionator.

A series of 3–4 compressors are used to increase the pressure of the lighter components to ~1.5 MPa. These compressors are driven by single/double extraction/condensing turbine, and the early/heavier condensates from them are redirected to the gasoline fractionator. There exists an acid gas removal system which may use dilute caustic soda solution, mono-ethanolamine (MEA) or di-ethanolamine (DEA) to reduce the CO_2 and H_2S concentration in the process stream below 1 ppm. This process stream then goes through a water wash system to remove hydroxide carryover. In case of sulfur content as high as 500–600 ppm, an amine regenerative system is also included. After another stage of compression up to 3.5 MPa and cooling by propylene refrigerant to slightly above hydrate inception temperature, the stream is flashed into vapour and condensate.

The flash vapour comprising C_2 and lighter components goes through molecular sieve driers to remove water completely. It is then subjected to stage-wise condensation using propylene–ethylene cascade refrigeration to

separate hydrogen and fuel gas. The stage condensates are directed to appropriate trays of demethanizer as feed streams. The demethanizer operates at 0.7 MPa, and the overhead stream comprises of 95 mol% methane, minor H_2 and CO amounts and traces of ethylene, and bottoms stream contains primarily C_2 and heavier products.

The condensate from the flash after last compression stage is fed into the condensate stripper whose overhead stream is returned for recompression. The bottoms of both condensate stripper and demethanizer are supplied to the deethanizer operating at 2.4-2.8 MPa. The overheads of deethanizer are mainly C_2's, namely, ethylene, ethane and acetylene, and the bottoms containing C_3's and higher are sent to the depropanizer.

There are two ways of dealing with acetylene in deethanizer overheads: a) recovery using extractive distillation and b) hydrogenation to produce more ethylene. In the event of recovery, the overhead stream is passed through acetylene recovery section. In the first tower, acetylene is absorbed in acetone, dimethylformamide or methylpyrollidinone. The second tower rejects the absorbed ethylene and ethane, and the third tower desorbs acetylene into the outlet stream. In case of hydrogenation, front-end removal is where the raw pyrolysis gas containing hydrogen and acetylene is treated before demethanizer. The back-end removal involves the deethanizer overheads heated to 20-100° C and treated with hydrogen over a fixed bed of palladium catalyst. This is mainly an exothermic reaction and requires intermediate cooling. However, it has higher selectivity and requires precise temperature control in comparison with front-end removal.

After the acetylene is recovered or hydrogenated, the dried gas is sent to ethylene fractionator which is an ethylene-ethane separator producing 99.9 mol% ethylene in overheads and more than 99 mol% ethane in bottoms. Here, condensed refrigerant vapour provides heat to the reboiler and the refrigerant boils at low pressure to generate the cooling required in the overhead condenser. The ethane is recycled to heaters for steam cracking into valuable products.

The depropanizer overheads are C_3 hydrocarbons including propylene, propane, methylacetylene and propadiene. This stream is sent to hydro-converters with catalysts that convert methyl-acetylene and propadiene to propene and propane. It is different from acetylene converter since the reaction occurs in liquid phase and at a lower temperature. The hydrogenated stream is sent to propylene fractionator operating at 1.8-2 MPa with more than 160 trays in a two-tower design producing polymer-grade propylene (99.5 %+) in overheads and propane with purity of more than 95%. The latter can either be recycled for steam cracking or used as fuel.

The depropanizer bottoms with C_4 and heavier hydrocarbons are fed into the debutanizer, operating at 0.4-0.5 MPa with steam heated reboilers and water-cooled condensers. The overheads of debutanizer comprise mainly of C_4's and bottoms are C_5's and higher [13].

2.1.2 Analysis and Optimization

Simulation and optimization of ethylene process has been carried out by a number of researchers in the past with the available technology and tools. These studies have given better insight into the process and identify the scope for modification at both structural and parametric fronts.

Rijckaert et al. [14] optimized a simplified model of ethylene plant using Geometric Programming. The prime focus was to optimize the naphtha cracker for maximizing the profit, using the mass flow through compressors, refrigeration system of ethylene as well as propylene as constraints. The four decision variables used were the mass flow of naphtha, the steam to oil ratio, the furnace outlet temperature and the furnace outlet pressure.

Bandoni et al. [15] created a fast and reliable process simulator for developing fast reduced models which in turn allowed implementation of a plant optimizer to find optimum operating conditions in a very short time. The authors came up with reduced models for pyrolysis section and cracked gas compressor and utility. Except demethanizer, rest of the columns and flash drums were kept at constant conditions. Three alternative objective functions, maximizing profits, minimizing power consumption and maximizing ethylene

production were used in the optimization. The solution of the NLP problem could be achieved in a few seconds.

Based on the ethylene plant framework presented in Bandoni et al. [15], Petracci et al. [16] performed optimization of an ethylene plant and its utility plant combined. Sequential Quadratic Programming (SQP) was used to solve the non-linear programming problem for maximizing gross benefit or maximizing ethylene production as objectives. Only ethane and propane rich feed was used. A limited section of the plant from reactor till demethanizer and related continuous variables like temperature and pressure of the high, medium and low pressure steam along with deaerator pressure were studied. The optimization variables of the ethylene plant were ethane conversion & steam dilution rate of the pyrolysis reactor, cracked gas compressor inlet pressure and demethanizer column pressure. The optimization results of ethylene plant and utility systems showed its economic potential and impact of ethylene price variations on the same.

The work of Petracci et al. [16] was followed by Eliceche et al. [17], which focused on the effect of variable feed conditions on the functioning of an ethylene plant and debottlenecking the plant as well. The optimization study was carried out for variable feed flow rate and variable ethane composition, individually as well as simultaneously. It was suggested that reducing the operation of 8 cracking furnaces to 7 could help deal with the active constraint of minimum feed flowrate through the reactor and a 1.6% increase in earnings was realized.

The behavior of the plant needs to be analyzed for significant feed disturbances. Flexibility of a plant takes into account the extent to which it can accommodate the uncertainty in variations of parameters. Petracci et al. [18], extending the work of Eliceche et al. [17], studied the flexibility analysis of ethylene plant. An active capacity constraint indicated the plant's debottleneck. The maximum deviations of parameters like variable feed conditions within their uncertain space demonstrated the plant operation behavior. Similar conclusions were drawn in Eliceche et al. [17].

The cold-end part of ethylene plant consists of three main components; the separation process, the heat-exchanger system and the refrigeration system. Pinch Analysis is crucial for carrying out successful heat integration of such process. Linnhoff and Dhole [19] presented the methodology of designing low temperature processes using pinch analysis and extended it to yield shaft-work targets from initial data, by-passing the interaction of heat-exchanger network and the refrigeration system.

Dhole and Linnhoff [20] integrated the optimization of a distillation column with the background process by setting certain heat loads and temperature targets. The concepts of minimum thermodynamic condition and column grand composite curve (CGCC) for targeting for different possible column modifications were applied, and a practical near-minimum thermodynamic condition (PNMTC) was developed which incorporated the column losses and inefficiencies for setting realistic targets. Instead of considering all components, only light and heavy key components were taken into account. The horizontal distance between the CGCC pinch point (minimum reflux ratio) and the vertical axis represented the potential reduction in reflux ratio. The column modifications were recommended in a sequence as follows: 1) reflux and pressure, 2) feed preheating/cooling and 3) side condensing/reboiling. Driving forces were related to the number of stages to expand the modifications beyond energy standpoint. The integration with the background process involved removing any overlaps of the column with the process on CGCC.

Dhole and Linnhoff [21] designed and analyzed low temperature processes based on a pinch and exergy analysis. The concept of 'process shaftwork targeting' established the resulting net shaftwork benefit from any column modification. There was a trade-off against capital cost which created scope for pre-optimizing distillation column after design step, bypassing the usual repeated column and refrigeration system simulations. Thereafter, these modifications were fine-tuned according to actual refrigeration levels and heat exchanger network (HEN) configurations, followed by overall optimization.

Castillo and Dhole [22] followed up on the work of Dhole and Linnhoff [21] addressing the interactions between the compression train, distillation columns and refrigeration system. It involved optimization of only feed stage location in each column and refrigeration level temperatures according to the changes in column temperature for the base case design. After that, this methodology is applied for designing processes at different pressures. Then optimal heat integration of columns with the heat-exchanger network and the refrigeration system is done with the help of pinch and exergy analyses. The difference in total shaft-work consumption between the base case and the low pressure case is negligible (only 1.7%). The reduced pressures spare capacity for processing extra feedstock.

Sobočan and Glavič [23] presented a new approach for arranging the heat integrated distillation sequences using pinch analysis. An ethylene case study was used to identify all the sequences and group them according to the separation in the first column. This was followed by comparing the sequences on the basis of max temperature difference. The process was simulated on Aspen Plus, and capital cost comparison was made. The process was divided into two parts: (a) fixed part which remains unaffected by the heat flow rates, condenser and reboiler duties and (b) variable part which is affected by the heat flow rates, condenser and reboiler duties. Sobočan and Glavič [23] claimed that this classification can result in correct ranking of the sequences.

The exergy analysis evaluates exergy losses and exergetical efficiencies for identifying potential process improvements. Exergoeconomic analysis, also called thermoeconomic analysis, is a combination of exergy analysis and economics. Chang [24] presented exergy and exergoeconomic analyses of an ethylene separation plant. The rigorous simulation of the plant was done on ChemCAD. A three-level exergy analysis was conducted for the ethylene process and the refrigeration system, namely, 1) unit operation level, 2) the subsystem level and 3) the overall process level. The cost to obtain a process stream in terms of exergy was called exergetic cost, and, in monetary terms, it is called thermo-economic cost. The results of exergy analysis indicated that the demethanizer and the debutanizer sections were highly inefficient.

Exergoeconomic analysis showed potential for energy improvement in the compression and the demethanizer sections.

Chang and Li [25] proposed an exergy analysis which considered intrinsic exergy destruction due to configuration constraints and transport rate limitations. Instead of interpreting exergy destruction as the amount of deviation from an ideal reversible operation, a two-level determination of the intrinsic and extrinsic exergy destructions was done. The process system was analyzed for thermodynamic equilibrium operation and actual operation of two case studies – ethylene plant and a distillation column for benzene/toluene separation. The configuration optimization was implemented to obtain the optimal base case, which was used as the initial case for transport rate optimization. However, the given analysis and the so-called lumped exergy analysis were not compared to show the improvement attained using this model.

Mafi et al. [26] performed exergy analysis for multistage cascaded low temperature refrigeration systems in olefin plants. The exergy destruction and exergetic efficiency for heat exchangers, compressors and expansion valves were calculated. The total exergy destruction in the system was related with the system's overall exergetic efficiency. The properties of incoming and outgoing process streams of refrigeration system and the ambient temperature determined the minimum work requirement. It was suggested that ethylene cannot be used for refrigeration below -101°C because the suction of ethylene compressor would be at sub-atmospheric pressure.

Huang and Shao [27] proposed pattern recognition method before optimization of an ethylene plant. The key parameters which influenced the target were first selected during preprocessing of data. The method of feature extraction was used for reducing the dimensionality of the pattern space of technological parameters. On the basis of these features, the samples were classified into zones of low quality product and high quality product using the Fisher rule and fractional correction rule which led to the development of a recognition model. Then, gradient descent algorithm was used to reach the

optimal operating conditions. The technique reduced the number of features by 33% while decreasing the recognition rate from 91.89 to 86.48%.

Díaz and Bandoni [28] discussed operation optimization of a real-world ethylene plant using outward approximation technique to solve the mixed-integer non-linear programming (MINLP) formulation. They used the OPTEAM program for optimization and interfaced it with a tailored process simulator called SISER. An ethylene plant was simulated covering pyrolysis furnaces right until the separation systems and heat-exchanger networks and simultaneous parameter and structural optimization was performed resulting in annual increase in gross profit by US$296337. Outward approximation technique dealt with MINLP in a way that it first solved the non-linear programming (NLP) and found the upper bound. At the maximum bound, it linearized the MINLP and solved the mixed-integer linear programming (MILP) to find the lower bound. The convergence was achieved when the lower bound from MILP became more than the upper bound of NLP. The structural parameters are included in the form of binary variables, and the model has a superstructure of utilities in place to optimize the utilities and their impact on cost.

Yan's thesis [29] submitted to the Department of Chemical Engineering at Texas Tech University was on plant-wide optimization of an ethylene plant with special focus on the design of the ethane/propane cracker and its kinetics. The author used an LSODE program to solve reactor model and carried out the optimization using NPSOL package where approximate models for distillation columns were used to simulate the final products and utility usage. The objective function was gross profit, and a number of decision variables and constraints were discussed.

Sobočan and Glavič [30] proposed two best sequences for distillation columns for a six-product separation from their previous works. They used two different simulators, Hysys and Aspen Plus to see their effect on the operating cost and other parameters. Optimization of distillation columns included different reflux ratios, pressures, side reboilers/condensers and preheating/cooling of feed mixture. Heat flow rates and temperature levels of

different sequences were calculated for selecting the best combination. The objective was to attain lowest possible temperature difference inside the column and the lowest possible heat flow rates for better thermal integration and lower utilities consumption. Heat integration between distillation columns was considered i.e. total condensers and total reboilers with condenser-reboiler matches for using every available hot and cold process streams for substituting new utilities. With the same process sequence and thermodynamic models, significant differences were observed in the total annualized cost (TAC) due to different heat flow rates and temperatures leading to different heat integration conditions. Aspen Plus-1 simulator had the greatest TAC but also the highest investment.

Wang and Smith [31] focused on synthesis and optimization of specialized sequences including flash drums, dephlegmators and simple/complex distillation columns. The various configurations of these units for a five-product separation system were suggested and their ways to model are also provided. Later, this was integrated with the refrigeration system through simple and multiple refrigeration cycles. The superstructure was then optimized using genetic algorithm. Two case studies, liquefied natural gas (LNG) separation train and ethylene cold-end process were presented to prove the application of the proposed technique. The objective function was to minimize total shaft power requirement of refrigeration system or total utility costs.

Van Geem and Marin [32] studied the design of an ethylene separation process using advanced computational methods, which were used to simulate the product yields for a given furnace, design new furnaces, minimize emissions of CO_2 and NO_X, evaluate process conditions and for feedstock selection. Another section of the paper dealt with designing cold-section of the ethylene plant and finding the best out of demethanizer-first, deethanizer-first and depropanizer-first in combination with front-end or back-end hydrogenation. In the simulation of the ethylene and propylene cooling cycles of the refrigeration section, Redlich-Kwong-Soave equation of state was used for simulating distillation columns in the separation section. Pinch analysis was applied for maximizing the process-to-process heat recovery and minimizing

the utility requirements. The demethanizer first with front-end hydrogenation design was superior to all other designs from energy efficiency point of view. However, using a front-end hydrogenation design implied that some valuable products such as butadiene could be partly lost, which may not be desirable.

Zhang et al. [33] modeled the chilling train before demethanizer supported by regressed data using Aspen Plus, and optimized it using GAMS. The multi-objective optimization had three objective functions: minimize ethylene loss, maximize hydrogen recovery and minimize exergy-accounted energy consumption. The equality constraints were ethylene loss and hydrogen recovery and the objective function was exergy consumption. DICOPT was employed as the solver whereas CPLEX and CONOPT were used to solve the MILP master problem and the NLP sub-problem, respectively. The 3D Pareto frontier showed that energy consumption and ethylene loss rate increased with increase in hydrogen recovery. When the ethylene loss rate increased, the energy consumption rate first increased and then decreased. The energy consumption was affected by hydrogen recovery more than the ethylene loss rate.

2.1.3 New Developments and Retrofitting

There have been efforts, in both industry and academia, to improve the conventional ethylene process. There have been many patents issued in this field for more than half a century to companies like Kellogg, Brown & Root, UOP, BP America, ExxonMobil and Shell. Table 2.1 lists patents, broadly classified on the basis of focus area with respect to technology used in the ethylene process under consideration. Apart from these patents, several papers have been published in the journals, and these are reviewed next.

The superstructures of a process can be large in numbers and bring upon various complexities during optimization. Shah and Kokossis [34] presented Conceptual Programming which employed task representations instead of unit-based representations. Task based representation embedded complex column configurations, sloppy-split arrangements and options for optimizing operating pressure. The synthesis framework was a super-task representation accounting for different designs of the ethylene cold-end process and the

effect of the feed compositions on the layout of design. The effect of operating pressure on various design options at the sequencing stage was studied. Peng-Robinson (PR) equation of state was used for property package and shortcut models were used to simulate the distillation columns. For every feed coming from three different crackers, naphtha, ethane-propane and ethane, two sequences were suggested with respect to two objective functions: conceptual cost and shaft-work targets.

Table 2.1: List of Industrial Patents

S. No.	Patent Area	Authors of Patents
1.	Addition of new equipments like compressors, dephlegmators, expansion motors, two/three-phase separators, membrane separator	Jackson [35], Pryor and Rowles [36], Rowles [37], Rowles et al. [38], Dinh et al. [39], Krause and Pasadyn [40]
2.	Change in operating conditions of columns like pressure, temperature	Davis [41], Nazar [42]-[43], Kuechler and Lumgair [44]
3.	Different column configurations and thermal coupling	Tedder [45], Di Cintio et al. [46], Kaiser et al. [47]-[48], Manley and Haddad [49], Ronczy [50], Reyneke et al. [51]-[52]
4.	Mixed refrigerant and related developments in refrigeration systems	Bernhard et al. [53], Howard and Rowles [54]-[55], Manley [56]
5.	Integration of two or more columns into one column	Stork [57]-[58], Van Zile and Harris [59], Reyneke et al. [60]

Chen et al. [61] illustrated the simplified ideal heat-integrated distillation column (SIHIDiC), constructed from the configuration of the ideal heat-integrated distillation column by employing three internal heat exchangers to imitate internal heat integration between the rectifying section and the stripping section. Theoretical stages were assumed to have perfect mixing and Peng-Robinson equation of state was employed. With the aid of constrained steepest gradient method, the operating cost was reduced to 45.52%, demonstrating that adjustment of locations and sizes of the three internal heat

exchangers enhanced the thermodynamic efficiency of the Base SIHIDiC. The effect of heat integration was observed through changes in the vapour and liquid flow rates in the rectifying and stripping sections respectively. While the relocation of the three internal heat exchangers in Optimum SIHIDiC reduced the capital investment by 2.42% as compared with the Base SIHIDiC, the redistribution of the internal heat transfer areas among them did not affect thermodynamic efficiency of the Optimum SIHIDiC. The Optimum SIHIDiC was shown to be a good replacement to the ideal heat-integrated distillation column (HIDiC) in terms of capital investment and operating cost.

Nawaz and Jobson [62] suggested a method to bypass the rigorous simulation of complex demethanizer separating multi-component mixtures. They proposed a semi-rigorous boundary value method to model demethanizer in MATLAB, and linked it with HYSYS for predicting physical and thermodynamic properties using a short-cut model. Then, distillation columns were simulated in five levels, 1) boundary value method with energy balance, 2) extended boundary value method for two-phase feed, 3) model extension for multi-component mixtures, 4) double-feed column design by boundary-value method, and 5) extended Boundary-value method for column with side reboilers. Thereafter, two industrial-level case studies, a typical turbo-expander flow sheet model and one based a US Patent, "Multiple reflux streams Hydrocarbon recovery process" were illustrated.

Hou et al. [63] worked upon simulation of an ethylene plant and developed a model which predicted industrial data accurately. They chose to work on rapid cooling oil systems because there is a huge difference in operation performance and design capacity as compared to the ethane cracker gas cooling system. They demonstrated the selection of right property package, and carried out all simulations on Aspen Plus. The petroleum distillates in the cracked gas are represented by virtual groups in simulation. Results showed that after the number of groups reaches certain number, predictions were close to the process data. Further increasing number of groups did not affect predictions much. This was followed by simulation of gas-phase purification system for compressed liquid, cold-box system and separation system using

shortcut models. The simulation results agree well with data such as stream flow rates, compositions and temperature provided by the vendor.

Tahouni et al. [64] performed parameter optimization of low-temperature separation in an olefin plant cold-end separation. They tried to do retrofitting of separation columns which involved reflux ratio optimization, feed conditioning and side condensing and reboiling. The objective of optimization was to minimize the utility costs comprising the compressor shaft powers, cooling water and low pressure steam (LPS) consumption. The base case was simulated on Aspen and HYSYS and the optimization was carried out by COLOM software using Genetic Algorithm. The column parameters were simultaneously optimized with refrigeration cycles and associated heat sink/source exchangers. Addition of 1 compressor and 2 heaters was recommended to increase the column pressures. Decrease in utility requirements and increase in temperatures reduced compressor power and cooling water consumption.

Tahouni et al. [65] modified the basic configuration of low temperature separation systems and associated refrigeration cycles for determining most economic separation schemes and integrated refrigeration systems. In the sequential approach, the separation system was synthesized first and accordingly, the cooling/heating requirements were supplied from external utilities and refrigeration cycles. In the simultaneous design, the process streams were matched with refrigeration systems simultaneously which resulted in considerable savings. Three case studies, LNG separation train, ethylene plant cold-end separation and 5-component separation were discussed.

2.2 Membranes for Olefin/Paraffin Separation

In Semenova [66], it was claimed that around 2000 articles were published in context of membrane applications for hydrocarbons separation in the last 30 years with one-third of it being patents. These statistics indicate the growing interest of researchers in hybrid membrane-distillation systems in olefin/paraffin separation for understanding its commercial prospects. This second section of literature review is divided into six sub-sections.

1. **Current Membrane Technologies**: This sub-section reviews various membranes developed for olefin/paraffin separation.
2. **Membrane Characteristics and Parameters**: This sub-section describes the effect of feed and permeate pressures, feed flowrate and other factors on the membrane performance.
3. **Membrane Separation Improvement Techniques**: This sub-section discusses various techniques developed to improve membrane characteristics.
4. **Membrane Modeling**: This sub-section covers different models developed to simulate a membrane.
5. **Hybrid Membrane-Distillation Systems**: This sub-section reviews various efforts at establishing hybrid-membrane distillation systems.

2.2.1 Current Membrane Technologies

The two most typical materials for the construction of membranes are polymers and ceramics. Ceramic membranes are capable of operating at higher temperatures and providing superior chemical and structural stability than polymeric membranes. The main advantages of polymeric membranes are their low production costs and versatility in construction. Since, crystalline polymers are essentially insoluble, difficult to prepare and show low permeability, it is preferable to use amorphous polymers for membranes [11] though polymeric membranes exhibit some limitations when used in harsh environments like instability at high temperatures [67]. Porous inorganic membranes, e.g., different zeolite types exhibit high thermal and chemical resistance. However, preparation of defect-free membranes is expensive which makes their implementation at industrial scale difficult.

Facilitated transport membranes (FTM's) have been extensively investigated for olefin/paraffin separation, which can be seen form a series of review articles published from time to time [68]-[75]. FTM's can be highly selective as well show high permeabilities, especially at low concentration driving forces. Azhin et al. [75] reviewed the application of the FTM's technology in olefin/paraffin separation, and mentioned about its general mechanisms under varying conditions. Different parameters influence the degree of facilitated

factor, permeance and selectivity. However, the commercialization of FTM's still under-developed due to their instability during long-term exposure caused by carrier poisoning and short membrane life.

Polymeric membranes without a carrier for olefin/paraffin separation are under extensive study for large scale applications. The gas separation in these membranes follows the solution-diffusion mechanism. These membranes can be categorized as glassy, cellulosic, and rubbery. Properties such as molecule size & shape, polymer structure, packing and rigidity govern the separation characteristics of the polymeric membranes [76]. Glassy polymers have been primarily used for olefin/paraffin separation and aromatic, aliphatic and alicyclic hydrocarbons separation. Since the interaction between the sulfonyl/amino/carbonyl groups of polyimides and an aromatic molecule is stronger than that for paraffin with the same number of carbon atoms, olefins can show similar behavior resulting in their higher solubility [77]. They exhibit high selectivity in conjunction with medium permeability due to low free volume with narrow distribution and less flexibility in polymeric chains. Within this class of polymers, polyimides are most attractive for set of membranes due to relatively better separation characteristics, decent thermal and chemical resistance and easy processing [78].

However, dense polymeric membranes produce less permeate quantities due to relatively high membrane thickness. Alternatively, low thickness asymmetric membranes can be used. Polyimides display sensitivity to plasticization towards hydrocarbons like propane, propylene and carbon-dioxide at high pressure feeds. Moreover, the trade-off between permeability and selectivity has reached an upper limit for polymeric membranes, which is still inadequate for commercial application [79].

Fluorinated polyimides are found to have relatively higher thermal and chemical stability. Various attempts have been made to separate organic liquid mixtures using fluorinated polyimides. Monomers like 6FDA dianhydride contain bulky $–CF_3$ groups which restrain mobility and packing in polymeric chains, which improve separation characteristics of the membrane [78]. Shimazu et al. [80]-[81] studied 1,3-butadiene/n-butane separation and

propylene/propane separation by determining solubility, diffusivity, and permselectivity in seven different polyimides. Chan et al. [82] investigated transport of C_2's and C_3's olefin and paraffin aromatic 6FDA-1,5-NDA dense membranes. Rungta et al. [83] discussed the upper bound on trade-off between permeability and selectivity for ethylene/ethane separation displayed by 6FDA-based polyimides. Burns and Koros [84] had previously done a similar study for propylene/propane separation.

Despite their relatively good chemical resistance, fluorinated polyimide membranes have not been commercialized for pervaporation separations. When exposed for long periods to aggressive hydrocarbons, they tend to plasticize and lose their separation capabilities. Incorporation of copolymers into membranes like fluorinated ethers and ethylene, perfluorinated homopolymers (polytetrafluoroethylene (PTFE)) can be very helpful in resisting plasticization. However, polyimide structures can be extremely rigid due to their (semi)-crystalline nature and hence, their derivative membranes provide only low trans-membrane flux, making them impractical for large feed volumes. Fluorinated ring structures were found to be suitable as copolymers for providing amorphous structure, better permeability and resistance to plasticization [11].

Carbon-based membranes can be categorized as carbon molecular sieve (CMS) membranes and carbon nanotubes (CNT) membranes. CMS membranes are usually prepared by pyrolysis of polymeric precursors which are basically polyimide materials in an inert gas environment. Release of small volatile gases like H_2, CO_2, CO, and CH_4 created slit-like micro pore structures inside the membrane which changed the gas permeation mechanism to molecular sieving diffusion. The separation performance is much better for ethylene/ethane or propylene/ propane gas separation. Nevertheless, better CMS membranes are being developed for olefin/paraffin separation across various research groups as it shows a great potential for commercialization [76].

Many polymer precursors have been identified for CMS membranes and various pyrolysis conditions are being tested for improving its separation

performance. Suda and Haraya [85] used Kapton polyimide film, pyrolyzed in vacuum conditions at 1000°C, followed by activation in water vapour to expand the pore dimension. Okamoto et al. [86] pyrolyzed an asymmetric hollow fiber polymer membrane of 3,3′,4,4′-biphenyltetracarboxylic dianhydride and aromatic diamines. Vu et al. [87] prepared CMS hollow fiber membranes from asymmetric polyimide precursor fibers, 6FDA/BPDA-DAM and Matrimid 5218 and applied high-pressure (< 1000 psia) mixed-gas feeds of CO_2/CH_4 at different temperatures. Steel and Koros [88] studied CMS membranes made from 6FDA/BPDA-DAM as precursor pyrolyzed at 550°C.

There are many disadvantages to CMS membranes like complex and expensive preparation procedures, aging, pore blocking by higher hydrocarbons and brittleness. Operation at sufficiently high temperatures can avoid pore-blocking and use of a pre-purifier can completely remove traces of strongly adsorbed vapours inside the pores. For operating at large trans-membrane pressures, brittleness of a membrane can be reduced by using CMS composite membranes which are made from a selective carbonized layer on a non-selective inorganic support. These membranes show high permeability, brilliant mechanical strength, thermal and chemical stability. Fluorinated or perfluorinated polymer like polyvinylidene fluoride, is preferred for making the micro porous support membrane with an asymmetric structure [11]. In Ma et al. [79], macro porous α- alumina support coated with a sol−gel derived mesoporous γ- alumina layer was used for CMS membranes.

The use of polyimides as precursors and pyrolysis at high temperatures results in complex making methods and high production costs. The carbon-based membranes may cost upto 1 to 3 orders of magnitude greater per unit area as compared to polymeric membranes. Therefore, less expensive materials like polyacrylonitrile [89], poly(furfuryl alcohol) [90] and phenolic resin [91]. Only high separation performance as compared to its peers can justify the high capital investment in CMS membranes [92]. This can lead to their efficient implementation of hybrid-membrane distillation systems.

Pervaporation has been used in dehydrating organic solvents (alcohols, ethers, esters, acids), removing dilute organic compounds from aqueous streams and

separating organic–organic mixtures like methyl tert-butyl ether (MTBE) or dimethyl carbonate (DMC) from methanol. Even though there is not much literature on olefin/paraffin separation using pervaporation, there exists a great potential in highly diffusion-selective polymeric membranes, nanoparticles-incorporated mixed matrix membranes, and single crystalline zeolite membranes for such separation [93]. In pervaporation, the mass transport of permeating species across the membrane can be modeled on solution-diffusion mechanism [94]. Since both gas permeation and pervaporation are based on similar mass transfer phenomena, conclusions drawn on the permeation behavior of membranes for gaseous olefin/paraffin separation are also valid for pervaporation [77].

Da Costa et al. [11] claimed that membranes formed from fluorinated polymers are suitable for pervaporation performing organic/organic separations. Although the separation factor of these membranes propylene/propane separation was as low as 3, they are extremely viable in industrial context with high feed pressure and ambient permeate pressure. CMS membranes from Kapton precursor, were examined for pure liquid sorbates which suggested that they have better potential for dehydrating bioethanol through pervaporation or vapour permeation than polymeric membranes [95]. It can be concluded that pervaporation can be a promising aspect of hybrid-membrane distillation system.

2.2.2 Membrane Characteristics and Parameters

Solubility and Selectivity

Olefins and paraffins with similar boiling points and molecular shapes may have similar diffusion coefficients which can lead to difficulty in their separation. Hence, solubility difference is a key factor to enhance selectivity which can be doing by choosing a polymer material with higher affinity to olefins over paraffins [77]. Gas or vapour sorption experiments can determine the solubility properties of a membrane for a given feed composition at various feed pressures and can help determine the plasticization behavior of the membrane [78]. Both solubility and diffusivity affect the membrane properties of selectivity and permeability (Appendix C). Mixed gas

selectivities are generally lower for mixed gas experiments due to competitive sorption of components as compared to pure gas experiments.

As it was aptly mentioned by Khalilpour et al. [96], permeance is more impactful on membrane performance than ideal selectivity. On one hand, high purity permeate is produced at low permeance whereas high permeance leads to high flux (stage-cut) at low selectivities. As evident from the literature, synthesis of membranes showing high selectivities is difficult and therefore, the objective of membrane separation must be efficient target component (TC) recovery at medium selectivity as well as permeance in a membrane. Exceptions can be made for cases where high flux or high purity is required. The stringent targets posed by the industry to manufacture high selectivity membranes have been criticized and production of membranes with good permeance and acceptable selectivity has been advised [96].

Plasticization and Membrane Swelling

According to dual sorption model, permeability is supposed to decrease with increasing feed pressures in glassy polymeric materials. However, in some cases, while the feed pressure is increased, permeability starts increasing after a certain pressure called plasticization pressure. The chain packing in the membrane material is disrupted by high gas concentrations. The polymer matrix incurs swelling, leading to increase in segmental mobility of polymeric chains. This causes permeabilities of all components to increase which decreases selectivity. 6FDA-TrMPD polyimides and PPO membranes showed plasticization at 5 atm and 2 atm pressure respectively for C_3H_6/C_3H_8 separation [97]. 6FDA-TrMPD plasticized at around 0.5 atm for 1,3-butadiene/n-butane separation [98]. Plasticization occurs in the membranes on facing high partial pressure of CO_2**,** hydrocarbons like propylene, propane, ethylene oxide etc**.** Partial dissolution of the membranes can also be caused by strong plasticization. Membrane swelling increases free volume at high feed pressures which reduces the transport resistance and bigger molecules can diffuse through the membrane easily. It is commonly observed in pervaporation membranes.

Effect of Feed Flowrate

Increase in the feed flowrate decreases TC recovery in permeate due to shorter contact time of the feed gas with the active membrane area [99]. In case of pervaporation, feed flow rates of about 300 ml/min were found effective in providing regular flow on the feed side, while higher circulation rates caused localized mechanical strain and possibly chemical erosion of the membrane [77].

Effect of Temperature

In PDMS membranes, it was shown that at constant pressure, with decrease in temperature (50°C to -20°C), selectivity of N_2 changed negligibly but increased for C_2H_4 < C_3H_6 < C_4H_8. As the temperature approached their condensation temperature, gases became more condensable, increasing their solubilities. In case of permeability, decrease in temperature decreased the permeability of C2H4 slightly but increased the permeabilities of C_3H_6 and C_4H_8 sharply [100]. For poly (ether block amide) membranes, the operating temperature and pressure determine the effect of diffusivity on perm-selectivity. Decrease in temperature and increase in pressure increase the olefin's sorption uptake, thereby increasing permeability and selectivity [101].

Effect of Feed Pressure

TC recovery in permeate stream can be increased with high feed pressure and/or high membrane areas. Increasing the feed pressure improves the selectivity at lower membrane areas. For higher membrane areas, this effect is observed only till certain extent beyond which selectivity starts to decrease [96]. In both pure as well as mixed gas experiments for C_2H_4/C_2H_6 separation, the permeability of both components and ethylene selectivity decreased with increase in the feed pressure which is attributed to "dual sorption and diffusion model" for low operating pressures. For C_3H_6/C_3H_8 separation, increase in feed pressure increased both propane and propylene permeabilities and decreased selectivity because of plasticization in polyimide [102]. The solubility coefficients increase in the order $S_{C4H8} > S_{C3H6} > S_{C2H4} > S_{N2}$ when pressure is increased from 1 to 20 atm at 25 ◦C, which is in the same order as their critical temperatures [100].

Membranes formed from fluorinated polymers can operate well under unusually high pervaporation feed pressures, such as 100 psig, 150 psig or above and permeate side of the membrane at atmospheric pressure [11]. For the ethylene glycol cross-linked 6FDA-4MPD/6FDA-DABA 4:1 copolyimide, plasticization effects were not observed up to 30 bar, due to restricted mobility of the polymer chains caused by crosslinking units [78].

Effect of Permeate Pressure

Changing the permeate pressure affects the trans-membrane flux due to change in chemical potential across the membrane. It can be maintained at the atmospheric pressure or above, depending upon the desired state of permeate, gas or vapour. The atmospheric pressure on the permeate side avoids the need for a vacuum pump, simplifying the recovery or further treatment of permeate. Alternatively, it can be reduced by drawing vacuum on the permeate side, sweeping the permeate side with an inert gas to continuously remove permeating vapour, or cooling the permeate vapour stream to induce condensation [11]. Increasing permeate pressure or decreasing feed pressure raises membrane area [103].

2.2.3 Membrane Separation Improvement Techniques

Membrane performances can be significantly improved for gas separation and pervaporation purposes by methods discussed below.

Cross-linking

Crosslinked copolyimide membranes exhibit high resistance to plasticization and low loss in selectivity when compared to non-crosslinked membranes on exposure to CO_2/CH_4 or toluene/cyclohexane mictures. Covalently crosslinked membranes must be preferred for long-term applications since they have better separation performance than ionically crosslinked membranes [104]. There are many ways of cross-linking through which the structural stability of the composite membranes can be improved like cross linking of the top layer, multi-layer structure strategy and integrally skinned structure approach.

Addition of metal-organic frameworks (MOFs)

Mixed-matrix membranes (MMMs) with metal–organic frameworks (MOFs) as additives (fillers) help in enhancing the membrane performance in terms of increased permeabilities and sometimes, selectivities, in comparison with the pure polymer. Since it is easier to modify membranes with MMM's, they are economically more attractive than inorganic membranes. Incorporation of MMM's also enhances physical, thermal, and mechanical properties for harsh operating conditions [92]. In Ploegmakers et al. [105], MMMs were prepared with different MOFs as fillers (Cu_3BTC_2, FeBTC and MIL-53(Al)) and characterized for ethylene/ ethane separation.

Inorganic Support

During the preparation of supported CMS membranes, the membrane thickness is reduced which results in increased gas permeance. However, certain non-selective defects are formed in the membrane which decreases selectivity. Shiflett and Foley [106] used the ultrasonic deposition method for preparing CMS membranes on a macroporous stainless steel tube for O_2/N_2 separation whose thickness (5-20 μm) depended on the number of coatings and the concentration of polymer solution. In Yamamoto et al. [107], a CMS membrane of BPDA-pp'ODA polyimide was prepared by coating/ imidization/pyrolysis process, for obtaining membrane of thickness of 5−6 μm.

2.2.4 Membrane Modeling

Tessendorf et al. [108] presented membrane models based on differential equations for counter- and cross-current flows which were solved using a procedure based on orthogonal collocation and tested in OPTISIM, an external simulator. In the case of liquid hydrocarbons separation in Sakellaropoulos et al. [77], a 1D single fibre model was developed for the pervaporation of a binary mixture through an asymmetric hollow fibre membrane with significant permeate pressure drop inside the fibre bore. Davis [94] developed mathematical models for gas permeation and pervaporation to be used in Aspen HYSYS, which included energy balance for taking into account the

temperature change during pervaporation. The logarithmic-mean trans-membrane partial pressure for counter-current flow is defined as

$$\overline{xp_F - yp_P} = \frac{(x_F p_F - y_P p_P) - (x_R p_F - y_i p_P)}{\ln\left(\frac{(x_F p_F - y_P p_P)}{(x_R p_F - y_i p_P)}\right)} \quad (2.1)$$

where y_i is the permeate composition at the retentate end of the membrane. A hybrid distillation-pervaporation process was illustrated in HYSYS for simulating ethanol purification [94].

Chatterjee et al. [109] presented a hollow fiber membrane model for CO_2 separation from CH_4. It was solved using finite-difference method and analyzed for different flow patterns and operating parameters. Counter-current flow showed higher efficiency, and increase in permeate pressure and/or decrease in feed pressure decreased the membrane area. In Ahmad et al. [110], a 2D cross-slow membrane model was simulated in Aspen HYSYS using Visual Basic (VB) sub-routine for designing the process of CO_2 capture from natural gas. Different design configurations were tested for parametric sensitivities as well as process economics, and the double stage with permeate recycle system was found to be the most optimum design. In Khalilpour et al. [96], a hollow fibre membrane system was modeled using a system of nonlinear differential algebraic equations for a multi-component gaseous feed. It was solved with the help of backward differentiation and Gauss–Seidel method, and parametric analyses were done in terms of feed quality, pressure, area, selectivity and permeance. Koch et al. [111] published a detailed model for pervaporation to account for pressure, temperature, composition and flux profiles inside the membrane module to handle temperature and concentration polarization as well as fluid dynamics.

2.2.5 Hybrid Membrane-Distillation Systems

Gottschlich and Roberts [112] carried out a study for US Department of Energy to identify governing principles behind the choice of hybrid separation systems over conventional columns. One of their case studies was propylene/propane separation where they examined factors characterizing energy consumption as well as overall costs for both membrane and non-membrane technologies which might affect the final choice between the two.

Three hybrid configurations were chosen and thermodynamic and economic evaluations as well as sensitivity analysis were carried out. It was concluded that high product purities resulted in lower efficiencies and higher processing costs for all systems. Secondly, the thermodynamic extent of separation in the membrane is a key parameter for a hybrid system.

Davis et al. [113] developed a facilitated transport membrane system for BP and grouped it with distillation column to carry out pilot plant experiments on propylene/propane and ethylene purge gas recovery. Results showed that membrane was stable over three to six months, and 98.5% or higher purity was guaranteed using refinery grade propylene feed. Optimization was carried out for hybrid systems with three configurations and the one using side draw from the distillation column proved to be most advantageous. The splitter could be debottlenecked to increase its capacity by 80% with no increase in utilities. This resulted in energy savings of 500 billion BTU per year for C_3-splitter producing 10,000 bbl/day of polymer grade propylene.

Moganti et al. [114] discussed the minimum area method and the Smoker' equation method for a hybrid membrane-distillation process to minimize the number of trays inside the C_3-splitter. The effect of membrane parameters on the number of trays was observed. The optimum membrane position was found to be near the feed stage of the column which reduced the tray number by ~25%, and increasing the membrane area increased the efficiency of the system only up to an extent. At a ratio of 0.1 mol/m^{2}s for feed flowrate to surface area of the membrane, maximum reduction of tray numbers could be achieved

Pettersen and Lien [115] proposed an algebraic model for designing vapour permeation systems with black-box representation of a membrane and carried out parametric studies. Results showed that the module cut rate i.e. the amount of water being removed was close to minimum value at high values of selectivity. The amount of permeate increased with decrease in selectivity. This reduced the permeate purity as well as the product recovery in the retentate and led to larger recycle of permeate stream to the column. A reduction of 50% in membrane area was observed on doubling the feed

pressure. In another study [116], parallel configuration for of hybrid membrane-distillation system was analyzed for propylene/propane separation. The optimum membrane feed stream was found to be near the main feed stage for the column.

Pressly and Ng [117] investigated the effect of various possible hybrid membrane−distillation configurations. A procedure for screening calculations is presented that allows the determination of the break-even cost for a membrane, above which the hybrid would be too costly to be competitive. This approach is applicable to the screening of all the types of membranes and can be used to target the desirable membrane properties. Screening calculations are performed for water - acetic acid, ethanol - water, and propylene - propane systems to demonstrate the inherent trade-offs of the hybrids and the effect of phase behavior on the performance. It was concluded that series or parallel configurations were preferred over top or bottom configurations for propylene/propane separations.

Fahmy et al. [118] presented a methodology to alter membrane parameters responsible for vapour permeation in a hybrid system, and a case study was performed on ethanol dehydration. For every specific range of separation, membranes with a wide range of selectivities were required. An early stage simulation and optimization of three configurations of the process provided useful information related to membrane properties. The whole membrane system was predesigned, sizing of major equipment was done and the annual cost was minimized. Results showed that for a very pure retentate, high selectivity membranes must be used.

Kookos [119] proposed a mathematical programming methodology for optimizing hybrid membrane-distillation systems efficiently through a modified superstructure representation of various configurations. Structural and parametric optimization was carried out for the hybrid system of propylene/propane separation. The objective of this study was to minimize the total annual cost which was dependant on installation costs and utility costs of compressor and steam. The annual cost was dominated by utility cost, and hardly affected by membrane bare module cost.

Kreis and Górak [120] focused on modeling, simulation and process analysis of hybrid membrane separations on distillation and pervaporation for separation of acetone, isopropanol and water. A flexible and robust simulation tool was described for pervaporation and vapour permeation, developed in ASPEN Custom Modeler^{TM}. Relevant model parameters were determined and the model was validated using binary and ternary lab-scale pervaporation experiments with satisfactory agreement. The simulation studies showed that it was necessary to maintain high membrane feed streams in order to obtain adequate module efficiencies to compensate for the temperature loss due to permeate vapourization. At the industrial scale, the minimal required membrane area for the given separation task was found in the region of high heat duties and large mass flows. However, the cost optimum of the hybrid process was localized at low heat duties and high side streams.

Takht Ravanchi et al. [121] reviewed different membrane processes and membrane reactors in petrochemical industry which included olefin-paraffin separation. They demonstrated the potential of hybrid membrane distillation systems in United States. They highlighted that, while searching for appropriate membranes, mechanical properties are as important as favorable combination of permeability and selectivity.

Caballero et al. [122] retrofitted and optimized a hybrid membrane–distillation system for ethylene/ethane separation with parallel configuration using a mathematical programming approach. A shortcut model was introduced to determine the viability of the hybrid system and gauge the order of magnitude for related energy savings. Thereafter, they proposed a superstructure optimization approach to minimize total annual savings which used rigorous models for simulating column as well as the membrane on MATLAB and optimized using MATLAB-TOMLAB. The savings of up to 30% were recorded for the ethylene/ethane separation. The potential savings were lowest for a 0.8 mole fraction ethylene in feed.

Bernardo and Drioli [123] focused on the application of membrane gas separation technology in oil-refining and petrochemical sector. The use of membrane as an alternative solution to distillation was considered. However,

due to similar molecular sizes and condensabilities of the components, the separation was quite difficult. Moreover, it was a challenge to operate the membranes in a hydrocarbon-rich environment under pressure. Hence, it was concluded that membranes must be able to perform adequately under conditions of exposure to organic vapours, especially C_3+ hydrocarbons, which are common in refineries, chemical plants or gas fields.

Ayotte-Sauvé et al. [124] presented a thermodynamic approach to find minimal energy requirement for a retrofitting hybrid membrane-distillation system. Examples of C_3 splitter and C_2 splitter were used to demonstrate this approach. The results were compared to a reference superstructure formulation, solved using GAMS-CONOPT for C_3-splitter and GAMS-CoinIpopt for C_2-splitter. The reflux ratio of the column in the hybrid setup was minimized by finding optimum membrane surface area, position of membrane feed and product streams along the column, feed stage and the hybrid profile of the column. The shortcut method calculated the minimal reflux ratios for C_3-splitter and C_2-splitter, which had errors of 2.4% and 1.52% from reference cases respectively, while significantly reducing the corresponding number of equations to be solved. The method proved useful for rapid and reliable screening of different membrane technologies.

Benali and Aydin [125] carried out optimization and economic analysis of numerous hybrid membrane distillation schemes to scrutinize their feasibility in applications to C_2- and C_3- splitters. The membrane cascade system resulted in significantly high capital and operating costs with the total savings of 54% compared to the base case and yielded highest ethylene purity of 99.99% for ethylene/ethane separation. The series configuration was comparatively more economical for C_2-splitter. The top configuration was better for C_3-splitter in terms of propylene purity and the top-bottom configuration for maximum cost savings when compared to the base case.

Naidu and Malik [126] optimized a hybrid pervaporation-distillation system with series, parallel and series-parallel configurations using a GAMS–CONOPT solver, and proposed a general method for the separation of azeotropes, close boiling mixtures and tangent pinch mixtures. The total

annual cost for the separation system was minimized by optimizing number of trays, feed tray location, reflux ratio, retentate recycle location, permeate recycle location, membrane feed location, number of pervaporation modules required, target composition and membrane selectivity. The separation of propylene-propane was studied as a close boiling mixture. The parallel arrangement of membrane modules was found to be more economical compared to series and series/parallel configurations.

Motelica et al. [127] presented a techno-economic evaluation of paraffin/olefin separation for determining the membrane potential for hybrid processes in ethylene/ethane separation. Two configurations with membrane in up-stream as well as down-stream were studied. Increasing the ethylene permeance (or selectivity) decreased the condenser duty. High membrane selectivity (> 60) or ethylene permeance greater than 1×10^{-4} mol/(m^2-s-kPa) is required for considerable savings.

Ploegmakers et al. [128] retrofitted an existing ethylene splitter with a membrane unit in series and parallel configurations. The membrane unit variables like feed pressure, permeate pressure and surface area were optimized to understand the effect of ethylene permeance and ethylene/ethane selectivity on the utility consumption of the hybrid membrane-distillation system. The series configuration with 2500 kmol/h membrane feed outperformed the series and parallel configurations with 1500 kmol/h membrane feed. Operating at high feed pressures increased the temperature inside the membrane which was favorable. High permeate pressures reduced the compression duty at the cost of driving force across the membrane, which led to lesser reduction in condenser and reboiler duties. High membrane surface area increased the permeate flow with increased reductions in column duties, but at the cost of high capital investment.

2.3 Conclusions

The conventional process design of ethylene plant is discussed in the firsts section of this literature review. Pinch [19]-[22] and exergy analysis [23]-[24] presented scope for heat integration in the process. Petracci et al. [16], Eliceche et al. [17] and Petracci et al. [18] optimized the process of an

ethylene plant and its utility plant combined using SQP, studied the effect of variable feed conditions on an ethylene plant i.e. flexibility analysis as well as possibility of debottlenecking. Díaz and Bandoni [28] optimized a real-world ethylene plant using outward approximation technique to solve the MINLP formulation. Sobočan and Glavič [30] and Wang and Smith [31] suggested optimal sequences for distillation columns for a multi-product separation. Tahouni et al. [64]-[65] performed parameter optimization and modified the basic configuration, respectively, of cold-end separation in an olefin plant.

Clearly, an ethylene plant creates avenues for multi-objective optimization (MOO). Tarafder et al. [129] carried out MOO of an industrial ethylene reactor using a nondominated sorting genetic algorithm. Zhang et al. [33] performed MOO on the cold-box of an ethylene plant. However, MOO on the separation train in the ethylene plant has not been subjected to MOO till yet. This has led us to focus our research on the MOO of cold-end separation of an ethylene plant.

The second section of this review explores the membrane application in an ethylene plant. CMS membranes with better rigidity and improved separation performances present a great potential for commercialization in hybrid membrane-distillation systems. Takht Ravanchi et al. [121] reviewed different membrane processes and membrane reactors and Bernardo and Drioli [123] focused on the application of membrane gas separation in petrochemical industry, especially olefin-paraffin separation.

It is important to understand the economics behind the application of such hybrid systems as done by Benali and Aydin [125] for different hybrid schemes for C_2- and C_3- splitters and Motelica et al. [127] in ethylene/ethane separation. Ploegmakers et al. [128] retrofitted an existing ethylene splitter with a membrane unit in series and parallel configurations and showed the effect of ethylene permeance on net savings for different selectivities using optimization. However, the literature values of these membrane parameters are much lower than projected by Ploegmakers et al. [128] for the system's commercial feasibility. As it is important to minimize the operating cost of the

hybrid system while minimizing related capital investment, it makes for an ideal case of MOO within the range of reasonable membrane parameters.

Chapter 3

MULTI-OBJECTIVE OPTIMIZATION OF A CONVENTIONAL COLD-END SEPARATION IN AN ETHYLENE PLANT

3.1 Introduction

Ethylene is a key building block in the petrochemical industry. Majority of ethylene is used in the production of ethylene oxide, ethylene dichloride, ethyl benzene, and a variety of homo- and co-polymers (i.e. plastics ranging from food wrap to impact-absorbing dashboards in cars). Increasing modernization and urbanization in developing countries in Asia have created new markets for these products, thereby accelerating the demand for ethylene. This has resulted in large ethylene capacity expansions in recent years, with capacity growing at a compound annual growth rate of 4% between 2007 and 2012, to reach 155.9 MTA in 2012 [1]. Ethylene plants are complex, large-scale factories that can process a variety of feed-stocks, ranging from gases (such as ethane, propane and liquefied petroleum gas) to naphtha, distillates and gas oils. Local market and extent of integration of ethylene units into refining and/or petrochemical complexes influence the products desired and the feed-stocks used. Main products are polymer-grade ethylene and propylene, and others such as butadiene-rich C_4 stream and C_6-C_8 aromatics-rich pyrolysis gasoline.

Many studies have been reported on analyzing ethylene production process, optimizing the process flow-sheet and suggesting modifications. These studies have helped gain better insight into the process and identify the scope for modification at both design and operation fronts. Bandoni et al.[15] developed a fast and reliable process simulator for ethylene plants which allowed implementation of a plant optimizer to find optimum operating conditions in a very short time. Based on this ethylene plant framework, Petracci et al.[16] performed optimization of a process consisting of pyrolysis furnaces, compressors and demethanizer in combination with its utility plant using two alternative objective functions: maximize gross benefit or maximize ethylene production. The results showed the economic potential of overall optimization of ethylene plant and utility systems. Subsequently, Eliceche et al. [17]

focused on the effect of variable feed conditions on the process operation and debottlenecking the plant as well. Petracci et al. [18] extended the work of Eliceche et al. [17], to conduct flexibility analysis of a given process.

Huang and Shao [27] proposed a pattern recognition method and used linear programming to obtain the optimal operating point of an ethylene process. Díaz and Bandoni [28] discussed operation optimization of an ethylene plant using outward approximation technique to solve the MINLP (mixed integer nonlinear programming) model. Shah and Kokossis [34] presented 'Conceptual Programming' which employed task representations instead of unit-based representations like complex column configurations, sloppy-split arrangements and options for operating pressure optimization. Sobočan and Glavič [23] presented a new approach for arranging the heat integrated distillation sequences using pinch analysis, which can provide correct ranking of the sequences. Yan's thesis [29] was on plant-wide optimization of an ethylene plant with special focus on the design of the ethane/propane cracker and its kinetics, and approximate models for distillation columns to simulate the final products and utility usage.

Sobočan and Glavič [30] performed optimization of two best sequences for distillation columns for a six-product separation, including a case study on ethylene process. Wang and Smith [31] focused on synthesis and optimization of specialized sequences including flash drums, dephlegmators and simple and complex distillation columns to minimize total shaft power requirement of the refrigeration system or total utility costs. Van Geem and Marin [32] studied the design of an ethylene separation process using advanced computational methods and found the best configuration out of demethanizer-first, deethanizer-first and depropanizer-first process design in combination with front-end or back-end hydrogenation. Zhang et al. [33] modeled the chilling train before demethanizer supported by regressed data using Aspen Plus, and optimized it using GAMS.

Hou et al. [63] studied simulation of an ethylene plant with focus on rapid cooling oil systems, and developed a model, which predicted industrial data accurately. Nawaz and Jobson [62] suggested a method to bypass the rigorous

simulation of complex demethanizer, in separating multi-component mixtures. They proposed a semi-rigorous boundary value method to model the equations of demethanizer on MATLAB and linked it with Hysys for prediction of physical and thermodynamic properties using a short-cut model. Tahouni et al. [64] performed operation optimization of low-temperature separation in an olefin plant. They studied retrofitting of separation columns, which involved reflux ratio optimization, feed conditioning and side condensing and reboiling. In another study, Tahouni et al. [65] modified the basic design procedure for ethylene plant cold-end separation and their associated refrigeration cycles, to determine appropriate and cost-effective separation schemes along with integrated refrigeration systems.

Thus, many attempts have been made to optimize the ethylene process with various objectives. However, these objectives may be conflicting and affect the process optimization in opposite directions. Hence, it is important to understand the nature of conflict between different objectives. Multi-objective optimization (MOO) has been applied on various chemical processes in recent years [130-131]. It provides a set of optimal solutions in the form of a Pareto-optimal front, where moving from one solution to another has some trade-off in at least one objective. Till now, MOO studies on ethylene process are limited to naphtha cracker only [129, 132-135] In the present study, the conventional cold-end separation section of ethylene production, which comes after the pyrolysis and compression sections, is analysed and optimized for multiple objectives. This study considers a train of distillation columns, intercepted by a methyl-acetylene propadiene hydrogenation (MAPDH) reactor and an acetylene recovery section, to produce ethylene, propylene, acetylene, ethane, propane, C4's and gasoline. The elitist non-dominated sorting genetic algorithm, NSGA-II is employed for MOO. Several bi-objective cases involving important and conflicting objectives are considered for MOO of cold-end separation process. The results including trade-off between objectives and optimal values of decision variables are presented and discussed for deeper insight into the process.

The rest of this chapter is organized as follows. Section 3.2 describes the ethylene production process. Section 3.3 presents the simulation and validation of the conventional cold-end separation process adopted for this study. Section 3.4 covers formulation of MOO problems, which includes selection of objectives, decision variables and constraints in the optimization problems studied. In section 3.5, results from the optimization of several combinations of two objectives are presented and discussed. Finally, conclusions of this study are given in section 3.6.

3.2 Process Description

In a conventional ethylene plant, hydrocarbons along with superheated steam at radiant-coil inlet temperature of about 600°C, are sent to tubular heaters for pyrolysis. Cracked gases leave the radiant coil of an ethylene furnace at 750 – 900 °C. Thereafter, the effluent is quickly cooled in exchangers by generating steam. Quench oil is directly sprayed into the cracker effluent which reduces the temperature quickly, in order to minimize further cracking into undesired products. This is followed by a gasoline fractionator to recover fuel oil and lighter components from the heavies in the cracked effluent whose top products are sent to a quench tower to condense all the steam and most of the pyrolysis gasoline components. A series of 3–4 compressor stages are used to increase the pressure of the quench tower exit stream to ~1.5 MPa. After an acid gas removal system, another stage of compression up to 3.5 MPa and cooling by propylene refrigerant to slightly above hydrate inception temperature, the stream is flashed into vapour and condensate. This flash vessel is the starting point of the cold section of an ethylene (or cold-end) separation process. The process studied in this work is shown in Figure 1, and it is briefly described below.

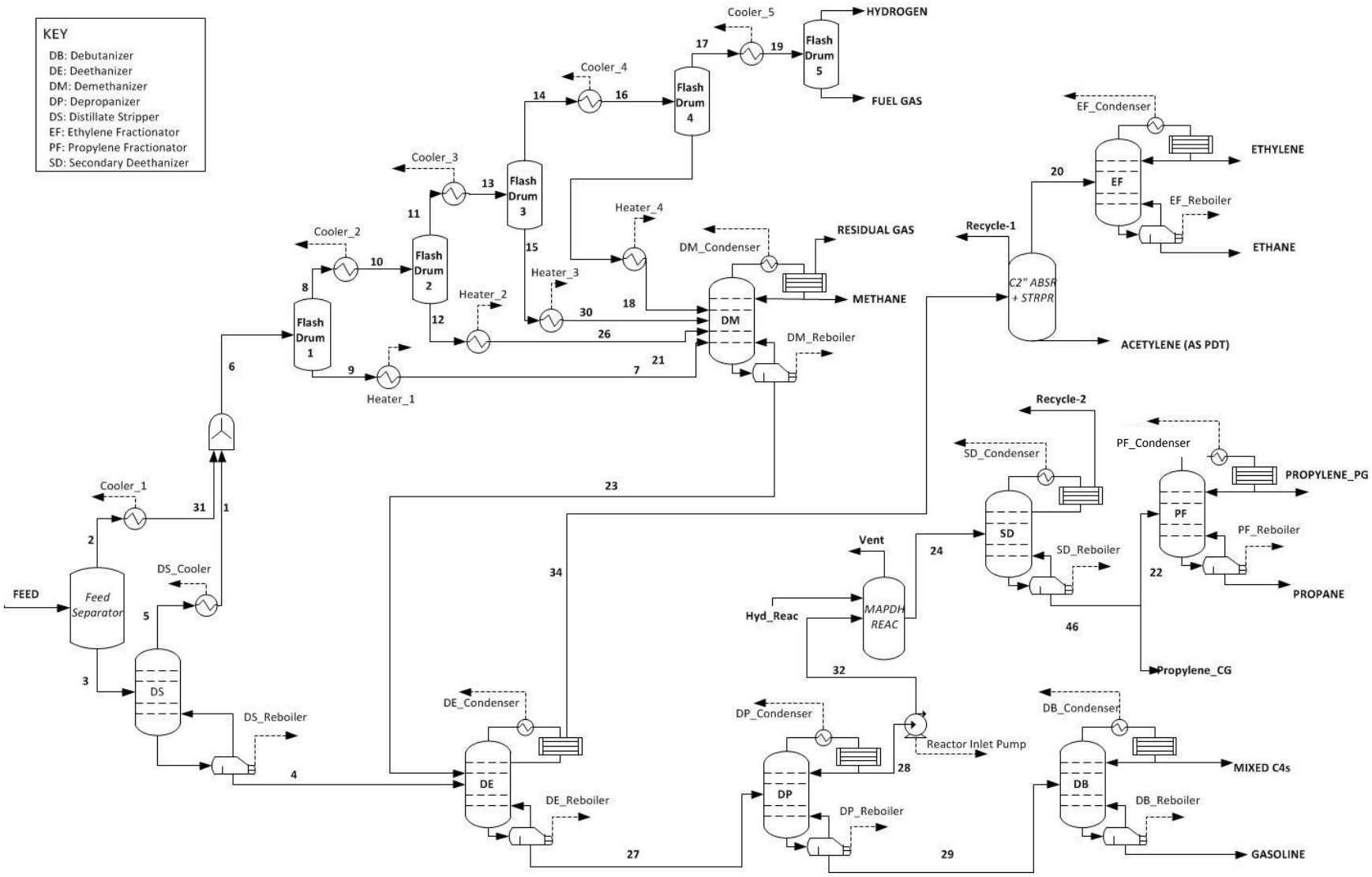

Figure 3.1: Process flow diagram of conventional cold-end separation of an ethylene plant

In the conventional separation process, the flash vapour from the flash vessel, Feed_Separator comprising C_2 and lighter components goes through stage-wise condensation using propylene–ethylene cascade refrigeration, also known as chilling box, to finally separate hydrogen and fuel gas in Flashdrum_5. The condensates from Flashdrum_1, Flashdrum_2, Flashdrum_3 and Flashdrum_4 are directed to appropriate trays in the demethanizer, DM as feed streams. DM's overhead vapour stream, RESIDUAL GAS comprises of 95 mol% methane and the rest is H_2 and CO with traces of ethylene; a distillate stream, METHANE, with traces of hydrogen and ethylene. DM's bottoms stream contains primarily C2 and heavier products.

The condensate from the Feed_Separator is fed into the distillate stripper, DS whose overhead stream containing lighter hydrocarbons up to C4's is sent to the chilling box. The bottoms from both DS and DM are supplied to the deethanizer, DE operating at ~2.6 MPa. The overhead stream of DE is mainly C_2's, namely, ethylene, ethane and acetylene, and the bottoms containing C_3's and higher. The acetylene in DE overheads is recovered using extractive distillation by passing through absorption-desorption towers [13]. In the first tower, acetylene along with some ethylene and ethane is absorbed in dimethylformamide. The second tower recovers the absorbed ethylene and ethane, and the third tower desorbs acetylene into the outlet stream. After the acetylene is recovered, the gas is sent to the ethylene fractionator, EF which is an ethylene-ethane separator typically producing 99.9 mol% ethylene in overheads and 99.5 mol% ethane in bottoms. Ethane is recycled to tubular heaters for steam cracking to valuable products.

The DE bottoms are fed to the depropanizer, DP. The overhead stream from DP is C_3 hydrocarbons including propylene, propane, methylacetylene and propadiene. This stream is sent to the hydro-converter, MAPDH_REAC with catalysts that convert methyl-acetylene and propadiene to propene and propane [13]. The hydrogenated stream is sent to the secondary deethanizer, SD whose vent is recycled and bottoms is supplied to the propylene fractionator, PF. PF operating at 1.8–2 MPa with more than 200 trays in two-tower design produces polymer-grade propylene (99.5 %+) in the overheads

and propane with purity of more than 95% in the bottoms. The latter can either be recycled to the steam cracker or used as a fuel. DP's bottoms with C_4 and heavier hydrocarbons is fed into the debutanizer, DB, operating at 0.4-0.5 MPa, where the overheads comprises mainly of C_4's and bottoms is C_5's and higher.

3.3 Simulation of the Cold-End Separation Process

The simulation of the cold-end separation process is performed using the commercial simulator, Aspen Hysys version 7.2. The cold-end separation section of the existing plant comprises of eight distillation columns, six flash drums, six coolers, four heaters and one reactor (Figure 1).

3.3.1 Property Package Selection

The simulation procedure in Aspen Hysys involves selection of a property package, which estimates thermodynamic and transport properties for the multi-component mixtures in the process. The two most important tasks to describe the physical properties successfully for simulation are: selecting the appropriate physical property methods, and validating the physical properties [136]. Preliminary selection of property methods requires consideration of four factors: (a) nature of properties of interest, (b) composition of the mixture, (c) pressure and temperature ranges, and (d) availability of parameters in the property model. Based on these considerations, two property models: Soave-Redlich-Kwong (SRK) and Peng-Robinson (PR) model catering to real and non-polar components, were selected for further deliberation

Extensive vapour-liquid equilibrium (VLE) validation was done to choose between SRK and PR equation of state models by simulating the experimental VLE data available in Gmehling et al. [137]. In total, seven binary VLE data for key components in the distillation columns involved were considered. Analysis of adjusted R^2 values between experimental and simulated VLE data showed that values predicted by PR model fitted the experimental data better than those by SRK model; therefore, the former was selected as the property package for simulating the cold-end separation process of the ethylene plant.

3.3.2 Details of the Process and Simulation

The cold-end separation process used in this study is based on a simplified and yet realistic process flow diagram, typical of plants built in early 80's using naphtha as the feedstock. The feed for the separation process is mixture of gases, leaving the multi-stage compression and caustic wash section. It comprises of hydrogen, methane, C_2's, C_3's, C_4's C_5's and C_6's, with typical composition shown in Table 3.1. The C_7's and higher components were combined together with C_6's and they are all considered as n-hexane. The stage numbering is based on bottom-up format as followed by the available data.

The distillation columns are simulated rigorously via stage-by-stage calculations. The operating pressure and number of trays are typical of actual operating plant. The bottom pressure is estimated assuming 0.1 psi pressure drop per tray. Since actual numbers of trays in the columns are known, overall efficiency of the column is used to find the number of ideal trays. It is calculated using the O'Connell correlation [149]:

$$E_0 = 51 - 32.5 \times \log(\mu_a \alpha_a) \tag{3.1}$$

This efficiency is based on feed liquid viscosity (μ) and the relative volatility of light-heavy key components ($\alpha_{LK\text{-}HK}$) at the column average conditions. Using equation (3.1), overall efficiency calculated for each column is consistent with the ranges given in the literature (Table 3.2). Based on these efficiencies, number of ideal trays was calculated as follows:

$$Number\ of\ Ideal\ Trays = Actual\ Number\ of\ Trays \times Overall\ Efficiency \tag{3.2}$$

In Aspen Hysys, stage/tray efficiency can be given for simulating distillation columns. The column model is probably based on equilibrium stages, and stage efficiency is used to correct compositions of liquid and vapour streams leaving a stage. This, according to Kaes [138], makes the column model inappropriate for prediction at other operating conditions, if stage efficiencies are used. It was suggested to use overall efficiency to translate the actual trays to ideal trays and then simulate the column with ideal trays. Hence, number of ideal trays calculated as above using the overall efficiency, were used in the

Hysys simulation of distillation columns. The feed stage for each column was changed according to its overall efficiency.

Table 3.1: Feed Composition for the Cold-End Separation Process

S. No.	Component	Molecular Formula	Mole Fraction
1.	Hydrogen	H_2	0.1445
2.	Methane	CH_4	0.2627
3.	Acetylene	C_2H_2	0.0056
4.	Ethylene	C_2H_4	0.3172
5.	Ethane	C_2H_6	0.0608
6.	Methyl-Acetylene	C_3H_4	0.0023
7.	Propadiene	C_3H_4	0.0023
8.	Propene	C_3H_6	0.1135
9.	Propane	C_3H_8	0.0053
10.	1,2-Butadiene	C_4H_6	0.0025
11.	1,3-Butadiene	C_4H_6	0.0227
12.	i-Butane	C_4H_{10}	0.0080
13.	n-Butane	C_4H_{10}	0.0088
14.	1-Butene	C_4H_8	0.0000
15.	i-Butene	C_4H_8	0.0080
16.	cis-2-Butene	C_4H_8	0.0020
17.	trans-2-Butene	C_4H_8	0.0020
18.	n-Pentane	C_5H_{12}	0.0155
19.	n-Hexane	C_6H_{14}	0.0150
20.	Carbon monoxide	CO	0.0012

Various configurations were used for different columns depending upon their reflux conditions in the actual plant. DM has a partial condenser, and hence its simulation requires three active specifications, which are overhead vapour stream flow rate, distillate stream flow rate and reflux ratio. DM and SD use full reflux conditions (i.e., with only a vapour stream as the distillate), and so vent rate and reflux rate are used as active specifications for their simulation. DP and DB use total condenser, and are simulated with specified distillate rate and reflux ratio. For the EF and PF, total condensers are used. Since these

produce final products, active specifications for their simulation are the product compositions as given in the design data.

Table 3.2: Key Components and Overall Efficiency for Columns in the Cold-End Separation Process shown in Figure 1

Distillation Column	**Light Key**	**Heavy Key**	**Overall Efficiency (%)**		
			Calculated	**Kaes (2000)**	**GPSA (2004)**
DS	Methane	n-Butane	43	40–50	-
DM	Methane	Propane	72	-	45– 60
DE	Ethane	Propene	79	65–70	60–75
DP	Propene	i-Butene	72	70–80	80–90
DB	Propane	n-Butane	73	85–90	85–95
SD	Ethane	Propane	84	65–70	-
PF	Propylene	Propane	95	95–100	-
EF	Ethylene	Ethane	87	95–100	-

In the present study, major heat-integrated networks inside chilling-box section before DM are not considered for simplicity. Data on the acetylene recovery section are not available due to proprietary reasons, and so it is replaced by a component splitter for simulation purpose. The MAPDH_REAC is simulated as a conversion reactor along with a component splitter to closely simulate this complex reactor system. A few streams are returned to the upstream section of the plant (i.e., steam cracker), and so they are considered as such without any recycle block in the Hysys simulation.

3.3.3 Validation of the Simulation

For validating the predictions by Aspen Hysys, all the units in the process shown in Figure 1 were simulated based on the design data of a typical operating plant outlined in the previous section. The product specifications were followed as per the design data as well. The solver used for all distillation columns was HYSIM inside-out algorithm except for DM which required the modified HYSIM inside-out for robust convergence. The component splitters for simulating the acetylene recovery section and MAPDH_REAC section have been assigned split values according to the design data. The predicted stream conditions are compared with the available

industrial design data, in Table 3.3 and 3.4. For each distillation column, absolute error is calculated in case of temperatures, and both absolute and percentage errors are given for the overhead and bottom flow rates.

Referring to the first three entries in Table 3.3, the difference in the predicted bottoms flow rate of DS from the design data is due to lesser amount of liquid from Feed_Separator flowing into DS as top stage feed. This may be due to the property package used in the simulation which affects the flash calculations of Feed_Separator. However, it is recovered back through the DM which is supplied with vapour from Feed_Separator through the chilling box.

Interestingly, the DM bottom flow rate error is 57 kg/h higher than the DS bottom flow rate error in the simulation (Table 3.3). This accounts for the extra 57 kg/hr of components coming into the DE from the DM bottoms, which were supposed to go out through Hydrogen & Fuel_Gas, as per the design data. Since DE vent rate was fixed according to the design data as an active specification for the column, predicted flow rate of DE bottoms is 57 kg/h higher than the design value since more of propene and ethane are driven to the DE bottoms. Similarly, distillate rate is specified for DP. Hence, extra propene entering the column is sent through overheads instead of some methyl-acetylene, butadienes and other C4's which go to the DP bottoms. Small errors in product flow rates of EF are partly attributed to the physical property model and partly due to the lesser amount of propene (22 kg/h) entering the column.

Results in Table 3.4 show that DS overhead temperature is predicted to be 6.8°C lower than the design value. This may be because of the physical property model used for this column in the present simulation and fir industrial design. Predicted temperatures of DP and DB bottoms are 4°C and 11.5°C higher than the design data due to more heavies going to DP and DB bottoms, relative to the design data. In general, most of the errors are small and the Aspen Hysys simulation model can be used for optimization.

Table 3.3: Comparison of Predicted Flow Rates with the Typical Design Data

Distillation Column	**Output Stream**	**Design Value (kg/h)**	**Predicted Value (kg/h)**	**Absolute Error (Percentage)**
Feed_Separator	Overheads	84788	86386	1598 (1.9%)
	Bottom	36018	34420	1598 (4.4%)
DS	Bottoms	28317	26720	1597 (5.6%)
DM	Bottoms	71382	73036	1654 (2.3%)
DE	Bottoms	49339	49396	57 (0.1%)
DP	Bottoms	25113	25170	57 (0.2%)
DB	Bottoms	11175	11232	57 (0.5%)
SD	Bottoms	24247	24241	6 (0.0%)
EF	Overheads	39830	39780	50 (0.1%)
	Bottoms	8227	8269	42 (0.5%)
PF	Overheads	15312	15308	4 (0.0%)
	Bottoms	1083	1084	1 (0.1%)

Table 3.4: Comparison of Predicted Temperatures with the Typical Design Data

Distillation Unit	**Output Stream**	**Design Value (°C)**	**Predicted Value (°C)**	**Absolute error**
DS	Overheads	36.7	29.9	6.8
	Bottoms	101.3	102.2	0.9
DM	Overheads	-96.3	-97.9	1.6
	Bottoms	6.9	6.0	0.9
DE	Overheads	-16.1	-15.9	0.2
	Bottoms	87.6	88.5	0.9
DP	Overheads	-1.1	-0.4	0.7
	Bottoms	67	71.0	4
DB	Overheads	37.8	39.3	1.5
	Bottoms	95	106.4	11.5
SD	Overheads	37.8	37.8	0.0
	Bottoms	51.9	52.2	0.3
EF	Overheads	-28.9	-29.0	0.1
	Bottoms	-5.7	-5.8	0.1
PF	Overheads	43.4	43.8	0.4
	Bottoms	55.6	53.9	1.7

3.4 Formulation of Multi-objective Optimization Problems

In large-scale processes like the cold-end separation under consideration, there are many factors which play a crucial role in the selection of objective functions. It is therefore important to study different objectives separately as well as together in right combinations to draw meaningful conclusions. Often, optimization is carried out to minimize the most common objective, namely, profit. Since profit is the difference of revenue and cost, reducing cost and/or increasing revenue drive the profit upwards. In the present case study, the prime source of revenue is from ethylene and propylene production. Therefore, they are selected as two objectives to be maximized. The counteracting forces for each of them are the net utility cost of distillation columns which increases with production rate. So, it is important to minimize the net utility cost; utility data and prices used in the present study are summarized in Table 3.5.

Here, net utility cost has been used to consider both cost of total utilities consumed and utility credits. There are two sources of credit for cold energy produced in the process: (a) utility used in DM reboiler is chilled water which leaves at about 5°C, and (b) utility used in EF reboiler is propylene leaving at about -2°C. These give rise to another objective function in the form of maximizing utility credit obtained from the plant.

For meaningful MOO, we need to couple the chosen objectives in a way that they are conflicting in nature. Hence, the following sets of binary objectives are considered for MOO.

- Case 1: Maximization of ethylene production and minimization of net utility cost
- Case 2: Maximization of propylene production and minimization of net utility cost
- Case 3: Maximization of utility credit and minimization of total utility cost

The equations for the objective functions chosen for MOO are:

Minimize Total Utility Cost, UC = Σ (Reboiler Utility Cost for DE, DP, DB, SD and PF) + Σ (Condenser Utility Cost for DM, DE, DP, DB, SD, EF and PF) + Σ (Cost of Utilities for all Coolers and Heaters)

Minimize Net Utility Cost, Net UC = Σ (Reboiler Utility Cost for DE, DP, DB, SD, PF) + Σ Condenser Utilities Cost (DM, DE, DP, DB, SD, EF, PF) + Σ (Cost of Utilities for all Coolers and Heaters) – (DM Reboiler Utility Credit + EF Reboiler Utility Credit)

Maximize Ethylene Production, EP = Ethylene Production (kg/h)

Maximize Propylene Production, PP = Propylene Production (kg/h)

Maximize Utility Credit, EC = DM Reboiler Utility Credit + EF Reboiler Utility Credit

Decision Variables: The important variables which can affect the performance of distillation columns were considered as decision variables. In

an actual plant, the manipulated variables in a distillation column are often reflux ratio and reboiler duty. Since the reboiler duty is affected by the reflux ratio/rate and overhead flow rate (i.e., vapour rate, distillate rate or vent rate), the reflux ratio/rate and overhead flow rate have been assumed as decision variables for the current study. These variables are listed in Table 3.6 along with their bounds for optimization. Bounds on reflux ratios/rates have been chosen to avoid any flooding or dry trays in the columns. Bounds on overhead flow rate of each column have been set to ensure convergence of the simulation.

Table 3.5: Utility Data and Prices used in the study

S. No.	**Utility**	**Temperature (**°C)	**Unit Price**	**Reference**
1.	Refrigerant (Ethylene)	-101	21 $/GJ	Values are interpolated using the data from Seider et al.[139]
2.	Refrigerant (Propylene)	-35	10.6 $/GJ	
3.	Refrigerant (Propylene)	-20	8.2 $/GJ	
4.	Refrigerant (Propylene)	-2	5.4 $/GJ	
5.	Chilled Water	5	4.4 $/GJ	
6.	Low Pressure Steam (1.03 barg)	120	29.3 $/t	Turton et al. [140]
7.	Cooling Water	35-40	0.0148 $/$m^3$	

Constraints: In the industrial scenario, it is common to require specifications of some intermediate streams depending on their downstream uses. Hence, these were included in the optimization problem as constraints. Composition of C4's in bottoms and heavies in overheads of DB were specified at 0.04 and 0.003 mole fraction, respectively. In addition, ethane in bottoms of DE was found to be within the range of 50 kg/h to 1070 kg/h for simultaneous convergence of EF and PF. Since these bounds cannot be specified inside the simulation, they are specified as constraints. Product specifications of ethylene

and propylene were given as active specifications of EF and PF for simulation. For optimization purposes, the current product specifications followed by the industry were used as given in Table 3.7.

Optimizer: For MOO of the cold-end separation process, the elitist non-dominated sorting algorithm (NSGA-II) implemented in MS Excel using binary coding was employed [141]. The optimizer in MS Excel generates trial solutions, each of which is sent to Aspen Hysys through the Excel-Hysys interface for simulating the cold-end separation process. The Hysys simulation provides results for computing objectives to the optimizer in Microsoft Excel through the Excel-Hysys interface. These steps of generating a trial solution (by the optimizer) and process simulation (in Hysys) are repeated numerous times for the specified maximum number of generations. More details on NSGA-II and its implementation in MS Excel can be found in Sharma et al. [141]. It has been successfully used in conjunction with process simulation in Hysys by Lee and Rangaiah [142], and Al-Mayyahi et al. [143] The optimization run was carried out up to 200 generations to find the Pareto-optimal front accurately. Other algorithm parameters used in the optimizer are: two-point crossover with probability = 0.8, bit-wise mutation with probability = 0.05, tournament selection, random seed = 0.5 and population size = 100.

Table 3.6: Decision Variables for Multi-Objective Optimization of Cold-End Separation

S. No.	**Decision Variable**	**Lower Bound**	**Upper Bound**
1.	DM Reflux Ratio	3	6
2.	DM Overhead Vapour Rate (kg/hr)	13360	13520
3.	DE Vent Rate (kg/hr)	50100	50360
4.	DE Reflux Rate (kg/hr)	38000	50000
5.	DP Distillate Rate (kg/hr)	20000	24226
6.	DP Reflux Ratio	1.27	1.57
7.	DB Distillate Rate (kg/hr)	12000	14000
8.	DB Reflux Ratio	0.87	1.27
9.	SD Vent Rate (kg/hr)	1000	3000
10.	SD Reflux Rate (kg/hr)	29000	39000

Note: DM Reflux Ratio and Overhead Vapour Rate are used in Cases 1 and 3 respectively

Table 3.7: Specifications of Main Products

Product	**Specification**
Ethylene	99.9 mol%
Ethane	99.5 mol%
Propylene	99.0 mol%
Propane	95.0 mol%

3.5 Results and Discussion

Three cases of bi-objective optimization were carried out, and the obtained results are presented and discussed in this section. For each case, two optimization runs were carried out: one with all decision variables and second with only a few significant variables based on the results of the first run; the second run is to improve/confirm the optimization results.

3.5.1 Case 1: Maximization of Ethylene Production and Minimization of Net Utility Cost

Ethylene production was considered to avoid the need for the selling price of ethylene, which is subject to market fluctuations throughout the year. Changes in ethylene production depend on ethylene loss in DM which is affected by its reflux ratio. So, only for this case, DM reflux ratio was considered as a decision variable along with others, which include vent rate and reflux rate for both DE and SD, and distillate rate and reflux ratio for DP and DB. Net utility cost was considered on annual basis assuming an operating time of 8760 h.

Figure 3.2a shows the Pareto-optimal front obtained by NSGA-II after 200 generations for maximizing ethylene production and minimizing net utility cost. The generated front shows a clear trend with reasonably well-distributed optimal solutions. As we move from one point to another towards the right of the front, ethylene production increases with increase in net utility cost. Thus, the solutions obtained after 200 generations comprise a Pareto-optimal front. Figure 3.2a also presents solutions at 50, 100 and 150 generations; these show that, after 100 generations, the Pareto front is nearly same with slight changes in the later part of the front. Hence, 200 generations are more than sufficient to find the Pareto-optimal front in this case. The net utility cost varied from \$23 to \$23.4 Million/yr which means that an annual saving of 1.3% is possible on utility costs but at the expense of decreased ethylene production 39820 to 39885 kg/h (Figure 3.2a). Since ethylene production increase is steep initially, a good trade-off solution is 39870 kg/h of ethylene production with net utility cost of \$23.1 Million/year. DM reflux ratio corresponding to this optimal solution is 4.6. All other decision variables are at their lower/upper bounds as shown in Figures 3.2 c-j.

The optimal values of four decision variables: DE vent rate, DP distillate rate and SD vent rate are near their respective upper bound (namely, 50360 kg/hr, 24226 kg/hr and 3000 kg/hr) with DB distillate rate near its upper bound at 13887 kg/hr. The feed to DE, DP, DB and SD is in liquid phase. Higher overhead flow rates in DE, DP, DB and SD correspond to higher reboiler and condenser duties. At the same time, they result in higher product flow rates. All the flow rates take upper bound values (and values close to upper bound for DB) since the objective of increasing ethylene production dominates the objective of decreasing utility cost. The optimal values of four other decision variables: DE reflux rate, DP reflux ratio, DB reflux ratio and SD reflux rate are near their respective lower bound (namely, 38000 kg/hr, 1.27, 0.87 and 29000 kg/hr) (Figure 3.2 g-j). This is due to the fact that when the reflux rates/ratios are low, condenser and reboiler duties are lower for fixed product purity specifications, which minimizes the objective of net utility cost.

The decision variable, affecting the two objectives in opposite directions, is DM reflux ratio. Figure 3.2b shows that DM reflux ratio has significant effect on ethylene production, in the beginning of the Pareto-optimal front; this corresponds to change in ethylene loss in DM condenser. This signifies the correlation between DM reflux ratio and EF distillate rate (recall that DE and the acetylene recovery section are between DM and EF). As the DM reflux ratio increases from 3 to 6, ethylene production increases by 65 kg/h. With this, duties of EF condenser and reboiler decrease slightly but DM condenser and reboiler duties increase significantly. This leads to an increase in net utility cost. An outlier appears at right end of the Pareto-optimal front (Figure 3.2a). It can be attributed to DM reflux ratio reaching its upper bound and increase in SD reflux rate (Figures 3.2b and 3.2j), which increases the net utility cost but has negligible effect on ethylene production.

To confirm the Pareto-optimal solutions, another optimization run was performed with only DM reflux ratio as the decision variable while all other decision variables were set at their optimum values found in the previous run (Figure 3.2). The obtained Pareto-optimal front is continuous and similar to that obtained in the previous run except for marginal differences at high net

utility cost (Figure 3.3). The outlier is no longer present, probably because SD reflux rate is no longer a decision variable. The results at different number of generations in Figure 3.3a show that the Pareto-optimal front is unchanged after 50 generations. This faster convergence is expected since there is only one decision variable in the second run.

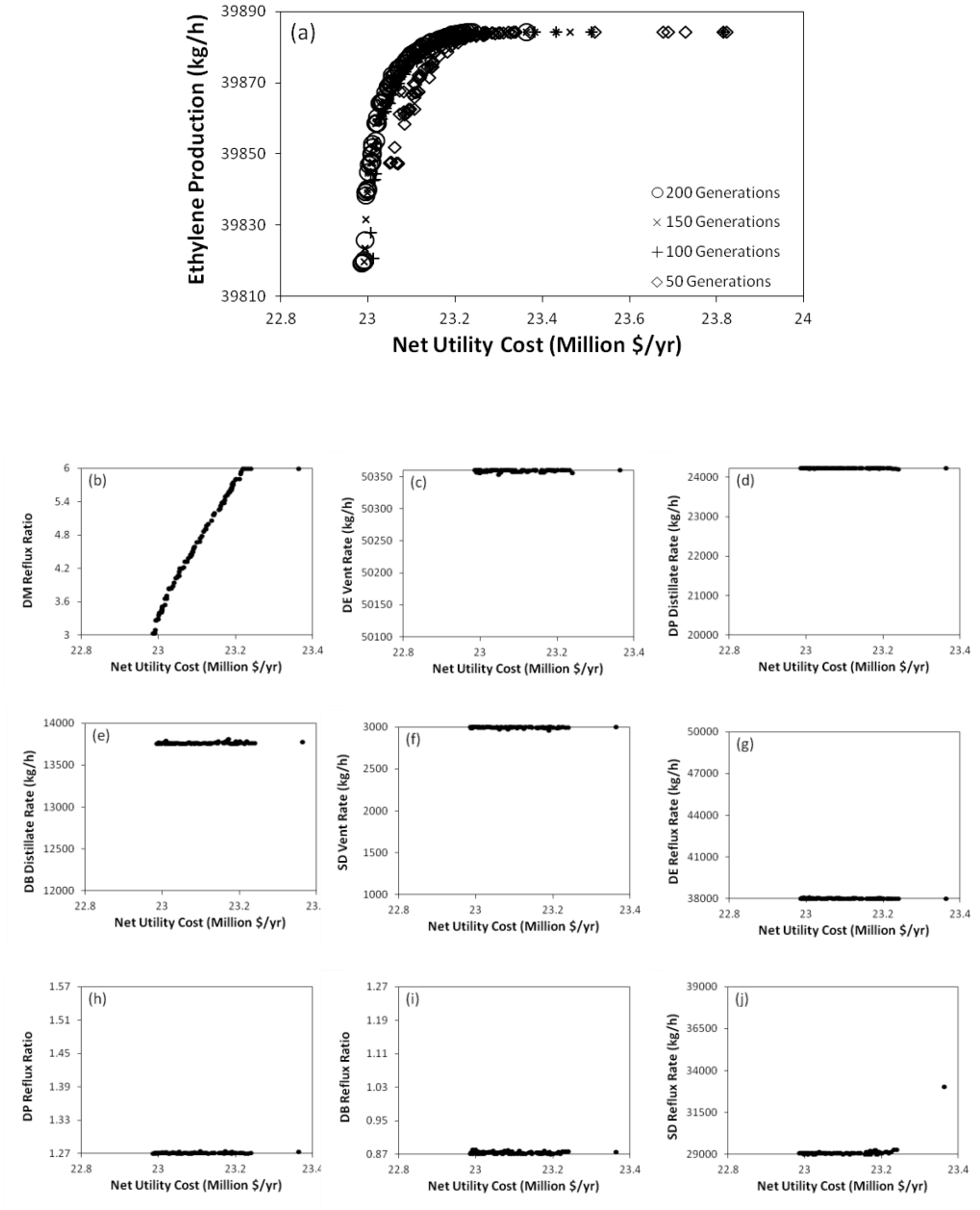

Figure 3.2: Pareto-optimal front for maximization of ethylene production and minimization of net utility cost (plot a); optimal values of decision variables corresponding to the Pareto-optimal front are shown in plots b to j.

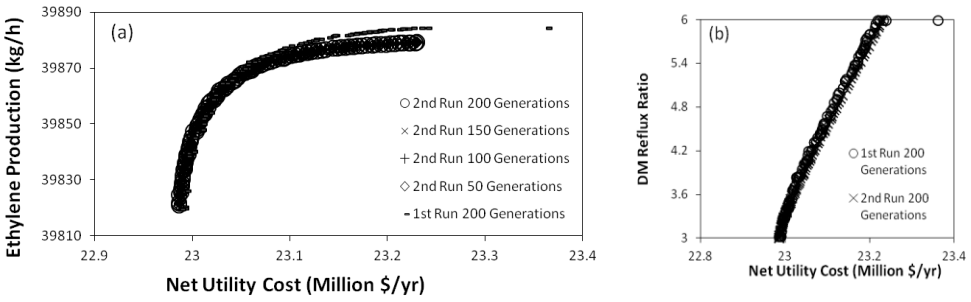

Figure 3.3: Pareto-optimal front for maximization of ethylene production and minimization of net utility cost with only DM reflux ratio as the decision variable and comparison of Pareto fronts obtained in the two runs are shown in plot a; optimal values of DM Reflux Ratio corresponding to the Pareto-optimal front for 1st and 2nd run are in plot b.

3.5.2 Case 2: Maximization of Propylene Production and Minimization of Net Utility Cost

Hourly propylene production was maximized instead of revenue from propylene sales for the same reason as for ethylene production. As before, net utility cost was calculated on annual basis. All decision variables other than those of DM in Table 3.6 affect propylene production as entire propylene input to DM goes into its bottoms. These are Vent Rate and Reflux Rate for both DE and SD, and distillate rate and reflux ratio for DP and DB. The Pareto-optimal sets obtained by NSGA-II at 50, 100, 150 and 200 generations for the maximization of propylene production and minimization of net utility cost (Figure 3.4a), show that, after 100 generations, the Pareto-optimal front is nearly same with slight changes in the later part of the front. Hence, 200 generations are more than sufficient to find the Pareto-optimal front in this case also. The Pareto-optimal set after 200 generations is smooth and nearly continuous in the first half of the range, and later it is nearly constant and somewhat discontinuous. The net utility cost increases by 2.1% from \$24.2 to \$24.7 Million/yr as propylene production increases by 10% from nearly 14000 to 15400 kg /h (Figure 3.4a). The corner point (15380 kg/hr propylene production at utility cost of \$24.7 Million/yr) in the Pareto-optimal front is the most likely choice to increase propylene production significantly with a small increase in the net utility cost. SD vent rate corresponding to this optimal solution is 3 which is its specified lower bound, and all other decision variables are at their lower/upper bound (Figure 3.4). When SD Vent rate is

the lowest possible, propylene loss from SD is the least but the reboiler utility cost is high. Since propylene loss costs more than the reboiler utility, maximizing propylene production is preferred with some trade-off in SD reboiler utility cost.

The optimal values of decision variables corresponding to the Pareto-optimal front are shown in Figure 3.4b–i. Optimum values of DE vent rate and DP distillate rate are at their respective upper bounds with DB distillate rate slightly away from its upper bound; these are same as in the previous case. SD vent rate is the main decision variable affecting both the objectives in the present case (Figure 3.4a). The Pareto-optimal front shows a linear increase which is caused by a linear decrease in SD vent rate. Initially, the higher vent rate corresponds to more propylene loss, resulting in less propylene production while incurring lower net utilities cost. As the vent rate decreases, more propylene is redirected to PF, increasing propylene production. However, reboiler utility cost of SD increases pushing up the net utilities cost.

The other four decision variables, DE reflux rate, DP reflux ratio, DB reflux ratio and SD reflux rate stay at their lower bounds until SD vent rate reaches its lower bound (Figures 3.4f–i). When SD vent rate is at its lowest bound, reflux ratios/rates of DP, DB, DE and SD start to increase; causing propylene production to increase marginally. However, during this course, net utility cost increases substantially due to direct correlation of these decision variables with the condenser and reboiler energy requirements.

To confirm this, second optimization run was carried out where SD vent rate was fixed at its lower bound and decision variables were reflux rates of DE and SD as well reflux ratios of DP and DB. Range of the Pareto-optimal front (Figure 3.5a) is limited since SD vent rate was fixed at its lower bound. Effect of decision variables in the second run (Figures 3.5b–e) is similar to that in Figure 3.4. Increasing trend of DE reflux rate and DP reflux ratio is evident; these two decision variables largely affect the net utility cost by nearly 1 Million $/yr in the Pareto-front. However, increase in propylene production is insignificant (Figure 3.5a) since propylene production is not much dependant on reflux rates/ratios of DE, SD, DP and DB. Further, DB reflux ratio and SD

reflux rate are mostly scattered near their respective lower bound (Figure 3.5d and 3.5e).

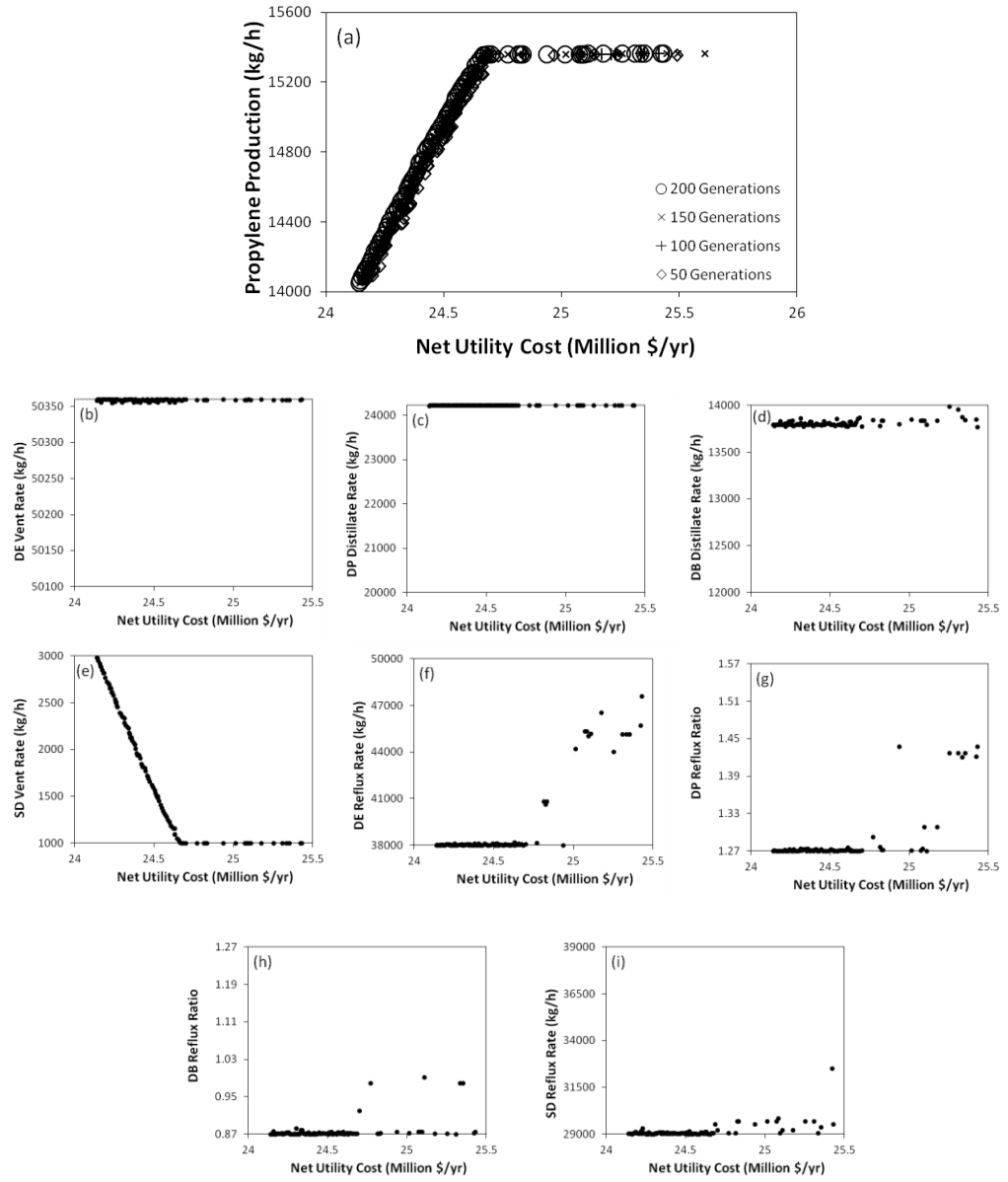

Figure 3.4: Optimal Pareto front for maximization of propylene production and minimization of net utility cost, at an interval of 50 generations (plot a); optimal values of decision variables corresponding to the Pareto-optimal front are shown in plots b to i.

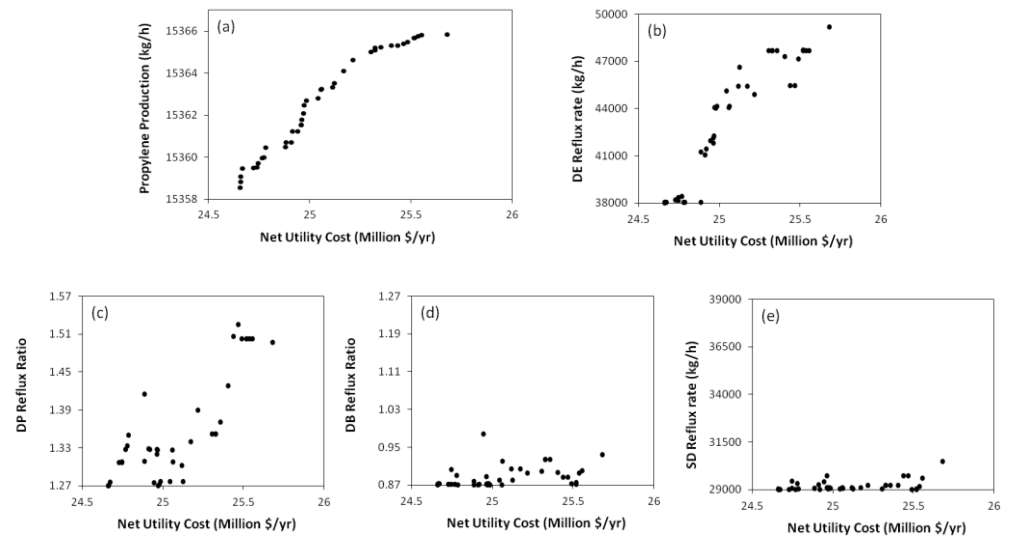

Figure 3.5: Optimal Pareto front for maximization of propylene production and minimization of net utility cost with reflux rates/ratios of DE, SD, DP and DB as decision variables (plot a); optimal values of decision variables corresponding to the Pareto-optimal front are shown in plots b to e.

3.5.3 Case 3: Maximization of Utility Credit and Minimization of Total Utility Cost

Figure 6a shows the Pareto-optimal set obtained by NSGA-II after 200 generations for maximizing utility credit and minimizing total utility cost. It also presents solutions at 50, 100 and 150 generations; these show that, after 100 generations, the Pareto-optimal front is nearly same with slight changes in the later part of the front. Hence, 200 generations are more than sufficient to find the Pareto-optimal front in this case, which shows a neat trend with three linear segments. As we move from one point to the other towards the right, utility credit increases with increase in total utility cost. Thus, the solutions obtained after 200 generations comprise a Pareto-optimal front. The total utility cost increases by 2.1% from \$15 million/yr to \$15.32 million/yr as the utility credit increases by 4.5% from \$2.69 million/yr to \$2.81 million/yr. The most likely choice for the optimal conditions would be to operate at the starting point of the curve as the increase in utility credit is lesser than the corresponding increase in utility cost.

The optimal values of four decision variables: DE vent rate, DP distillate rate, DB distillate rate and SD vent rate are near their respective upper bounds (Figures 3.6c to 3.6f) whereas those of four other decision variables: DE reflux

rate, DP reflux ratio, DB reflux ratio and SD reflux rate are near their respective lower bounds (Figure 3.6g to 3.6j). All these can be correlated to one of the objectives, i.e., minimizing total utility cost. Since utility credit comes from the DM reboiler and EF reboiler only, decision variables related to other columns comply with lowest utility cost conditions. In this case, the decision variable leading to the Pareto-optimal front is DM Vent Rate (Figure 3.6b), which affects DM reboiler duty as well as the condenser and reboiler duties of other columns.

The Pareto-optimal front shows a linear increase due to a nearly linear decrease in DM Vent Rate (Figures 3.6a and 3.6b). In the beginning of the Pareto-optimal front, the points correspond to high vent rate, requiring lower condenser and reboiler duty from EF while generating higher reboiler utility credit from DM. As the DM Vent Rate decreases, the condenser and reboiler utility costs of DE, SD, PF, and EF increase while the DM reboiler duty decreases. Since the utility credit is a sum of DM and EF reboiler utility credit, the slight decrease in DM reboiler utility credit is countered by major increase in EF reboiler utility credit. Hence, overall utility credit increases with decrease in DM vent rate.

The outliers generated in 50^{th}, 100^{th} and 150^{th} generations are probably due to sudden increase in DP reflux ratio. To confirm this, one more optimization run was carried out to see the individual effect of the main decision variable i.e. DM vent rate along with DP reflux ratio on the Pareto-optimal front. The Pareto-optimal front (Figure 3.7) is similar to that in the 1^{st} optimization run; however, there is an outlier found at the 200^{th} generation. Once DM vent rate reaches its lower bound, DP reflux ratio increases causing increase in the total utility cost. However, since DP reflux ratio does not affect the reboiler duties of DM and EF, there are no significant effects on the utility credit. Nevertheless, changing the DM vent rate only, while fixing overhead flow rates to their respective upper bounds and reflux ratios/ rates to their respective lower bounds, in other columns is sufficient for obtaining the Pareto-optimal front in this case.

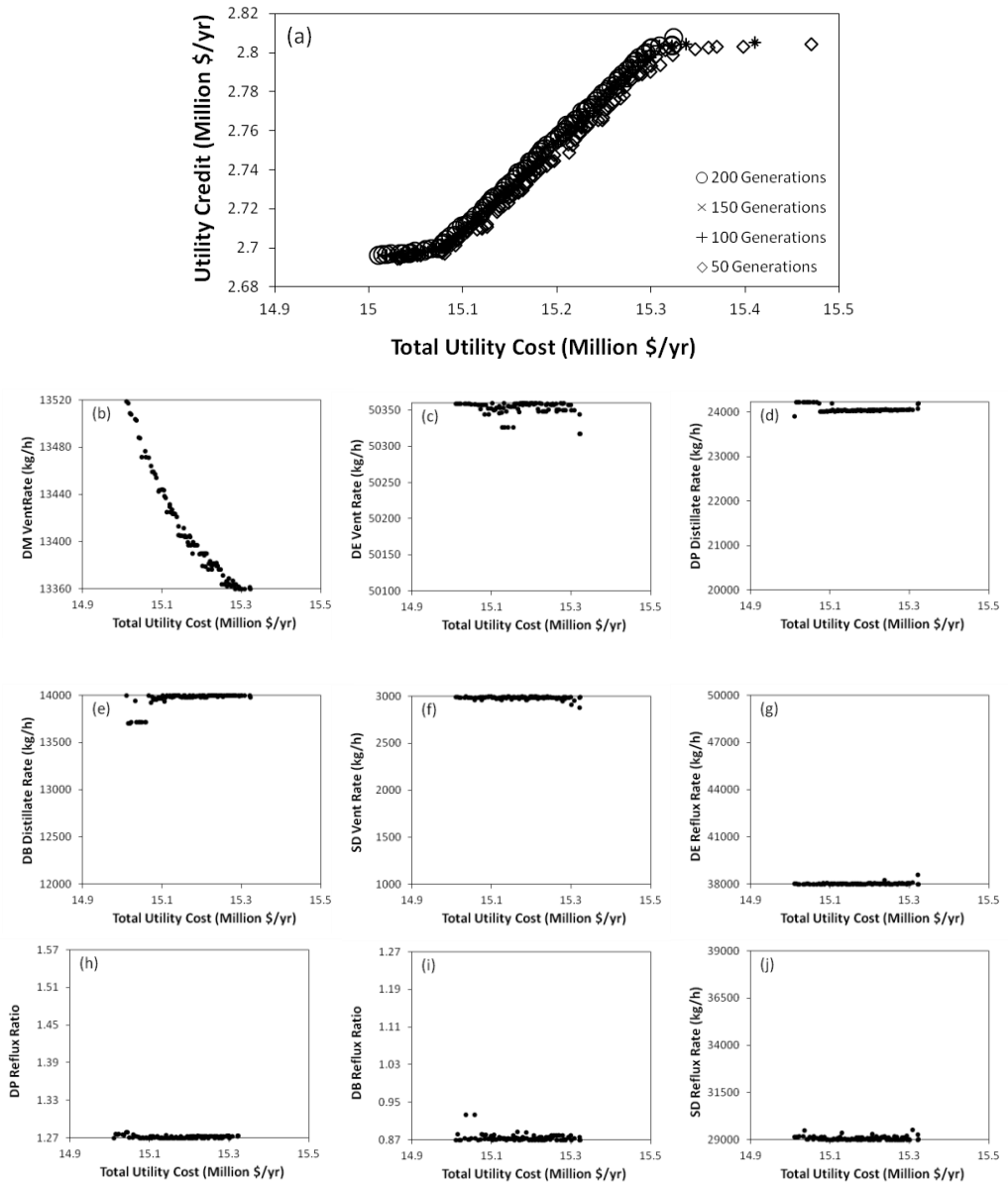

Figure 3.6: Optimal Pareto front for maximization of utility credit and minimization of total utility cost, at an interval of 50 generations (plot a); optimal values of decision variables corresponding to the Pareto-optimal front are shown in plots b to j.

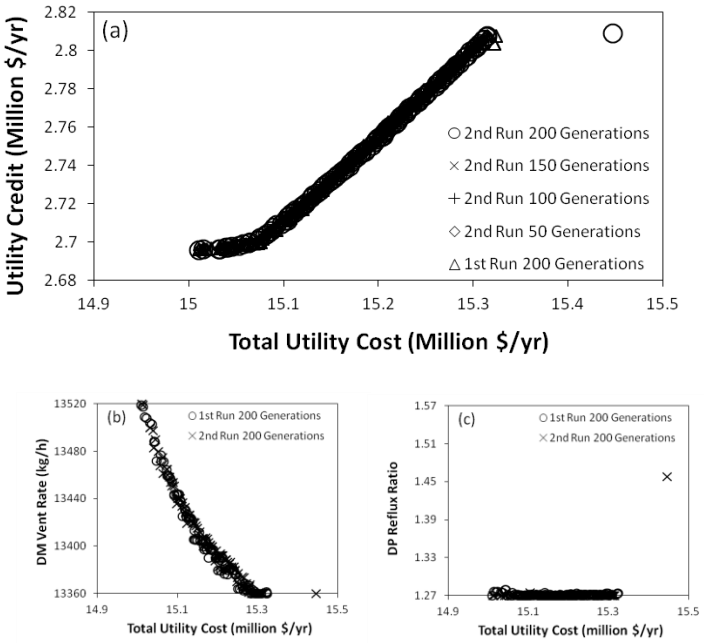

Figure 3.7: Optimal Pareto front for maximization of utility credit and minimization of total utility cost, at an interval of 50 generations, with only DM vent rate and DP reflux ratio as decision variables (plot a); optimal values of decision variables corresponding to the Pareto-optimal front from 1st and 2nd run are shown in plots b to c.

3.6 Conclusions

The conventional cold-end separation in an industrial ethylene plant was simulated using Aspen Hysys. The elitist non-dominated sorting genetic algorithm, NSGA-II implemented in Excel and Excel- Hysys interface were then employed for MOO. For validating the Hysys model, the cold-end separation process was successfully simulated based on typical design data of cold-end separation of a conventional ethylene plant. Operation optimization of this process was then studied for 3 cases of two simultaneous objectives. The Pareto-optimal set for maximizing ethylene production and minimizing net utility cost in the first case, was incremental over the range: 39820–39885 kg/h and 23.0–23.4 Million $/yr respectively. Hence, annual ethylene production could be increased by 0.57 Million kg which corresponds to 0.73 Million $/yr increase in revenue at the cost of 0.4 Million $/yr in utility consumption. The Pareto-optimal front in the second case for maximizing propylene production while minimizing net utility costs, increased linearly over the range: 14000-15400 kg/h of propylene production and utility cost of

24.2-24.7 Million $/yr. For the third case to study the conflicting nature of total utility cost of the process with the utility credit from DM and EF reboilers, the best operating point from the Pareto-optimal front is the one with the lowest utility cost. In all cases, variation of optimal values of decision variables with the objectives can be explained qualitatively, which supports MOO results obtained by NSGA-II. The simulation and optimization methodology of this study can be applied to other schemes of the cold-end separation process of an ethylene plant.

Chapter 4

RETROFITTING SELECT DISTILLATION COLUMNS IN COLD-END SEPARATION WITH A MEMBRANE UNIT

4.1 Introduction

In recent years, a lot of research was carried out on membranes for ethane/ethylene and propane/propylene separations. Various kinds of membranes were tested to identify their permeability and selectivity for olefins and paraffins. The prime reason to analyze a hybrid-membrane distillation (HMD) is reduction of energy consumption by a conventional distillation column. Many papers have shown that significant savings can be achieved by retrofitting a conventional column with a membrane module. Such arrangements are able to provide equivalent or better purities for lower utility costs. However, these systems have not been exploited much on industrial scale due to lack of general design methodologies and membrane's inability to withstand harsh processing conditions.

Olefin/paraffin separation, often categorized as one of the difficult separations in petrochemical industry due to the small differences in boiling points between them, has lately been under the purview of research. This is after significant membrane technologies have been developed in the areas of dehydration of organic solvents and aromatic/paraffin separation. Membranes may not be able to replace distillation columns but the two can be coupled in the form a hybrid system for an enhanced separation.

Gottschlich and Roberts [112] carried out a study to identify general principles behind the choice of hybrid separation systems over conventional columns; they concluded that high product purities resulted in lower efficiencies and higher processing costs for all systems, with the thermodynamic extent of separation being a key parameter for a hybrid system. Davis et al. [113] developed a hybrid facilitated transport membrane-distillation system to carry out pilot plant experiments on propylene/propane and ethylene purge gas recovery. The splitter capacity could be increased by 80% with no increase in

utilities, which resulted in energy savings of 500 billion BTU per year for a 10,000 bbl/day grassroots facility producing polymer grade propylene. In Pettersen and Lien [116], a parallel configuration for propylene/propane separation was investigated, and it was found that the optimum membrane stream composition to be near the column feed stream composition, where distillation is the least efficient. Pressly and Ng [117] investigated the effect of possible HMD configurations through screening calculations, and concluded that series or parallel configurations are preferred over top or bottom configurations for propylene/propane separations.

Caballero et al. [122] proposed a mathematical programming approach to optimize and retrofit HMD system for ethylene/ethane separation with parallel configuration; their study showed potential energy saving of up to 30%. Bernardo and Drioli [123] focused on the application of membrane gas separation technology in oil-refining and petrochemical sector, and concluded that membranes must be able to perform adequately under conditions of exposure to organic vapours, especially C_3+ hydrocarbons, which are common in refineries, petrochemical plants and gas fields. Benali and Aydin [125] carried out optimization and economic analysis of various HMD configurations to scrutinize their feasibility in applications to C_2 and C_3 splitters. Motelica et al. [127] presented techno-economic evaluation for determining the increased energy efficiency and debottlenecking of ethylene/ethane separation, in relation to the required membrane performances. It was found that high membrane selectivity (> 60) and/or ethylene permeance of at least 1×10^{-4} mol/(m^2-s-kPa) are required for considerable savings. Ploegmakers et al. [128] studied retrofitting an existing distillation column with a membrane unit for ethylene/ethane separation. Membrane parameters like feed pressure, permeate pressure and membrane surface area were optimized to understand the effect of ethylene permeance and ethylene/ethane selectivity on the energy requirements of the HMD configurations.

The prime reason for analyzing retrofitting distillation columns to HMD systems is the reduction of energy consumption for separation, thus improving the economic and environmental sustainability of existing plants. A techno-

economic evaluation can reveal viability of the HMD system for retrofitting different columns in an ethylene separation process. The study of Ploegmakers et al. [128] established the limits of ethylene permeance and ethylene/ethane selectivity for economical retrofitting of an ethylene/ethane splitter with a membrane unit. However, these limits are far removed from the observed parameter values of membranes used for olefin/paraffin separation as reported by Faiz and Li. [76] It is, henceforth, important to carry out optimization considering bounds on membrane selectivity and permeance, which are reported or expected from near-future developments in membrane technologies. Moreoever, Ploegmakers et al. [128] considered the reboiler duty of ethylene fractionator as a cost; however, this duty should be considered as a credit since chilled water can be produced during the vaporization of the bottom stream (at -8°C) in the reboiler.

Multi-objective optimization (MOO) of a process gives a set of optimal solutions for process design and operation, in the form of a Pareto-optimal front. It not only shows the trade-off between the chosen objectives, but also identifies the effect of decision variables considered on the objective functions. As reflected from the reviews by Masuduzzaman et al. [130], and Sharma et al. [131], MOO has not been applied for retrofitting columns into HMD systems in petrochemical plants. Hence in this study, retrofitting four selected columns for the olefin/paraffin separation of an ethylene plant, with a membrane unit is optimized for maximizing annual utility cost savings and minimizing the capital cost simultaneously.

The rest of this chapter is organized as follows. Section 4.2 describes the procedure of simulating a HMD system. Section 4.3 covers formulation of MOO problems, which includes selection of objectives, decision variables and constraints in the optimization problems studied. In Section 4.4, results from the optimization of two objectives for various cases are presented and discussed. Finally, conclusions of this study are given in Section 4.5.

4.2 Retrofitting Conventional Distillation with a Membrane Unit

4.2.1 HMD Modeling and Simulation

For each HMD system, the stream and column specifications are from a typical design data of a conventional ethylene plant as given later in Table 4.2. All simulations of processes similar to Figure 2 were carried out in Aspen HYSYS v7.2. The feed streams for DE, DP and PF are in liquid form which can be processed by a membrane through pervaporation. However, there is not enough literature on pervaporation experiments using carbon-molecular sieve membranes, and so series configuration is not feasible. Hence, only gas separation membranes are considered in the following case studies, with parallel arrangement where side draw of vapor stream is taken from a suitable stage in the column. The stage for side draw is kept near the feed stage for DP, EF and PF. The feed stages for their respective permeate and retentate streams are selected based on preliminary analysis.

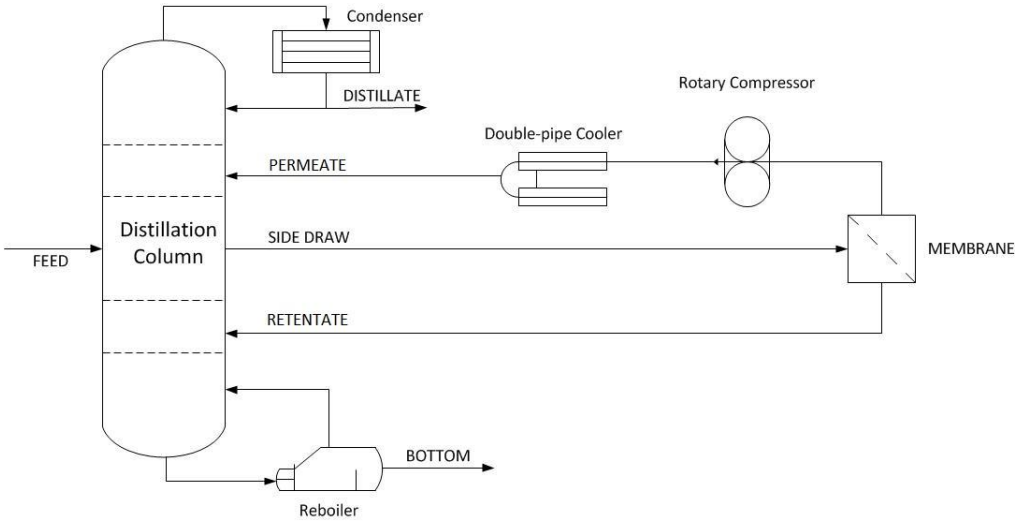

Figure 4.1: Process Flow Diagram of a HMD System: Parallel Arrangement

The Membrane Unit v3.0a extension obtained from the Aspen Tech website, is used for simulating a membrane module in Aspen HYSYS. It uses the following equation for solving fluxes for each component in the membrane feed:

$$Q_x = Per_x \times A \times N \times \frac{(Px_1 - Px_2)}{\ln\left(\frac{Px_1}{Px_2}\right)} \quad (4.1)$$

where molar flow rate of component x in the permeate, Perx = permeability (flux) of component x, Am = membrane area per unit, N = total number of units, Px1 = partial pressure of component x in feed, and Px2 = partial pressure of component x in retentate. To solve for the output partial pressure, an iterative method is used such that mass is conserved over the unit. Membrane Unit v3.0a extension is also capable of doing an energy balance on request. This requires the user to specify the retentate and permeate side pressures. Permeate stream is simulated as leaving at its dew point (i.e., vapour fraction is 1). So, it is sent to a compressor to recompress the stream to column pressure (Figure 4.1). The recompression raises the stream temperature, which requires cooling.

4.2.2 Techno-Economic Feasibility of Retrofit Operation

A preliminary techno-economic evaluation is helpful in understanding the viability of a HMD system. Capital and operating costs of the base case (i.e., distillation only) and the corresponding HMD case are evaluated using the equations given in Appendix C. Table 4.1 1 shows annual net savings calculated for each of the columns under consideration. This evaluation gives some idea on the feasibility of retrofitting to a HMD system for each case. Values of decision variables used for results in Table 4.1 are average of the respective lower and upper bounds for individual cases. In the case of EF, reboiler duty is considered as utility credit because the bottoms stream temperature entering the reboiler is -6°C which can cool the propylene utility, and so it shall be deducted from the total utility cost of the corresponding base and retrofitted cases. From the preliminary techno-economic evaluation, it can be concluded DE and EF may not be suitable for retrofitting to HMD systems. On the other hand, net savings for DP and PF in Table 4.1 are promising for retrofitting them with a membrane unit. To validate these findings, MOO for maximizing utility cost savings and minimizing capital cost is carried out for each of the four columns. It will help in quantifying the benefits of retrofitting each column, with deeper insight on tradeoff between objectives and on effect of decision variables considered on the column performance.

Table 4.1: Preliminary techno-economic evaluation of HMD systems for four columns

Column	**Case**	**Condenser Duty (GJ/h)**	**Reboiler Duty (GJ/h)**	**Capital Cost (US$/yr)**	**Operating Cost (MM US$/yr)**	**Net Savings**	
						(MM US$/yr)	**%**
Deethanizer (DE)	Base	11.27	26.38	-	3.88	-0.16	-4
	HMD	11.95	27.00	18812	4.02		
Depropanizer (DP)	Base	21.22	13.77	-	2.61	0.35	13
	HMD	18.56	10.89	78211	2.18		
Ethylene Fractionator (EF)	Base	54.47	39.73	-	3.178	-0.02	-1
	HMD	54.28	39.48	20368	3.182		
Propylene Fractionator (PF)	Base	53.91	53.48	-	6.35	0.44	7
	HMD	48.06	48.51	95429	5.81		

Table 4.2: Feed and product specifications for various columns

No.	Components in Feed	Feed Composition	Feed Conditions	Product Purity or Other Specs	Other Conditions
1	**Deethanizer**				
	DM Bottom Feed				
	Methane	0.0025	2246 kgmol/h	Ethylene in	Overhead Column Pressure:
	Acetylene	0.0110	3200 kPa	overheads = 0.8259	2583 kPa
	Ethylene	0.6346	6°C	mol frac	Pressure Drop/Tray: 0.1 psi
	Ethane	0.1145	N_F = 37		No. of Ideal Trays: 51
	M-Acetylene	0.0029		Ethane in bottoms =	Full Reflux Condenser
	Propadiene	0.0031		155 kg/hr	Peng-Robinson Model
	Propene	0.1677			
	Propane	0.0075			
	12-Butadiene	0.0017			
	13-Butadiene	0.0200			
	i-Butane	0.0077			
	n-Butane	0.0077			
	i-Butene	0.0073			
	cis2-Butene	0.0015			
	tr2-Butene	0.0016			
	n-Pentane	0.0061			
	n-Hexane	0.0025			
	DS Bottom Feed		502 kgmol/h		

	Acetylene	0.0028	3556 kPa		
	Ethylene	0.0877	102.2°C		
	Ethane	0.0499	N_F = 19		
	M-Acetylene	0.0084			
	Propadiene	0.0076			
	Propene	0.2989			
	Propane	0.0156			
	12-Butadiene	0.0157			
	13-Butadiene	0.1201			
	i-Butane	0.0392			
	n-Butane	0.0466			
	i-Butene	0.0410			
	cis2-Butene	0.0116			
	tr2-Butene	0.0113			
	n-Pentane	0.1165			
	n-Hexane	0.1271			
2	**Depropanizer**				
	Ethane	0.0053	969 kgmol/h	Propylene in	Overhead Column Pressure:
	M-Acetylene	0.0111	2649 kPa	overheads: 0.9116	576 kPa
	Propadiene	0.0111	89°C	mol frac	Pressure Drop/Tray: 0.1 psi
	Propene	0.5426	N_F = 30		No. of Ideal Trays: 42
	Propane	0.0255		Methyl-acetylene in	Total Condenser
	12-Butadiene	0.0121		bottoms: 0.0013	Peng-Robinson Model

	13-Butadiene i-Butane n-Butane i-Butene cis2-Butene tr2-Butene n-Pentane n-Hexane	0.1086 0.0382 0.0421 0.0382 0.0095 0.0095 0.0744 0.0716		mol frac	
3	**Ethylene Fractionator** Methane Ethylene Ethane Propene	 0.0003 0.8388 0.1604 0.0005	 1693 kgmol/h 2056 kPa -24.4°C N_F = 40	 Ethylene in overheads: 0.999 mol frac Ethane in bottoms: 0.995 mol frac	 Overhead Column Pressure: 1997 kPa Pressure Drop/Tray: 0.1 psi No. of Ideal Trays: 125 Total Condenser Peng-Robinson Model
4	**Propylene Fractionator** Propene Propane i-Butane	 0.9390 0.0600 0.0010	 388 kgmol/h 2141 kPa 52.2°C N_F = 99	Propylene in overheads: 0.99 mol frac Propane in bottoms: 0.95 mol frac	Overhead Column Pressure: 1792 kPa Pressure Drop/Tray: 0.1 psi No. of Ideal Trays: 200 Total Condenser Peng-Robinson Model

4.2.3 Assumptions for Membrane Simulation

In order to simulate a HMD system, certain assumptions need to be made.

1. Membrane performance does not deteriorate within its life expectancy of 5 years.
2. Membrane is able to handle the high pressure conditions and large feed flowrates without any signs of plasticization
3. Compressor and cooler have a life expectancy of 10 years.
4. The permeance ratio of propylene to ethylene is kept as 5 due to higher permeability shown by C_3 components as compared to C_2 components, as deduced from Faiz and Li [76]. Permeance of i-butene is assumed to be same as that of ethylene since their permeabilities are very similar in the literature. This is probably due to bigger size of C4 molecules despite their higher solubility in polymers as compared to C2's. Permeance of ethyl-acetylene and propadiene are assumed to be same as that of propylene. Cis/trans-2-butene and 13/12-butadiene permeate at the same rate as i-butene.
5. In general, when selectivities are plotted against their corresponding permeances for a given set of olefin/paraffin on a log-log plot, a linear upper bound can be observed with negative slope as mentioned in previous papers [83-84]. This leads to the following correlation between selectivity and permeance:

$$\alpha_{AB} = \frac{\beta_{AB}}{P_A^{\lambda_{AB}}} \tag{4.2}$$

where P_A is the permeance of fast-permeating component A, α_{AB} is the selectivity of A shown by the membrane as compared to slow-permeating component B, β_{AB} (in Barrer) is called the front factor of the upper bound and λ_{AB} is called the slope. The parameter values (Table 4.3) used for each set of olefin and paraffin are based on the literature data for different olefin/paraffin sets compiled by Faiz and Li [76]. Thus, Equation 4.2 was used to relate selectivity with permeability using the parameter values in Table 4.3, for each set of hydrocarbons.

According to Vu et al. [144], polymeric membranes cost around \$20/m^2. Ockwig and Nenoff [145] stated that the carbon-based membrane cost is 1 to 3 orders of magnitude higher, as compared to polymeric membranes. However, because of large scale application and decreasing trend of prices of membranes, as seen in the last many years, lower cost of membranes can be achieved. Lie et al. [146] assumed a value of \$15/m^2 for in-house tailored carbon-molecular sieve membranes with a bare module cost factor of 3.5. In the current study, total module cost of \$100/m^2 is assumed for carbon-molecular sieve membranes, which includes labour and installation costs.

Table 4.3: Values of slope and front-factor of the upper-bound for olefin/paraffin membrane separation

	β_{AB}	λ_{AB}
Ethylene/Ethane	7.2364	-0.212
Propylene/Propane	25.294	-0.244
i-Butylene/Butane	61.977	-0.242

4.3 Formulation of Multi-Objective Optimization

There are two major costs which play an important role in HMD feasibility as an alternative to the distillation alone. One of them is the capital cost of the membrane module along with compressor, cooler and associated installation, piping and labor costs. The other one is the utility cost which includes the condenser and reboiler duties, electricity cost for compressor and utility cost for cooler. Clearly, both the capital and utility costs need to be minimized in order to obtain more savings from the retrofitted HMD system. At the same time, production rates and quality of products from the retrofitted system should remain the same so that they do not affect other columns/units in the plant.

Higher membrane area will lead to more separation for a given feed flowrate and membrane permeate pressure. This may lead to reduction in condenser and reboiler duties of the associated column. Hence, while there is a decrease in utility cost of the column, there is an increase in capital cost of the

membrane. So, there is conflict between the two cost objectives, which can be studied using MOO. The unit prices of utilities used in various equipments are as mentioned in Table 3.4. The compressor used in the HMD system is driven by an internal combustion engine which requires Fuel Oil No. 2 given in Table 4. Note that utility used in EF reboiler is propylene refrigerant leaving at about -2°C, which can be considered as utility credit (with unit price of $5.4/GJ) and will be multiplied by -1 in calculating the objective function of utility cost for EF.

The MOO is carried out for maximizing utility cost savings and minimizing capital cost simultaneously for retrofitting DE (Case 1), DP (Case 2), EF (Case 3) and PF (Case 4), with a membrane unit. The equations for these objective functions are:

Maximize Utility Cost Savings = $OPEX_{hyb} - OPEX_{base}$

where OPEX the sum of utility cost of reboiler, condenser, permeate compressor and cooler. In the base case, permeate compressor and cooler are absent, and so utility cost for them is zero.

Minimize Annualized Capital Cost, CAPEX = (Membrane Unit Purchase Cost / Membrane Life Expectancy) + (Compressor Cost + Cooler Cost) / Equipment Life Expectancy

Decision Variables: The important variables affecting the performance of the HMD system were considered as decision variables. As mentioned before, membrane area is an important factor determining the capital cost as well as the utility cost, and is one of the prime decision variables. The permeances of slow- and fast-permeating components in every case can be varied (as per equation 4.2) to see their effect on HMD performance. The permeate flowrate changes the load on the following compressor, to recompress the permeate stream to the column pressure. More compression results in higher temperature of the stream which requires cooling; for this, cheap utility like cooling water can be used. Therefore, while a better separation is guaranteed, there is tradeoff in employing high flowrate through the membrane in terms of utility cost. The third active specification is side draw rate for all columns,

which is a decision variable. The feed flowrate to the membrane determines the extent of separation affected by the membrane and its impact on the column duties. It also depends upon the amount of feed entering the column, and one has to be careful while choosing its value so that the hydrodynamic conditions of the column are not disturbed. Bounds on the permeances of components are determined by the values available in the membrane literature [76]. The bounds for side draws depend upon the vapour flowrates inside the column. Membrane areas are reasonably bounded for attaining positive net savings. The decision variables with their respective bounds are given in Table 4.4.

Table 4.4: Decision variables for MOO of various distillation columns

Column	**Deethanizer**		**Depropanizer**		**Ethylene Fractionator**		**Propylene Fractionator**	
Bound*	LB	UB	LB	UB	LB	UB	LB	UB
Membrane Feed Flowrate (kg/h)	900	1500	100	600	100	300	50	300
Membrane Area (m^2)	500	3000	500	1500	1000	4000	100	600
Permeance (kgmole/1000h-m^2-kPa)	0.0008	0.002	0.01	0.1	0.001	0.008	0.01	0.1

* LB: Lower Bound, UB: Upper Bound, a: Ethylene Permeance b: Propylene Permeance

Constraints: A rotary compressor has been considered for the permeate stream compression. It requires a minimum operating power requirement of 18 kW which is kept as a constraint in the given problem.

Optimizer: For MOO of the retrofitted hybrid membrane-distillation systems, the elitist non-dominated sorting algorithm (NSGA-II) implemented in MS Excel using binary coding was employed [141]. The optimization run was carried out up to 100 generations to find the Pareto-optimal front accurately. Other algorithm parameters used in the optimizer are: two-point crossover

with probability = 0.8, bit-wise mutation with probability = 0.05, tournament selection, random seed = 0.5 and population size = 100.

4.4 Results and Discussion

4.4.1 Case 1: HMD System for Deethanizer

Deethanizer (DE) is used for separating C2 olefins and paraffins from C3's and heavies. It is fed by the bottom streams from demethanizer and distillate stripper (Figure 3.1). Decision variables with their bounds for optimizing DE retrofit with a membrane unit are given in Table 4.4. The side draw is taken from stage 34, and retentate and permeate streams are fed at stages 35 and 33 respectively, these are based on preliminary testing for optimum stages. Here, the retentate is sent to the tray above the side draw as it is richer in ethylene. This is because the membrane has higher permeance of ethylene. The condenser uses propylene (-20°C) as utility, and the reboiler uses low pressure steam. The permeate pressure is kept at 400 kPa as assumed by Ploegmakers et al. [128]

Non-dominated solutions obtained by EMOO program at 60^{th}, 80^{th} and 100^{th} generations for maximizing the utility cost savings and minimizing the capital cost are shown in Figure 4.2a. There is minor improvement between the Pareto fronts at 80^{th} and 100^{th} generations, and so it can be concluded that 100 generations are sufficient for obtaining the Pareto-optimal front, which comprises of discrete non-dominated solutions. The utility cost savings increase from -0.01 to 0.132 Million $/yr whereas the capital cost increases slightly from 0.062 to 0.072 Million $/yr. Membrane feed flowrate is near its upper bound of 1500 kgmol/h (Figure 4.2b), membrane surface area increases from to 2200 m^2 to 2700 m^2 (Figure 4.2c), and ethylene permeance decreases slightly from its upper bound to 0.194 kgmole/1000h-kPa-m^2 (Figure 4.2d). These changes in decision variables lead to the Pareto-optimal solutions.

From Figure 4.2a, the best utility savings is 0.132 Million $/yr, which requires capital cost of 0.072 Million $/yr for DE retrofitting with a membrane unit. This will generate net savings of 0.06 Million $/yr which is approximately 1.5% of the base utility cost. This is relatively low. Note that the membrane

permeance and selectivity values for ethylene and other components are based on current literature. Hence, for the available membrane technology, retrofitting DE with a membrane unit is not attractive. However, this will change if there are significant increases in membrane performance and/or utility costs in the future.

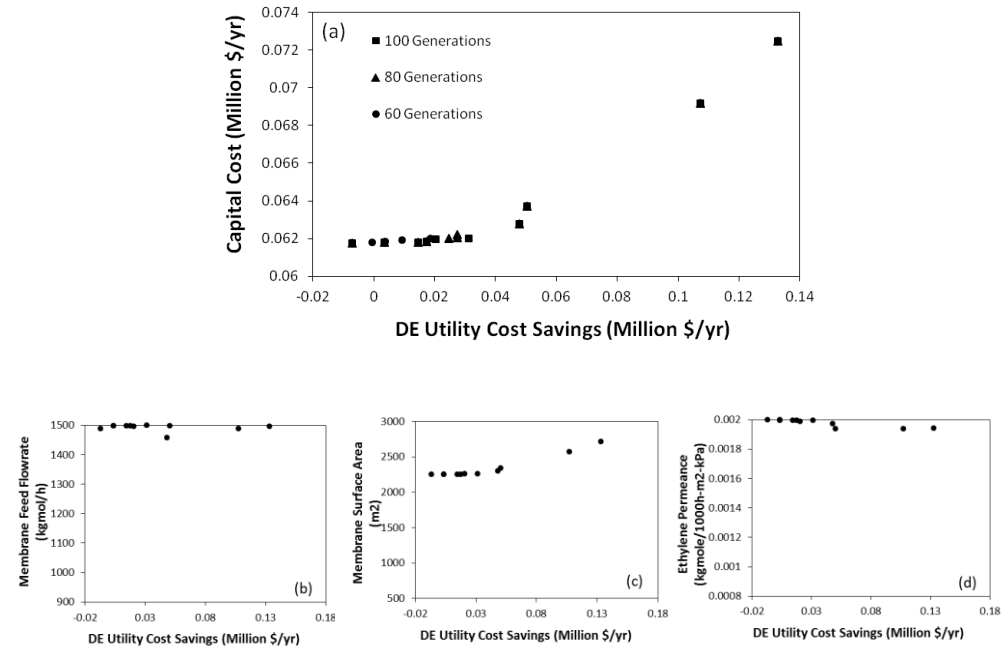

Figure 4.2: Non-dominated solutions for maximization of utility cost savings and minimization of capital cost for retrofitting DE to a HMD system (plot a); corresponding optimal values of decision variables are shown in plots b to d.

4.4.2 Case 2: HMD System for Depropanizer

Depropanizer (DP) is used to separate C3 olefins and paraffins from the C4's and the heavies. Details of decision variables chosen for MOO of HMD for DP retrofitting are given in Table 4.4. The side draw is taken from stage 30 near the feed stage of the column, and retentate and permeate streams are fed at stages 25 and 35 respectively. The condenser uses propylene (-2°C) as utility, and the reboiler uses low pressure steam. The permeate pressure is kept at 100 kPa. This pressure was considered lower than the previous case since it involves multi-component feed with C3's and C4's and better driving force is required for separation across membrane. Figure 4.3a shows the Pareto-optimal set obtained by EMOO after 100 generations for maximizing the utility cost savings and minimizing the capital cost. It also includes non-

dominated solutions at 60th and 80th generations, showing that the Pareto-optimal front is nearly same with negligible changes between 60 and 100 generations. Further, the front is almost continuous with numerous solutions. The utility cost savings increase by 22% from \$0.37 Million/yr to \$0.45 Million/yr as the capital cost increases from \$0.027 Million/yr to \$0.1 Million/yr (Figure 4.3a). The last point on the front (with utility cost savings of \$0.45 Million/yr at \$0.1 Million/yr capital cost) is the best choice for the membrane unit design to retrofit DP. It gives net savings of \$0.35 Million/yr, i.e., 13.4% of the utility cost of the base case.

Optimal values of membrane feed flowrate in Figure 4.3b are scattered, which means it does not affect the membrane operation significantly. In Figure 4.3c, optimal value of membrane area is at its lower bound for the initial part of the graph, and then increases linearly to reach the upper bound of the membrane area. The optimal value of propylene permeance (Figure 4.3d) increases initially, after which it is slightly scattered close to its upper bound. This may be causing the initial increase in the Pareto-optimal front while the membrane area values are at their lower bound. Hence, both membrane area and propylene permeance affect the Pareto-optimal front in this case of retrofitting DP.

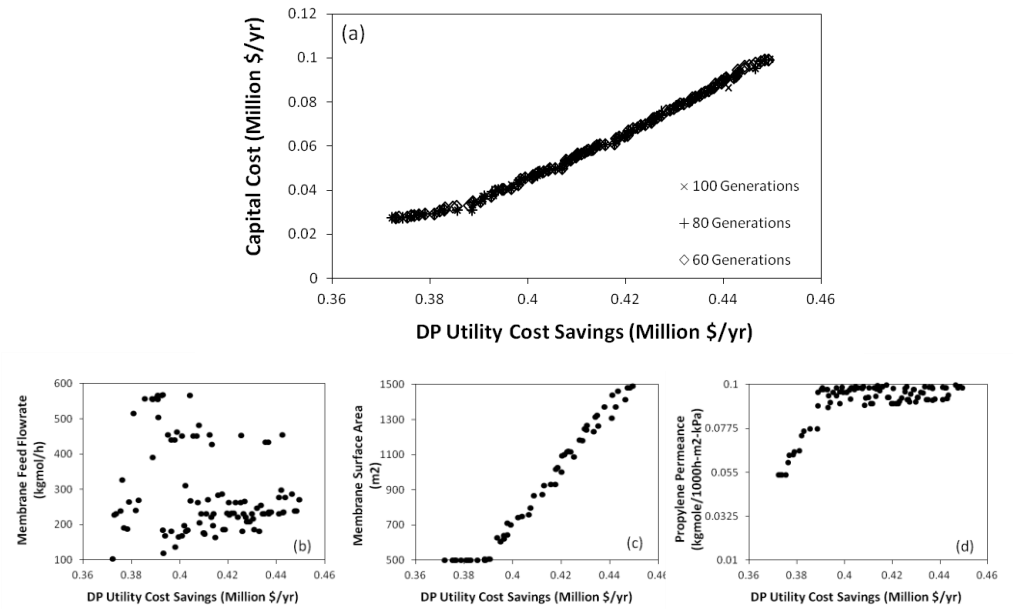

Figure 4.3: Optimal Pareto front for maximization of utility cost savings and minimization of capital cost for retrofitting DP to a HMD system (plot a); optimal values of decision variables corresponding to the Pareto-optimal front are shown in plots b to d.

4.4.3 Case 3: HMD System for Ethylene Fractionator

Ethylene fractionator (EF) produces 99.9 mol% ethylene as the top product and 99.5 mol% ethane as the bottom product. Decision variables for the MOO of HMD system for EF retrofitting are given in Table 4.4. The side draw is taken from stage 40, and retentate and permeate streams are fed at stages 31 and 59 respectively. The condenser uses propylene (-35°C) as utility, and the reboiler uses propylene (-2°C); the latter is considered as utility credit. The permeate pressure is kept at 400 kPa [128]. The non-dominated solutions obtained by EMOO after 60, 80 and 100 generations for the maximization of utility cost savings and minimization of the associated capital cost of the membrane unit (Figure 4.4a), show that there are no positive utility cost savings for most part of the optimal front. One main reason for this is utility credit from reboiler duty; this is further discussed later.

Optimal values of decision variables corresponding to the Pareto-optimal front after 100 generations are shown in Figures 4.4b-d. Membrane feed flowrate values are scattered (Figure 4.4b). Optimal values of membrane area are at 1100 m^2 (Figure 4.4c), and ethylene permeance values are mostly closer to their upper bound of 0.008 kgmole/1000h-m^2-kPa (Figure 4.4d). This may be

due to the objective function of minimizing capital cost. Two outliers in Figure 4.4a occur due to increase in the membrane surface area to nearly 2600 m^2 (Figure 4.4c) and decrease in the ethylene permeance (Figure 4.4d), both of which lead to higher capital cost.

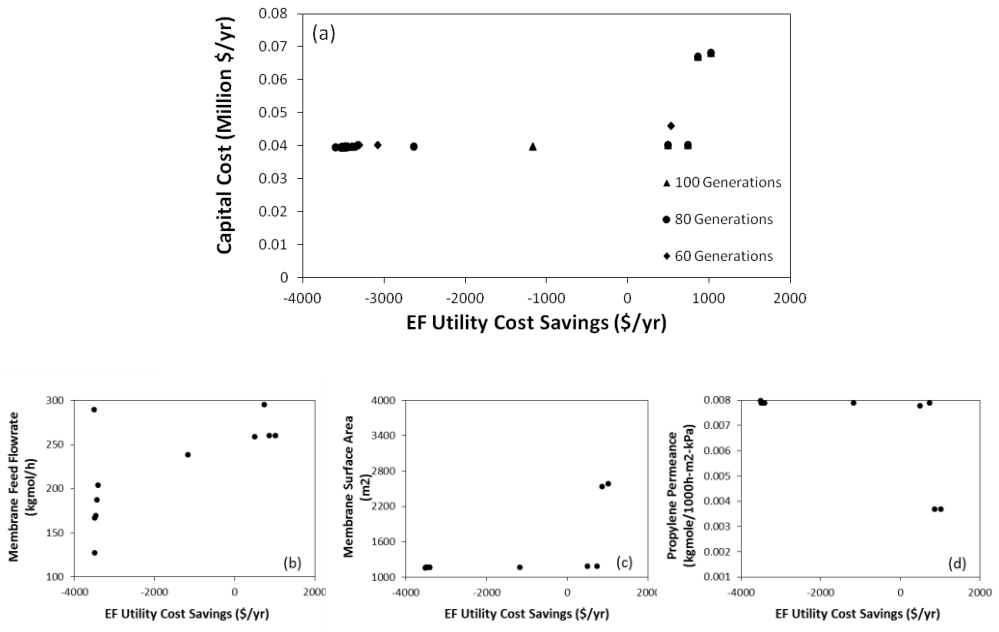

Figure 4.4: Non-dominated solutions for maximization of utility cost savings and minimization of capital cost for retrofitting EF to a HMD system, considering reboiler duty as utility credit (plot a); optimal values of decision variables corresponding to the Pareto-optimal front are in plots b to d.

Ploegmakers et al. [128] claimed 16% savings on total annualized cost (TAC) from retrofitting EF with a membrane unit in series. They used cooling water in reboiler as utility cost and membrane selectivity of over 30. In the current study assuming reboiler duty as utility credit in both base and hybrid cases, savings in the condenser utility cost are not enough to compensate for the utility cost of compressor used in the hybrid system. Even though there are some positive utility cost savings towards the end of the Pareto-optimal front (Figure 4.4a), corresponding capital cost is higher which means net savings is still negative. This makes EF retrofitting to a HMD system uneconomical.

Another set of optimization run was carried out where the reboiler duty of EF was considered as utility cost with cooling water as utility, as in Ploegmakers et al. [128]. The non-dominated solutions obtained by EMOO after 60, 80 and 100 generations for the maximization of utility cost savings and minimization

of the associated capital cost of the membrane unit are given in Figure 4.5a; 100 generations are enough for convergence in this case. Optimal values of decision variables corresponding to the Pareto-optimal front are shown in Figures 4.5b-d. It can be seen from Figure 4.5a that utility cost savings increases from 0.08 to 0.1 Million $/yr while the capital cost increases from 0.04 to 0.12 Million $/yr.

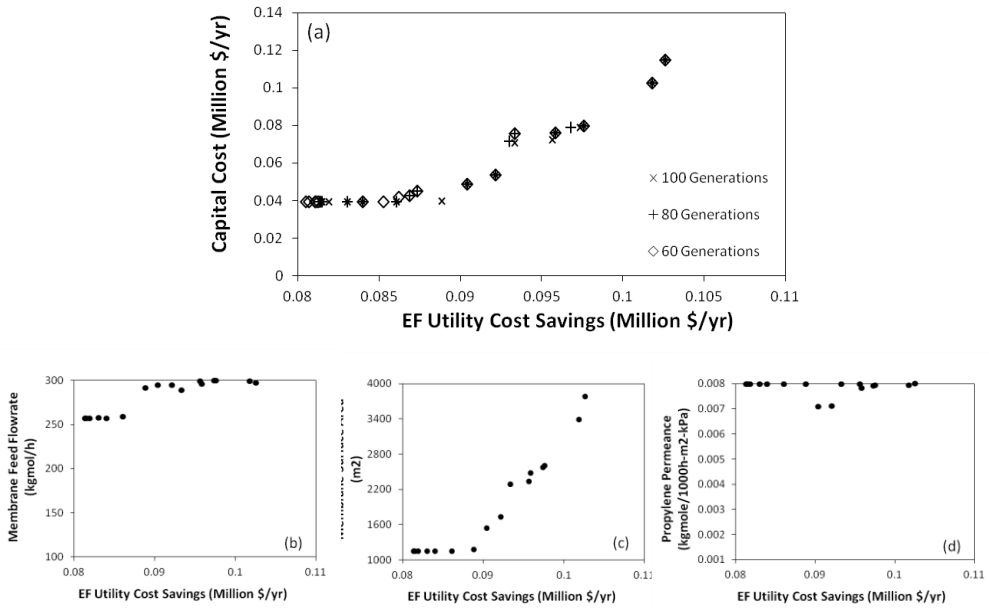

Figure 4.5: Non-dominated solutions for maximization of utility cost savings and minimization of capital cost for retrofitting EF to a HMD system, considering reboiler duty as cost (plot a); optimal values of decision variables corresponding to the Pareto-optimal front are in plots b to d.

Since the change in capital cost is higher than utility cost savings, the maximum savings can be obtained at the starting point of the Pareto-optimal front, which is 0.08 Million $/yr with capital cost of 0.04 Million $/yr. This corresponds to membrane feed flowrate of around 250 kgmol/hr, and will result in net savings of around 1.3% which is still not attractive for retrofitting EF to a HMD system.

4.4.4 Case 4: HMD System for Propylene Fractionator

Propylene fractionator (PF) produces propylene (99 mol% purity) in overheads and propane (95 mol% purity) in bottoms. Decision variables for the MOO of PF retrofitting to a HMD system are as per Table 4.4. The side draw for feeding the membrane is taken from stage 99 which is same as the

feed stage for the column, and retentate and permeate streams are fed at stages 90 and 122 respectively. The condenser uses cooling water as utility whereas the reboiler uses low pressure steam. The permeate pressure is kept at 400 kPa [128].

Non-dominated solutions obtained by EMOO at 60, 80 and 100 generations for the maximization of utility cost savings and minimization of the associated capital cost of the membrane unit, show that the Pareto-optimal front remains same after 60 generations with no significant changes (Figure 4.6a). Hence, 60 generations are sufficient to find the Pareto-optimal front in this case. The Pareto-optimal set after 100 generations is smooth, continuous and nearly linear. The net utility cost savings increase by \$0.602 Million/yr from \$0.028 to \$0.63 Million/yr as the corresponding capital cost increases from \$0.019 to \$0.112 Million/yr (Figure 4.6a); the relationship between these is nearly linear. The extreme point (\$0.63 Million/yr utility cost savings at \$0.112 Million/yr capital cost) is probably the best choice for retrofitting the PF to a HMD system. It will result in net savings of \$0.518 Million/yr (i.e., 8% savings on the current utility cost), which is attractive.

Optimal values of decision variables corresponding to the Pareto-optimal front after 100 generations are shown in Figures 4.6b-d. Membrane feed flowrate is scattered with an increasing trend (Figure 4.6b); there seems to be a minimum feed flowrate corresponding to each optimal value of membrane surface area above which the membrane feed flowrate does not have much effect on the Pareto front. For example, a minimum feed flowrate of 150 kgmol/h is required to attain the utility cost saving of \$0.3 Million/yr (Figures 4.6a and 4.6b). Lower membrane surface area results in lower separation by the membrane unit, leading to decreased reduction in condenser and reboiler duties. As the membrane surface area increases (Figure 4.6c), the associated capital cost increases but also generates comparatively higher utility cost savings. Optimum values of the propylene permeance (Figure 4.6d), which is the controlling factor of permeances of all components and selectivity of the membrane, are near its upper bound of 0.1 kgmole/1000m^2-h-kPa (Figure 4.6d). This is expected as best membrane available is required for the most efficient HMD system.

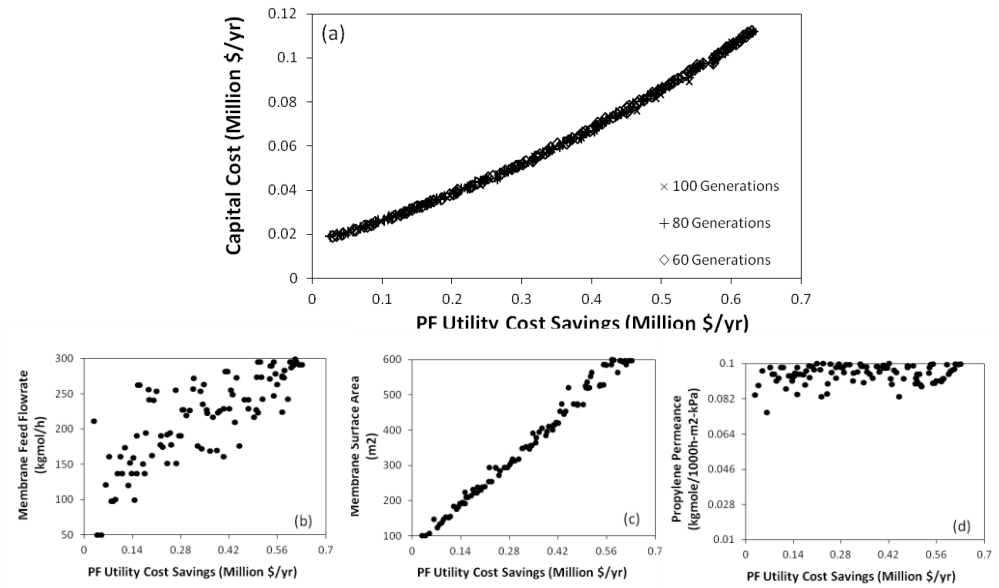

Figure 4.6: Non-dominated solutions for maximization of utility cost savings and minimization of capital cost for retrofitting PF to a HMD system (plot a); optimal values of decision variables corresponding to the Pareto-optimal front are shown in plots b to d.

4.5 Conclusions

The olefin/paraffin separation of an industrial ethylene plant was simulated using Aspen HYSYS, and then four distillation columns in this plant were selected for retrofitting to HMD systems in parallel configuration. The elitist non-dominated sorting genetic algorithm implemented in Excel and Excel-HYSYS interface were employed for simultaneously maximizing the utility cost savings and minimizing the associated capital cost for retrofitting with the membrane unit. Retrofitting DE showed around 1.5% savings for the HMD system; such low savings do not make it attractive. On the contrary, retrofitting DP and PF showed 13% and 8% utility savings, respectively, and are attractive for retrofitting them with a membrane unit. EF retrofitting showed negative utility savings; this can be attributed to the utility credit generated by its reboiler, which is deducted from the utility cost in both base and HMD cases. For the four distillation columns studied, high permeances of olefins are preferred over high selectivities, and increasing the membrane area was found to have an incremental effect on the Pareto-optimal front, since it affects both the objective functions.

Chapter 5

CONCLUSIONS AND RECOMMENDATIONS

5.1 Conclusions of this Study

Ethylene separation is one of the most energy-intensive processes in the petrochemical industry. This is due to the cryogenic distillation employed for separation of close boiling-point hydrocarbons like ethylene/ethane and propylene/propane. Operation optimization of cold-end separation of a conventional ethylene process for multiple objectives and techno-economic evaluation of retrofitting selected columns to hybrid membrane-distillation systems were studied in this thesis.

The cold-end separation of a conventional ethylene plant was simulated in Aspen Hysys and validated with industrial design data. Then, using this simulation model, MOO of the cold-end separation was studied for 3 cases of two objectives using the elitist non-dominated sorting genetic algorithm. Results show that the plant can be operated at different optimal conditions, each of which involves some trade-off among the objectives of interest. In the first case, annual ethylene production could be increased by 0.57 Million kg which corresponds to 0.73 Million $/yr increase in revenue at the cost of 0.4 Million $/yr for utilities. The second case showed linear increase in Pareto front for maximizing propylene production while minimizing net utility cost. Propylene production increased by 10% on the Pareto-optimal front over the utility cost range of 24.2-24.7 Million $/yr. The conflicting nature of total utility cost of the process with the utility credit from DM and EF reboilers was also studied, where it is advisable to operate at the lowest utility cost on the Pareto-optimal front. In all cases, variation of optimal values of decision variables with the objectives can be explained qualitatively, which supports MOO results obtained by NSGA-II.

In the second part of this thesis, membrane separations were added to select distillation columns in the ethylene plant, namely, deethanizer, depropanizer, and ethylene and propylene fractionator. Thereafter, each hybrid membrane-distillation system was optimized for maximizing utility cost savings and

minimizing associated capital cost simultaneously. Values of permeances were bounded by those available in the literature and reasonable assumptions were made for the corresponding selectivities and permeances of other components in the membrane feed. Retrofitting deethanizer, although projected nearly 3% savings, did not generate many Pareto-optimal solutions, which was attributed to significant change in stage compositions throughout this column and it may require simultaneous optimization of feed stages of both permeate and retentate streams. The hybrid system for ethylene fractionator was found to be uneconomical, probably because reboiler duty was considered to be giving utility credit. Retrofitting the depropanizer and propylene fractionator with a membrane unit was found attractive with 13.4% and 8% utility savings respectively, as compared to their corresponding base case. With preference to high permeances of components in all cases, membrane surface area was found to be the crucial decision variable which clearly had an incremental effect on the Pareto-optimal front.

5.2 Recommendations for Future Work

Based on this research, the following studies are recommended for further investigation.

1. Combined MOO of Cold-box and Demethanizer: In this study, MOO was done for the separation train only. MOO of cold-box before demethanizer which includes a series of flash vessels and heat exchangers, has been conducted by Zhang et al. [33]. These two sections can be together studied for MOO.

2. MOO of other configurations of cold-end separation: This study focused on a conventional ethylene separation process with back-end hydrogenation. Due to advancements in distillation technologies, many new configurations have been developed. Simulation and MOO of these configurations can be performed for deeper insight.
3. Retrofitting to Dividing-Wall Columns: In this study, retrofitting with a membrane unit was considered for selected columns in the cold-end separation, and their feasibilities were evaluated. Recently, dividing-wall

columns have been studied for many applications. Their techno-economic feasibility can be analyzed for combining deethanizer and depropanizer, and for secondary deethanizer and propylene fractionator in the conventional cold-end separation.

REFERENCES

[1] ICB: ICIS Chemical Business.2012 *http://www.icis.com/Articles/2012/11/22/9617145/gpca+ethylene+continues+expansion+in+2012.html* (Date of Access: 07-08-2013)

[2] Gerhartz,W., Yamamoto, Y. S., Laudy, K., Rounsaville, J. F., and Schulz, G. 2009. *Ullmann's Encyclopedia of Industrial Chemistry*, 5th Edition. John Wiley & Sons Canada, Ltd.

[3] Eramo, M. 2013. Shale energy resources driving resurgence for ethylene industry. *http://www.hydrocarbonprocessing.com/IssueArticle/3183764/Archive/Shale-energy-resources-driving-resurgence-for-ethylene-industry.html* (Date of Access: 14-09-2013)

[4] Ethylene Process Design Optimization. *http://www1.eere.energy.gov/manufacturing/resources/chemicals/pdfs/ethyleneoptimization.pdf* (Date of Access: 14-09-2013)

[5] Rosneft, Mitsui plan Russia Far East olefins project. 2013. *http://www.hydrocarbonprocessing.com/Article/3198286/Latest-News/Rosneft-Mitsui-plan-Russia-Far-East-olefins-project.html* (Date of Access: 14-09-2013)

[6] Dow to build world-scale ethylene plant by 2017 at Freeport complex. 2012. *http://www.hydrocarbonprocessing.com/Article/3014435/Dow-to-build-world-scale-ethylene-plant-by-2017-at-Freeport.html?LS=EMS765468* (Date of Access: 14-09-2013)

[7] Thinnes, B. 2012. Increased coal-to-olefins processes in China. *http://www.hydrocarbonprocessing.com/Article/3096211/Increased-coal-to-olefins-processes-in-China.html* (Date of Access: 14-09-2013)

[8] KBR wins licensing, process design deal for China olefins recovery project. 2012. *http://www.hydrocarbonprocessing.com/Article/3096994/Search/KBR-wins-licensing-process-design-deal-for-China-olefins.html* (Date of Access: 14-09-2013)

[9] SK Global signs final deal with Sinopec for Chinese petrochemical venture. 2013.

http://www.hydrocarbonprocessing.com/Article/3224758/Latest-News/SK-Global-signs-final-deal-with-Sinopec-for-Chinese-petrochemical-venture.html (Date of Access: 14-09-2013)

[10] ExxonMobil launches new Singapore cracker. 2013. *http://www.hydrocarbonprocessing.com/Article/3212505/Channel/194955/ExxonMobil-launches-new-Singapore-cracker.html* (Date of Access: 14-09-2013)

[11] Da Costa, A. R., Daniels, R., Jariwala, A. D. 2009. *Liquid-phase separation of low molecular weight organic compounds.* United States Patent no. 7,479,227 B2.

[12] Ethylene Plantwide Control and Optimization. *http://ieeecss.org/sites/ieeecss.org/files/documents/IoCT-Part2-07EthylenePlant-HR.pdf* (Date of Access: 14-09-2013)

[13] Kroschwitz, J. I. and Kirk-Othmer 2004. *Kirk-Othmer Encyclopedia of Chemical Technology*, John Wiley & Sons, Ltd.

[14] Rijckaert, M. J., Martens, X. M. and Desarnauts, J. 1978. Ethylene plant optimization by geometric programming. *Computers & Chemical Engineering,* 2**,** pp. 93-97.

[15] Bandoni, J. A., Eliceche, A. M., Serrani, A., Debeistegui, R., and Brignole, E. A. 1990. Optimal operation of ethylene plants. *Computer Applications in Chemical Engineering.* Proceedings from 21st European Symposium on Computer Applications in Chemical Engineering, ComChem'90, Hague, Netherleands (7 - 9 May, 1990) pp.177.

[16] Petracci, N., Eliceche, A. M., Bandoni, A., and Brignole, E. A. 1993. Optimal operation of an ethylene plant utility system. *Computers & Chemical Engineering,* 17(Suppl. 1)**,** pp.S147-S152.

[17] Eliceche, A. M., Petracci, N. C., Hoch, P., and Brignole, E. A. 1995. Optimal operation of an ethylene plant at variable feed conditions. *Computers & Chemical Engineering,* 19(Suppl. 1)**,** pp.223-228.

[18] Petracci, N. C., Hoch, P. M., and Eliceche, A. M. 1996. Flexibility analysis of an ethylene plant. *Computers & Chemical Engineering,* 20(Suppl. 1)**,** pp.S443-S448.

[19] Linnhoff, B. and Dhole, V. R. 1992. Shaftwork targets for low-temperature process design. *Chemical Engineering Science,* 47**,** pp. 2081-2091.

[20] Dhole, V. R. and Linnhoff, B. 1993. Distillation column targets. *Computers & Chemical Engineering,* 17**,** pp. 549-560.

[21] Dhole, V. R. and Linnhoff, B. 1994. Overall design of low temperature processes. *Computers & Chemical Engineering,* 18, Supplement 1**,** pp. S105-S111.

[22] Castillo, F. J. L. and Dhole, V. R. 1995. Pressure analysis of the ethylene cold-end process. *Computers & Chemical Engineering,* 19(Suppl. 1), pp. 89-94.

[23] Sobočan, G., and Glavič, P. 1999. A new method for studying thermally integrated distillation sequences. *Computers & Chemical Engineering,* 23(Suppl. 1)**,** pp.S899-S902.

[24] Chang, H. 2001. Exergy analysis and exergoeconomic analysis of an ethylene process. *Tamkang Journal of Science and Engineering,* 4**,** pp. 95-104.

[25] Chang, H. and Li, J. W. 2005. A new exergy method for process analysis and optimization. *Chemical Engineering Science,* 60**,** pp. 2771-2784.

[26] Mafi, M., Naeynian, S. M. M. and Amidpour, M. 2009. Exergy analysis of multistage cascade low temperature refrigeration systems used in olefin plants. *International Journal of Refrigeration,* 32**,** pp. 279-294.

[27] Huang, S. N. and Shao, H. H. 1994. Application of pattern recognition to ethylene production optimization. *Engineering Applications of Artificial Intelligence,* 7**,** pp. 329-333.

[28] Díaz, M. S. and Bandoni, J. A. 1996. A mixed integer optimization strategy for a large scale chemical plant in operation. *Computers & Chemical Engineering,* 20**,** pp. 531-545.

[29] Yan, M. 2000. Simulation and optimization of ethylene plant. Master of Science Thesis, Texas Tech University. *http://repositories.tdl.org/ttu-ir/bitstream/handle/2346/16119/31295016605676.pdf?sequence=1* (Date of Access: 13-08-2013)

[30] Sobočan, G., and Glavič, P. 2001. Optimization of ethylene process design. *11th European Symposium on Computer Aided Process Engineering*, Kolding, Denmark (27 – 30 May, 2001) 9, pp.529-534

[31] Wang, J. and Smith, R. 2005. Synthesis and Optimization of Low-Temperature Gas Separation Processes. *Industrial & Engineering Chemistry Research,* 44**,** pp. 2856-2870.

[32] Van Geem, K., and Marin, G. B. 2010. Computer aided design and optimization of olefin production plants. *http://www.aidic.it/escape20/webpapers/574Marin.pdf* (Date of Access: 07-08-2013)

[33] Zhang, J., Wen, Y. and Xu, Q. 2010. Multiobjective optimization for design and operation of the chilling train system in ethylene plants. *Industrial & Engineering Chemistry Research,* 49**,** pp. 5786-5799.

[34] Shah, P. B. and Kokossis, A. C. 1999. Novel designs for ethylene cold-end separation using conceptual programming technology. *Computers & Chemical Engineering*, 23**,** pp. S895-S898.

[35] Jackson, S. B. 1972. *Low pressure ethylene recovery process*. United States Patent no. 3675435.

[36] Pryor, J. A. and Rowles, H. C. 1977. *Recovery of C. sub. 2+ hydrocarbons by plural stage rectification and first stage dephlegmation*. United States Patent no. 4002042.

[37] Rowles, H. C. 1987. *Process for recovery and purification of C. sub. 3-C. sub. 4+ hydrocarbons using segregated phase separation and dephlegmation*. United States Patent no. 4714487.

[38] Rowles, H. C., Grassi, K. S. & Bernhard, D. P. 1988. *Process for the recovery and purification of ethylene*. United States Patent no. 4720293.

[39] Dinh, C. X., Petterson, W. C., Rastogi, A. and Verma, V. K. 1995. *Olefin recovery method*. United States Patent no. 5452581.

[40] Krause, W. A. and Pasadyn, R. C. 1997. *Method and Apparatus for Recovery of H2 and C2 and Heavier Components*. United States Patent no. 5689032.

[41] Davis, J. S. 1979. *Ethylene separation process*. United States Patent no. 4167402.

[42] Nazar, B. 1997. *Rectified reflux deethanizer*. United States Patent no. 5678424.

[43] Nazar, B. 1999. *Rectified reflux deethanizer*. United States Patent no. 5884504.

[44] Kuechler, K. H. and Lumgair, D. R. 2001. *Production of ethylene using high temperature demethanization*. United States Patent no. 6212905.

[45] Tedder, D. W. 1984. *Fractional distillation of C2/C3 hydrocarbons at optimum pressures*. United States Patent no. 4430102.

[46] Di Cintio, R., Picciotti, M., Kaiser, V. and Pocini, C. A. 1993. *Method and apparatus for recovery of ethylene and propylene from gas produced by the pyrolysis of hydrocarbons*. United States Patent no. 5253479.

[47] Kaiser, V., Laugier, J. P. and Simon, Y. 2003. *Process and installation for recovery and purification of ethylene produced by pyrolysis of hydrocarbons, and gases obtained by this process*. United States Patent no. 6578378.

[48] Kaiser, V., Laugier, J. P. and Simon, Y. 2008. *Process and installation for recovery and purification of ethylene produced by pyrolysis of hydrocarbons, and gases obtained by this process*. United States Patent no. RE40124.

[49] Manley, D. and Haddad, H. 1997. *Low cost thermal coupling in ethylene recovery*. United States Patent no. 5675054.

[50] Ronczy, S. E. 2007. *Secondary deethanizer to debottleneck an ethylene plant*. United States Patent no. 7207192.

[51] Reyneke, R., Foral, M., Papadopoulos, C. G., Logsdon, J. S., Eng, W. W. Y., Lee, G. C. and Sinclair, I. 2007. *Distillation sequence for the purification and recovery of hydrocarbons*. United States Patent no. 7311813.

[52] Reyneke, R., Foral, M. J., Lee, G. C., Eng, W. W. Y., Sinclair, I. and Lodgson, J. S. 2008. *Recovery and purification of ethylene*. United States Patent no. 7437891.

[53] Bernhard, D. P., Evans, M. H., Freeman, R. P. and Rowles, H. C. 1994. *Process for the recovery of C. sub. 2+ or C. sub. 3+ hydrocarbons*. United States Patent no. 5287703.

[54] Howard, L. J. and Rowles, H. C. 1995. *Mixed refrigerant cycle for ethylene recovery*. United States Patent no. 5379597.

[55] Howard, L. J. and Rowles, H. C. 1996. *Mixed refrigerant cycle for ethylene recovery*. United States Patent no. 5502972.

[56] Manley, D. B. 1998. *Pre-fractionation of cracked gas or olefins fractionation by one or two mixed refrigerant loops and cooling water*. United States Patent no. 5746066.

[57] Stork, K. 2000. *Integrated deethanizer/ethylene fractionation column*. United States Patent no. 6077985.

[58] Stork, K. 2001. *Integrated low pressure depropanizer/debutanizer column*. United States Patent no. 6291734.

[59] Van Zile, C. P. and Harris, J. W. 2003. *Dividing wall column control system*. United States Patent no. 6551465.

[60] Reyneke, R., Foral, M. J. & Lee, G. C. 2006. *Low capital implementation of distributed distillation in ethylene recovery*. United States Patent no. 7129387.

[61] Chen, H., Huang, K. & Wang, S. 2010. A novel simplified configuration for an ideal heat-integrated distillation column (ideal HIDiC). *Separation and purification technology,* 73**,** pp. 230-242.

[62] Nawaz, M. & Jobson, M. 2011. A boundary value design method for complex demethaniser distillation columns. *Chemical Engineering Research and Design,* 89**,** pp. 1333-1347.

[63] Hou, J., Bai, Y., Gao, F., and Fu, X. 2011. Research of ethylene separation process simulation technology. *Chemical Industry and Engineering Progress***,** S2, pp.70-79.

[64] Tahouni, N., Bagheri, N., Towfighi, J., and Panjeshahi, M. 2011a. Retrofit of low-temperature gas separation section of an olefin plant. *4th International Conference on Modeling, Simulation and Applied Optimization (ICMSAO),* Kuala Lumpur (19 – 21 April 2011) pp.1-4.

[65] Tahouni, N., Panjeshahi, M., and Ataei, A. 2011b. Comparison of sequential and simultaneous design and optimization in low-temperature liquefaction and gas separation processes. *Journal of the Franklin Institute,* 7**,** pp.1456-1469.

[66] Semenova, S. I. 2004. Polymer membranes for hydrocarbon separation and removal. *Journal of membrane science,* 231**,** pp. 189-207.

[67] Lutze, P. and Gorak, A. 2013. Reactive and membrane-assisted distillation: Recent developments and perspective. *Chemical Engineering Research and Design*.

[68] Way, J. D., Nobel R.D., Flynn, T. M. and Sloan, E. D. 1982. Liquid membrane transport: a survey. *Journal of Membrane Science*, 12, pp. 239–259.

[69] King, C. J. 1988. Separation processes based on reversible chemical complexation. *Handbook of Separation Processes*. Edited by R. W. Rousseau, John Wiley & Sons, Inc., New York, USA, pp. 760–774.

[70] Way, J. D. and Noble, R. D. 1992. Facilitated transport. *Membrane Handbook*. Edited by K. K. Sirkar and W. S. Ho , Van Nostrand Publishing Company, New York, USA.

[71] Eldridge, R. B. 1993. Olefin/paraffin separation technology: A review. *Industrial and Engineering Chemistry Research,* 32**,** pp. 2208-2212.

[72] Cussler, E. L. 1994. Facilitated and active transport. *Polymeric Gas Separation Membranes.* Edited by D. R. Paul and Y. P. Yampol'skii, CRC Press, Boca Raton, FL, USA, pp. 273–300.

[73] Liu, Z. M., Xu, Z. K., Kou, R. Q. and Dai, Q. W. 2002. Facilitated transport membranes for olefin/paraffin separation - an overview. *Petrochemical Technology,* 31**,** pp. 753-758.

[74] Noble, R. D. and Koval, C. A. 2006. Review of Facilitated Transport Membranes. *Materials Science of Membranes for Gas and Vapour Separation.* John Wiley & Sons, Ltd.

[75] Azhin, M., Kaghazchi, T. and Rahmani, M. 2008. A review on olefin/paraffin separation using reversible chemical complexation technology. *Journal of Industrial and Engineering Chemistry,* 14**,** pp. 622-638.

[76] Faiz, R. and Li, K. 2012. Polymeric membranes for light olefin/paraffin separation. *Desalination,* 287**,** pp. 82-97.

[77] Sakellaropoulos, G. P., Plaggesis, H., Koops, G.-H. and Makhlouf, M. 2010. Membrane Separation of Olefins from FCC Naphtha and Gases for Production of Reformulated Gasoline. *Chemical Process*

Engineering Research Institute. *http://cordis.europa.eu/documents/documentlibrary/50781711EN6.pdf* (Date of Access: 14-09-2013)

[78] Schmeling, N., Konietzny, R., Sieffert, D., Rölling, P. and Staudt, C. 2010. Functionalized copolyimide membranes for the separation of gaseous and liquid mixtures. *Beilstein Journal of Organic Chemistry,* 6**,** pp. 789-800.

[79] Ma, X., Lin, B. K., Wei, X., Kniep, J. and Lin, Y. S. 2013. Gamma-alumina supported carbon molecular sieve membrane for propylene/propane separation. *Industrial and Engineering Chemistry Research,* 52**,** pp. 4297-4305.

[80] Shimazu, A., Miyazaki, T., Matsushita, T., Maeda, M. and Ikeda, K. 1999. Relationships between chemical structures and solubility, diffusivity, and permselectivity of 1,3-butadiene and n-butane in 6FDA-based polyimides. *Journal of Polymer Science, Part B: Polymer Physics,* 37**,** pp. 2941-2949.

[81] Shimazu, A., Miyazaki, T., Maeda, M. and Ikeda, K. 2000. Relationships between the chemical structures and the solubility, diffusivity, and permselectivity of propylene and propane in 6FDA-based polyimides. *Journal of Polymer Science, Part B: Polymer Physics,* 38**,** pp. 2525-2536.

[82] Chan, S. S., Wang, R., Chung, T. S. and Liu, Y. 2002. C2 and C3 hydrocarbon separations in poly(1,5-naphthalene-2,2′-bis(3,4-phthalic) hexafluoropropane) diimide (6FDA-1,5-NDA) dense membranes. *Journal of membrane science,* 210**,** pp. 55-64.

[83] Rungta, M., Zhang, C., Koros, W. J. and Xu, L. 2013. Membrane-based ethylene/ethane separation: The upper bound and beyond. *AIChE Journal,* 59**,** pp. 3475-3489.

[84] Burns, R. L. and Koros, W. J. 2003. Defining the challenges for C3H6/C3H8 separation using polymeric membranes. *Journal of membrane science,* 211**,** pp. 299-309.

[85] Suda, H. and Haraya, K. 1997. Alkene/alkane permselectivities of a carbon molecular sieve membrane. *Chemical Communications***,** pp.93-94.

[86] Okamoto, K. I., Kawamura, S., Yoshino, M., Kita, H., Hirayama, Y., Tanihara, N. and Kusuki, Y. 1999. Olefin/paraffin separation through carbonized membranes derived from an asymmetric polyimide hollow fiber membrane. *Industrial and Engineering Chemistry Research,* 38**,** pp. 4424-4432.

[87] Vu, D. Q., Koros, W. J. and Miller, S. J. 2002. High pressure CO2/CH4 separation using carbon molecular sieve hollow fiber membranes. *Industrial and Engineering Chemistry Research,* 41**,** pp. 367-380.

[88] Steel, K. M. and Koros, W. J. 2005. An investigation of the effects of pyrolysis parameters on gas separation properties of carbon materials. *Carbon,* 43**,** pp. 1843-1856.

[89] David, L. I. B. and Ismail, A. F. 2003. Influence of the thermastabilization process and soak time during pyrolysis process on the polyacrylonitrile carbon membranes for O2/N2 separation. *Journal of membrane science,* 213**,** pp. 285-291.

[90] Chen, Y. D. and Yang, R. T. 1994. Preparation of carbon molecular sieve membrane and diffusion of binary mixtures in the membrane. *Industrial and Engineering Chemistry Research,* 33**,** pp. 3146-3153.

[91] Katsaros, F. K., Steriotis, T. A., Stubos, A. K., Mitropoulos, A., Kanellopoulos, N. K. and Tennison, S. 1997. High pressure gas permeability of microporous carbon membranes. *Microporous Materials,* 8**,** pp. 171-176.

[92] Bernardo, P., Drioli, E. and Golemme, G. 2009. Membrane gas separation: A review/state of the art. *Industrial and Engineering Chemistry Research,* 48**,** pp. 4638-4663.

[93] Shao, P. and Huang, R. Y. M. 2007. Polymeric membrane pervaporation. *Journal of membrane science,* 287**,** pp. 162-179.

[94] Davis, R. A. 2002. Simple gas permeation and pervaporation membrane unit operation models for process simulators. *Chemical Engineering and Technology,* 25**,** pp. 717-722.

[95] Liao, K. S., Fu, Y. J., Hu, C. C., Chen, J. T., Lin, D. W., Lee, K. R., Tung, K. L., Jean, Y. C. and Lai, J. Y. 2012. Microstructure of carbon molecular sieve membranes and their application to separation of aqueous bioethanol. *Carbon,* 50**,** pp. 4220-4227.

[96] Khalilpour, R., Abbas, A., Lai, Z. and Pinnau, I. 2013. Analysis of hollow fibre membrane systems for multicomponent gas separation. *Chemical Engineering Research and Design,* 91**,** pp. 332-347.

[97] Tanaka, K., Taguchi, A., Hao, J., Kita, H. and Okamoto, K. 1996. Permeation and separation properties of polyimide membranes to olefins and paraffins. *Journal of membrane science,* 121**,** pp. 197-207.

[98] Okamoto, K., Noborio, K., Hao, J., Tanaka, K. and Kita, H. 1997. Permeation and separation properties of polyimide membranes to 1,3-butadiene and n-butane. *Journal of membrane science,* 134**,** pp. 171-179.

[99] Shamsabadi, A. A., Kargari, A., Farshadpour, F. and Laki, S. 2012. Mathematical Modeling of CO2/CH4 Separation by Hollow Fiber Membrane Module Using Finite Difference Method. *Journal of Membrane and Separation Technology,* 1**,** pp. 19-29.

[100] Choi, S. H., Kim, J. H. and Lee, S. B. 2007. Sorption and permeation behaviors of a series of olefins and nitrogen through PDMS membranes. *Journal of membrane science,* 299**,** pp. 54-62.

[101] Liu, L., Chakma, A. and Feng, X. 2006. Sorption, diffusion, and permeation of light olefins in poly(ether block amide) membranes. *Chemical Engineering Science,* 61**,** pp. 6142-6153.

[102] Staudt-Bickel, C. and Koros, W. J. 2000. Olefin/paraffin gas separations with 6FDA-based polyimide membranes. *Journal of membrane science,* 170**,** 205-214.

[103] Ahmad, F., Lau, K. K. and Shariff, A. M. 2010. Modeling and Parametric Study for CO2/CH4 Separation using Membrane Processes *World Academy of Science, Engineering and Technology* 48**,** pp. 455-460.

[104] Hunger, K., Schmeling, N., Jeazet, H. B. T., Janiak, C., Staudt, C. and Kleinermanns, K. 2012. Investigation of cross-linked and additive containing polymer materials for membranes with improved performance in pervaporation and gas separation. *Membranes,* 2**,** pp. 727-763.

[105] Ploegmakers, J., Japip, S. and Nijmeijer, K. 2013a. Mixed matrix membranes containing MOFs for ethylene/ethane separation Part A:

Membrane preparation and characterization. *Journal of membrane science,* 428**,** pp. 445-453.

[106] Shiflett, M. B. and Foley, H. C. 2000. On the preparation of supported nanoporous carbon membranes. *Journal of membrane science,* 179**,** pp. 275-282.

[107] Yamamoto, M., Kusakabe, K., Hayashi, J. I. and Morooka, S. 1997. Carbon molecular sieve membrane formed by oxidative carbonization of a copolyimide film coated on a porous support tube. *Journal of membrane science,* 133**,** pp. 195-205.

[108] Tessendorf, S., Gani, R. and Michelsen, M. L. 1999. Modeling, simulation and optimization of membrane-based gas separation systems. *Chemical Engineering Science,* 54**,** pp. 943-955.

[109] Chatterjee, A., Ahluwalia, A., Senthilmurugan, S. and Gupta, S. K. 2004. Modeling of a radial flow hollow fiber module and estimation of model parameters using numerical techniques. *Journal of membrane science,* 236**,** pp. 1-16.

[110] Ahmad, F., Lau, K. K., Shariff, A. M. and Murshid, G. 2012. Process simulation and optimal design of membrane separation system for CO 2 capture from natural gas. *Computers and Chemical Engineering,* 36**,** pp. 119-128.

[111] Koch, K., Sudhoff, D., Kreiß, S., Górak, A. and Kreis, P. 2013. Optimisation-based design method for membrane-assisted separation processes. *Chemical Engineering and Processing: Process Intensification,* 67**,** pp. 2-15.

[112] Gottschlich, D. E. and Roberts, D. L. 1990. Energy minimization of separation processes using conventional/membrane hybrid systems. EG and G Idaho, Inc., Idaho Falls, ID (USA). *http://www.osti.gov/bridge/purl.cover.jsp?purl=/6195331-h2d2wl/* (Date of Access: 14-09-2013)

[113] Davis, J. C., Valus, R. J., Eshraghi, R. and Velikoff, A. E. 1993. Facilitated transport membrane hybrid systems for olefin purification. *Separation science and technology,* 28**,** pp. 463-476

[114] Moganti, S., Noble, R. D. and Koval, C. A. 1994. Analysis of a membrane/ distillation column hydrid process. *Journal of membrane science,* 93**,** pp. 31-44.

[115] Pettersen, T. and Lien, K. M. 1995. Design of hybrid distillation and vapour permeation processes. *Journal of membrane science,* 102**,** pp. 21-30.

[116] Pettersen, T., Argo, A., Noble, R. D. and Koval, C. A. 1996. Design of combined membrane and distillation processes. *Separations Technology,* 6**,** pp. 175-187.

[117] Pressly, T. G. And Ng, K. M. 1998. A Break-Even Analysis of Distillation-Membrane Hybrids. *AIChE Journal*, 44, 93-105.

[118] Fahmy, A., Mewes, D. & Ebert, K. 2001. Design methodology for the optimization of membrane separation properties for hybrid vapour permeation-distillation processes. *Separation science and technology,* 36**,** pp. 3287-3304.

[119] Kookos, I. K. 2003. Optimal design of membrane/distillation column hybrid processes. *Industrial & Engineering Chemistry Research,* 42**,** pp. 1731-1738.

[120] Kreis, P. and Górak, A. 2006. Process analysis of hybrid separation processes: Combination of distillation and pervaporation. *Chemical Engineering Research and Design,* 84**,** 595-600.

[121] Takht Ravanchi, M., Kaghazchi, T. and Kargari, A. 2009. Application of membrane separation processes in petrochemical industry: a review. *Desalination,* 235**,** pp. 199-244.

[122] Caballero, J. A., Grossmann, I. E., Keyvani, M. and Lenz, E. S. 2009. Design of hybrid distillation-vapour membrane separation systems. *Industrial & Engineering Chemistry Research,* 48**,** pp. 9151-9162.

[123] Bernardo, P. and Drioli, E. 2010. Membrane gas separation progresses for process intensification strategy in the petrochemical industry. *Petroleum Chemistry,* 50**,** pp. 271-282.

[124] Ayotte-Sauvé, E., Sorin, M. and Rheault, F. 2010. Energy requirement of a distillation/membrane parallel hybrid: A thermodynamic approach. *Industrial & Engineering Chemistry Research,* 49**,** pp. 2295-2305.

[125] Benali, M. and Aydin, B. 2010. Ethane/ethylene and propane/propylene separation in hybrid membrane distillation systems: Optimization and economic analysis. *Separation and purification technology,* 73**,** pp. 377-390.

[126] Naidu, Y. and Malik, R. K. 2011. A generalized methodology for optimal configurations of hybrid distillation–pervaporation processes. *Chemical Engineering Research and Design,* 89**,** pp. 1348-1361.

[127] Motelica, A., Bruinsma, O. S. L., Kreiter, R., Den Exter, M. and Vente, J. F. 2012. Membrane Retrofit Option for Paraffin/Olefin Separation- A Technoeconomic Evaluation. *Industrial & Engineering Chemistry Research,* 51**,** pp. 6977-6986.

[128] Ploegmakers, J., Jelsma, A. R. T., Van Der Ham, A. G. J. and Nijmeijer, K. 2013b. Economic evaluation of membrane potential for ethylene/ethane separation in a retrofitted hybrid membrane-distillation plant using Unisim Design. *Industrial and Engineering Chemistry Research,* 52**,** pp. 6524-6539.

[129] Tarafder, A., Lee, B. C. S., Ray, A. K., and Rangaiah, G. P. 2005. Multiobjective optimization of an industrial ethylene reactor using a nondominated sorting genetic algorithm. *Industrial and Engineering Chemistry Research*, 44, pp. 124-141.

[130] Masuduzzaman, Rangaiah, G. P. 2009 Multi-objective optimization applications in chemical engineering, in *Multi-Objective Optimization: Techniques and Applications in Chemical Engineering*; World Scientific, Singapore.

[131] Sharma, S., Rangaiah, G. P. 2013 Multi-objective optimization applications in chemical engineering. *Multi-Objective Optimization in Chemical Engineering*, John Wiley & Sons, Ltd.

[132] Gao, X., Chen, B., He, X., Qiu, T., Li, J., Wang, C., and Zhang, L. 2008. Multi-objective optimization for the periodic operation of the naphtha pyrolysis process using a new parallel hybrid algorithm combining NSGA-II with SQP. *Computers & Chemical Engineering*, 32, pp. 2801-2811.

[133] Li, C., Zhu, Q., and Geng, Z. 2007. Multiobjective particle swarm optimization hybrid algorithm: an application on industrial cracking

furnace. *Industrial and Engineering Chemistry Research*, 46, pp. 3602-3609.

[134] Nabavi, S.R., Rangaiah, G.P., Niaei, A., and Salari, D. 2009. Multiobjective optimization of an industrial LPG thermal cracker using a first principles model. *Industrial and Engineering Chemistry Research*, 48, pp. 9523-9533.

[135] Nabavi, R., Rangaiah, G.P., Niaei, A. , and Salari, D. 2011. Design optimization of an LPG thermal cracker for multiple objectives. *International Journal of Chemical Reactor Engineering*, 9(Article A80), pp. 1-34.

[136] Carlson, E. C. 1996. Don't gamble with physical properties for simulations. *Chemical Engineering Progress*. October 1996. pp. 35-46.

[137] Gmehling, J., Onken, U., Arlt, W. 1980 Vapour-Liquid Equilibrium Data Collection, Chemistry Data Series.Vol.1, Part 6 (a&b), The DECHEMA.

[138] Kaes, G. 2000. A Practical Guide to Steady State Modeling of Petroleum Processes (Using Commercial Simulators); 1st Edition, The Athens Printing Company.

[139] Seider, W. D., Seader, J. D., Lewin, D. R., and Widagdo, S. 2010 *Product and Process Design Principles – Synthesis, Analysis and Evaluation*. 3rd Edition , John Wiley & Sons.

[140] Turton, R., Bailie, R. C., Whiting, W. B., and Shaeiwitz, J. A. 2009. *Analysis, Synthesis and Design of Chemical Processes*, 3rd Edition. Pearson Education, Inc.

[141] Sharma, S., Rangaiah, G. P., and Cheah, K. S. 2012. Multi-objective optimization using MS Excel with an application to design of a falling-film evapourator system. *Food and Bioproducts Processing,*90, pp. 123-134.

[142] Lee E.S.Q., and Rangaiah,G.P. 2009. Optimization of recovery processes for multiple economic and environmental objectives. *Industrial and Engineering Chemistry Research*, 48, pp. 7662-7681.

[143] Al-Mayyahi M.A., Hoadley A.F.A, and Rangaiah G.P. 2013. CO_2 Emissions targeting for petroleum refinery optimization, in *Multi-Objective Optimization in Chemical Engineering: Developments and*

Applications. Edited by G.P. Rangaiah and A. Bonilla-Petriciolet, John Wiley & Sons, Ltd.

[144] Vu, D. Q., Koros, W. J. and Miller, S. J. 2003. Mixed matrix membranes using carbon molecular sieves: I. Preparation and experimental results. *Journal of membrane science*, 211, pp. 311-334.

[145] Ockwig, N. W. and Nenoff, T. M. 2007. Membranes for hydrogen separation. *Chemical Reviews*, 107, pp. 4078-4110.

[146] Lie, J. A., Vassbotn, T., Hägg, M. B., Grainger, D., Kim, T. J. and Mejdell, T. 2007. Optimization of a membrane process for CO2 capture in the steelmaking industry. *International Journal of Greenhouse Gas Control*, 1, pp. 309-317.

[147] Ghosal, K. & Freeman, B. D. 1994. Gas separation using polymer membranes: An overview. Polymers for Advanced Technologies, 5, pp. 673-697.

[148] Typical Overall Heat Transfer Coefficients (U - Values) *http://www.engineeringpage.com/technology/thermal/transfer.html* (Date of Access: 23-09-2013)

[149] Sinnott, R., and Towler, G. 2009. *Chemical Engineering Design*. 5th Edition, Butterworth-Heinemann .

Appendix A

Validation of Thermodynamic Models and Flash Calculations

Every simulation in HYSYS requires selection of an appropriate fluid package which determines the thermodynamic model for given components in distillation columns and other unit operations. In the present study, Peng-Robinson (PR) and Soave-Redlich-Kwong (SRK) models were validated for components of interest, against vapour-liquid-equilibrium (VLE) experimental data available [137]. Since we were dealing with multi-component mixtures, a binary mixture of light and heavy key components corresponding to each distillation column in the simulation was selected. A flash vessel is equivalent to one ideal stage in a distillation column. For different component ratios in the binary mixture entering as feed into the vessel, flash calculations were made for bubble pressure/temperature at constant flash temperature/pressure, which are selected considering the column operating conditions and available experimental data. The predicted data were compared with the experimental data in Gmehling et al. [137].

RESULTS AND DISCUSSION

Demethanizer Column

Methane and propane were chosen as light and heavy key components, respectively. Predicted data were generated using PR and SRK models at 27.579 bar and compared with the experimental data as shown in Figure A.1.

Deethanizer Column

Ethane and propene were chosen as light and heavy key components, respectively. Predicted data were generated using PR and SRK models at 38.78 °C and compared with the experimental data as shown in Figure A.2.

Depropanizer Column

Propene and i-butene were chosen as light and heavy key components, respectively. Predicted data were generated using PR and SRK models at 38.78 °C and compared with the experimental data as shown in Figure A.3.

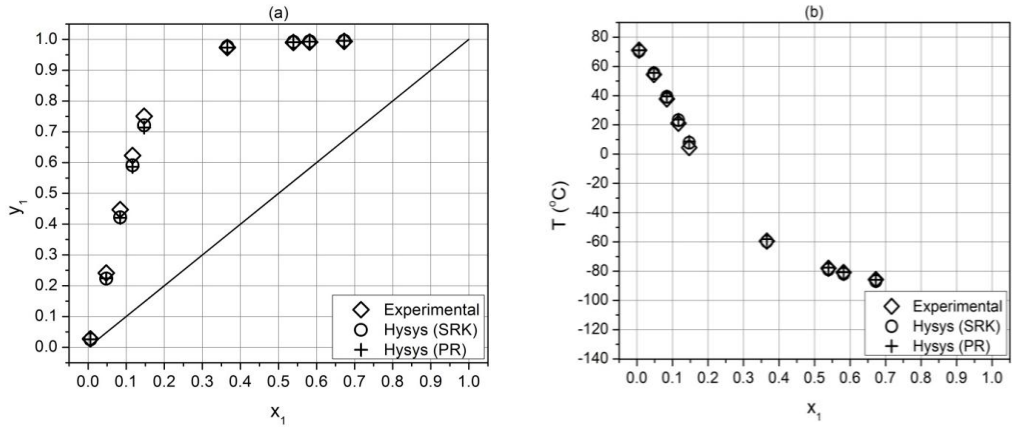

Figure A.1: Comparison of Experimental and Predicted Data for Methane (1) – Propane (2) Mixture: (a) x-y Plot and (b) T-x Plot

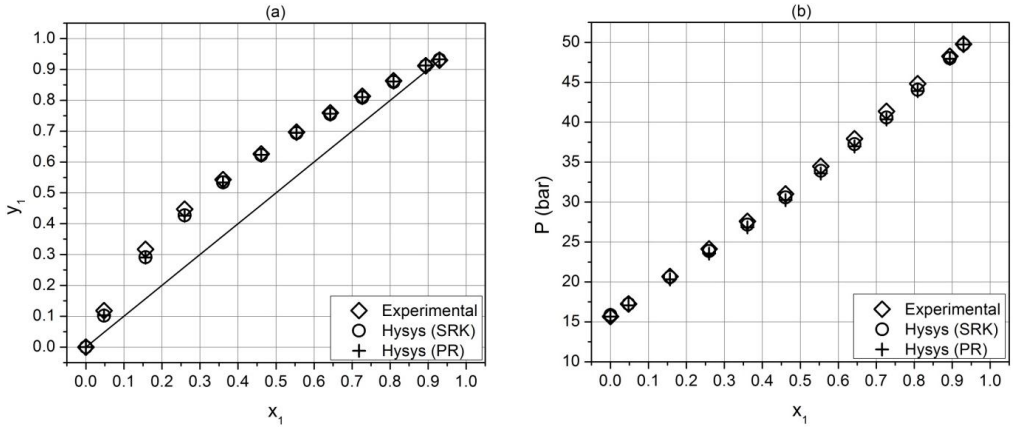

Figure A.2: Comparison of Experimental and Predicted Data for Ethane (1) – Propene (2) Mixture: (a) x-y Plot and (b) P-x Plot

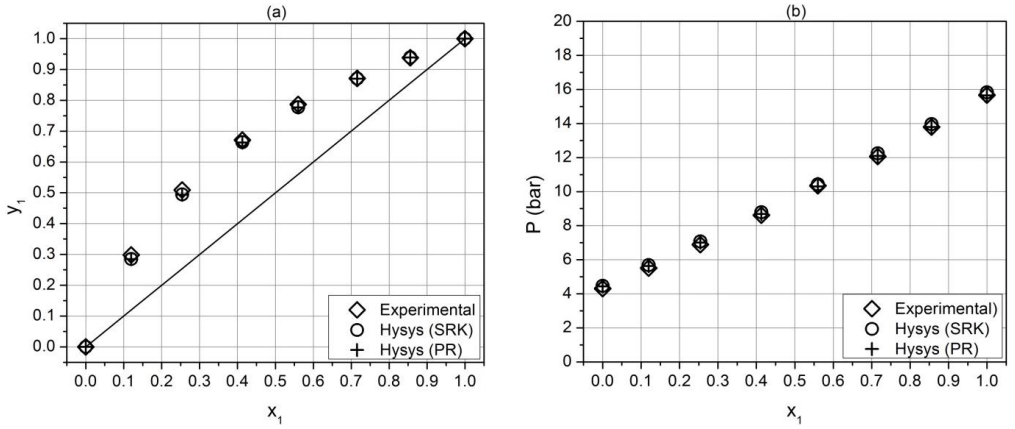

Figure A.3: Comparison of Experimental and Predicted Data for Propene (1) – i-Butene (2) Mixture: (a) x-y Plot and (b) P-x Plot

Debutanizer Column

Propane and pentane were chosen as light and heavy key components, respectively. Predicted data were generated using PR and SRK models at 50 °C and compared with the experimental data as shown Figure in A.4.

Ethylene Fractionator

Ethene and Ethane were chosen as light and heavy key components, respectively. Predicted data were generated using PR and SRK models at -17.78 °C and compared with the experimental data as shown in Figure A.5.

Secondary Deethanizer

Ethane and propane were chosen as light and heavy key components, respectively. Predicted data were generated using PR and SRK models 48.89 °C and compared with the experimental data as shown in Figure A.6.

Propylene Fractionator

Propene and Propane were chosen as light and heavy key components, respectively. Predicted data were generated using PR and SRK models at 48.89 °C and compared with the experimental data as shown in Figure A.7.

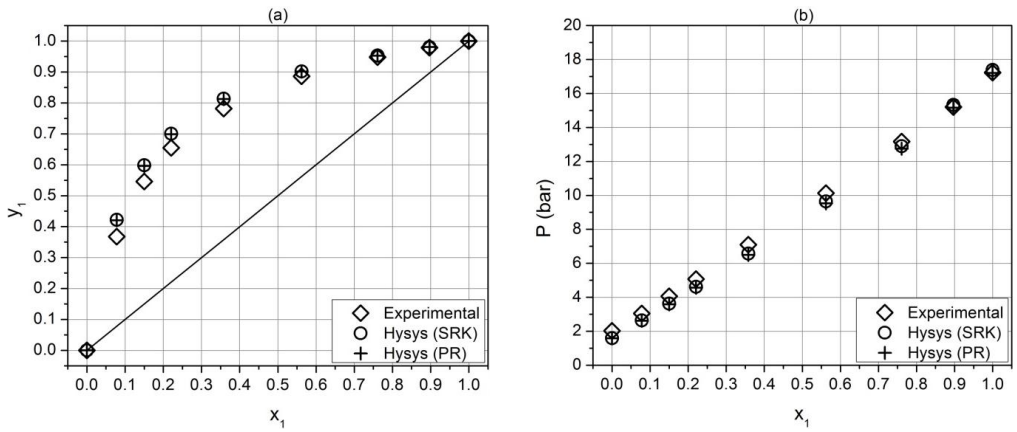

Figure A.4: Comparison of Experimental and Predicted Data for Propane (1) – Pentane (2) Mixture (a) x-y Plot and (b) P-x Plot

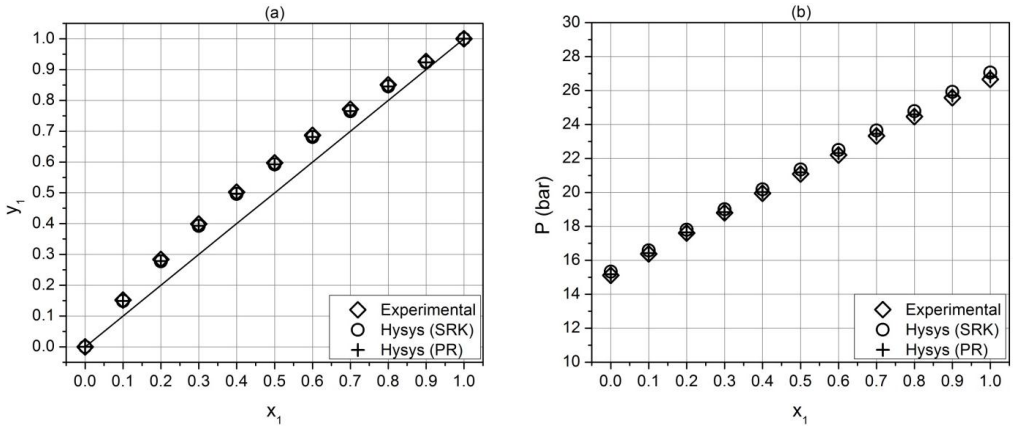

Figure A.5: Comparison of Experimental and Predicted Data for Ethene (1) – Ethane (2) Mixture: (a) x-y Plot and (b) P-x Plot

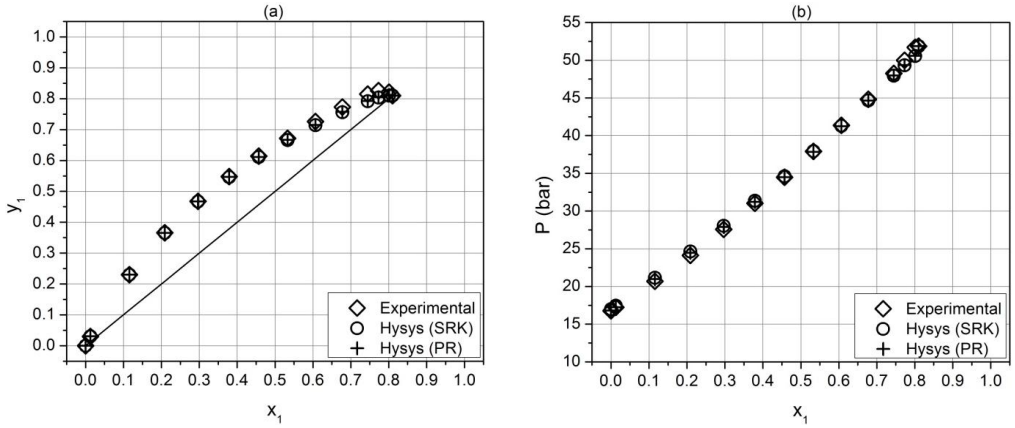

Figure A.6: Comparison of Experimental and Predicted Data for Ethane (1) – Propane (2) Mixture: (a) x-y Plot and (b) P-x Plot

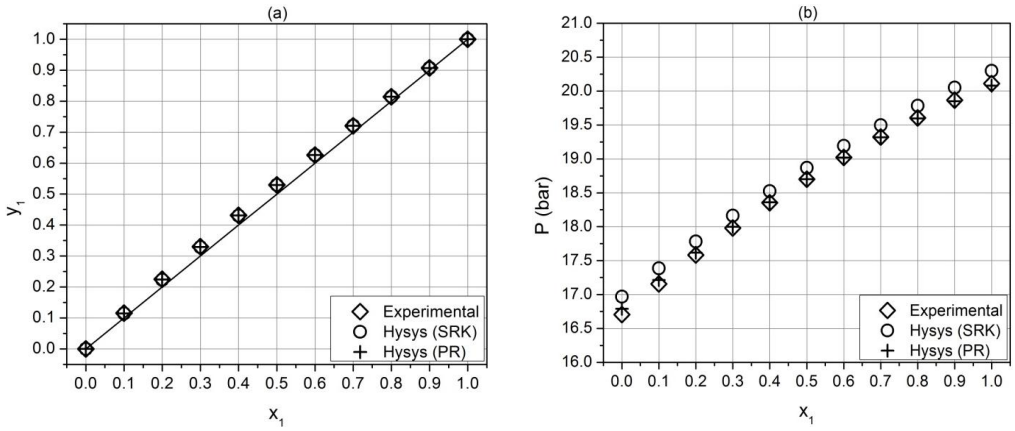

Figure A.7: Comparison of Experimental and Predicted Data for Propene (1) – Propane (2) Mixture: (a) x-y Plot and (b) P-x Plot

Predictions by PR and Soave-Redlich-Kwong models have also been compared using Adjusted R^2 values obtained with respect to the experimental data for each column. The results are presented in Tables A.1. From Figures A.1 to A.7 and Table A.1, it can be seen that both PR and SRK models are suitable for nearly all the binary mixtures of the respective distillation columns in the present study. However, in case of Propylene Fractionator, pressure values were better predicted by PR model. Hence, this model was chosen as the property (fluid) package for the simulation and optimization of the separation process system in this study.

Table A.1: Comparison of Adjusted R^2 for Predicted Data with Experimental Data

S. No.	**Column**	**Adjusted R^2 for y_1**		**Adjusted R^2 for P / T**	
		PR	**SRK**	**PR**	**SRK**
1.	Demethanizer (T)	0.996	0.997	0.999	0.999
2.	Deethanizer (P)	0.998	0.998	0.996	0.998
3.	Depropanizer (P)	0.999	0.999	1.000	0.998
4.	Debutanizer (P)	0.989	0.989	0.992	0.994
5.	Ethylene Fractionator (P)	1.000	1.000	0.999	0.994
6.	Secondary Deethanizer (P)	0.998	0.999	0.999	0.999
7.	Propylene Fractionator (P)	1.000	1.000	0.999	0.964

T: Temperature; P: Pressure

Appendix B

Theory of Membrane Separations

The separation mechanism in membranes having pore size greater than 2 nm is based on size exclusion. Such membranes are suitable for separation of components with significant size difference viz. dialysis, waste water treatment and functional clothing. Ceramics, metal, glass, polymers and zeolites are some of the materials used for membrane construction.

For separating components with similar sized molecules or ions, membranes based on solution-diffusion mechanism are used. The size of the target components (TC) is often less than 1 nm such as gas, vapour or liquids to be removed from process streams. A hydrocarbon mixture is sent on the feed side of the membrane. Different components have different permeances corresponding to a particular membrane. The identified target is first absorbed on the feed side of the membrane. It then diffuses through the free volume of the polymer. Finally, it desorbs on the permeate side of the membrane. Hence, the stream leaving the permeate side, also called the permeate stream, is enriched in TC concentration. The stream which leaves on the same side of the membrane as the feed is called retentate and is depleted of TC concentration as expected. Gas permeation is used for separating gaseous TC from a gaseous mixtures and pervaporation is used for separating gaseous TC from a liquid mixture.

The solution-diffusion membranes contain free volume sites by the virtue of restricted motion and intrinsic packing density of the polymer chains. These sites cannot be occupied due to conformational constraints. However, there exist certain transient gaps within this free volume to accommodate gas molecules. The driving force for the trans-membrane permeation of components is provided by the difference in chemical potential between the feed and permeate sides by keeping the permeate pressure much lower compared to the feed pressure. This pressure difference can be generated in a variety of ways, for example, by heating the feed liquid or maintaining a partial vacuum on the permeate side. It helps in transporting components in

transient gaps near the feed towards those closer to the permeate side in a successive movement. The components are moved through the microvoids due to the thermal motion of segments in the polymer chains [78].

Polymeric membranes are characterized through transport properties like permeability (measure of productivity of the membrane) and selectivity (measure of separation efficiency). The permeation of low molecular weight hydrocarbons through polymeric membranes is often determined by both thermodynamics (sorption) and kinetic (diffusion) properties. For polymer films without any support, the flux (n_A), normalized by the transmembrane partial pressure (Δp_A) and thickness (ℓ), the permeability ($P_{A,l}$) is defined, as:

$$P_{A,l} = n_A \frac{l}{\Delta p_A} \tag{B.1}$$

In gas separation devices the permeability values are typically reported in Barrer,

$$1\ Barrer = \ 10^{-10} \frac{cc(STP).cm}{cm^2.cm\ Hg.s} = 3.44 \times 10^{-16} \frac{kmol.m}{m^2.s.\ kPa}$$

whereas in pervaporation processes the mass flux is reported in $kg{\cdot}\mu m{\cdot}m^{-2}{\cdot}h^{-1}$. The ideal selectivity (i.e. pure feed components) between A and B is defined as the ratio of their permeabilities.

$$\alpha_{AB} = \frac{P_A}{P_B} \tag{B.2}$$

The permeability, P_A can be written as the product of the diffusion coefficient D_A, and the solubility coefficient S_A, assuming that diffusion and solubility coefficients of penetrating gas molecules are independent of the operating pressure.

$$P_A = \ D_A S_A \tag{B.3}$$

Diffusivity is a kinetic parameter which indicates the speed with which a penetrant is transported through the membrane, and is influenced by the molecular size, i.e., Lennard–Jones diameter, σ, and the free volume of the polymer membrane. Solubility is a thermodynamic parameter which gives a

measure of the amount of penetrant sorbed by the membrane under equilibrium condition. The solubility coefficient S_A is determined by the polymer-penetrant interactions (gas condensability) and by the amount of free volume in the polymer [147].

The gas condensability is represented by several physical properties such as boiling temperature, T_b, critical temperature, T_c, or the Lennard–Jones parameter, (ε/k). The average diffusion coefficient D_A is a measure of the mobility of the penetrants between the feed and permeate side of the membrane. It depends on packing and motion of the polymer segments and on the size and shape of the penetrating molecules [78]. Gas solubility in polymers generally increases with increasing gas condensability.

It has been found that polymeric membranes show a trade-off relationship between permeability and selectivity for separation of gases [83-84]. If their respective data for P_A (in Barrer) and α_{AB} is plotted on a log-log plot, it can be shown that there exists a linear upper bound to this data with P_A being inversely proportional to α_{AB}:

$$\alpha_{AB} = \frac{\beta_{AB}}{P_A^{\lambda_{AB}}} \tag{B.4}$$

where λ_{AB} is called the slope and β_{AB} (in Barrer) is called the front factor of the upper bound.

Appendix C

Costing of HMD System

For the techno-economic evaluation of retrofitting a distillation column to a HMD system, the most important indicator is the net savings (NS %/yr). It is the percentage of difference in the capital and operating costs of the base case and of the HMD case, to the operating cost of the base case. It can be calculated using the following equation:

$$NS\ \% = \frac{OPEX_{bas} - (CAPEX+OPEX)_{hyb}}{OPEX_{bas}} 100\% \quad \text{(C.1)}$$

Since retrofitting is considered in this study, $CAPEX_{base}$ is set to 0 \$/yr. The $CAPEX_{hyb}$ is given by:

$$CAPEX_{hyb} = \frac{(C_{comp} + C_{drive} + C_{cool})}{10} + \frac{100A_m}{5} \quad \text{(C.2)}$$

where A_m is the surface area (m^2) of the membrane and C(\$) is the cost of an equipment like compressor, drive and cooler in this case. The life expectancy of equipments is assumed as 10 years and that of the membrane unit is 5 years. The OPEX is calculated using utility requirement of the equipment and current utility prices based on the total operating time of 8760 annually.

$$OPEX_{hyb} = OPEX_{condenser} + OPEX_{reboiler} + OPEX_{compressor} + OPEX_{cooler} \quad \text{(C.3)}$$

Turton et al. [140] provide the following relation for calculating the purchase cost of equipment (PCE) for compressor and drive.

$$\log(PCE) = K_1 + K_2\log(S) + K_3[\log(S)]^2 \quad \text{(C.4)}$$

where S (kW) is the power input required by the cooler or drives and K_1, K_2 and K_3 are coefficients, whose values are available in Turton et al. [140]. The total module cost is:

$$C = (1 + 0.15 + 0.03) \times F_{bm} \times PCE \left(\frac{650}{397}\right) \quad \text{(C.5)}$$

where 15% is for contingency and 3% for contractor's fees. F_{bm} accounts for equipment erection, piping, instrumentation, electrical, buildings and process,

design and engineering. Chemical Engineering Plant Cost Index (CEPCI) is taken as 650. Its value was 397 in the period: May to September 2001 when the PCE data were obtained [140].

Table C.1: Calculation Parameters for Compressor and Drives [140]

Equipment	K_1	K_2	K_3	Unit	Min	Max	F_{bm}
Compressor (Rotary/ Carbon Steel)	5.0355	-1.8002	0.8253	kW	18	950	2.4
Drives (Internal Combustion)	2.7635	0.8574	-0.0098	kW	10	10000	2

For calculating the cooler size, the logarithmic mean temperature difference (LMTD) is computed with cooling water entering the at 30°C and leaving at 40°C and the process stream leaving the cooler at 35°C. Value of U is assumed as 350 W/m^2.K corresponding to cooler with hot fluid as light oils and cold fluid as water [148]. Then area of the cooler is obtained from:

$$Q = U\ A_c\ LMTD \tag{C.6}$$

Assuming a double-pipe heat exchanger (for heat exchange surface area in the range of 2 to 200 ft^2), PCE is calculated using: [139]

$$PCE_{cool} = \exp(7.1460 + 0.16 \times \ln(A_c)) \tag{C.7}$$

F_p is calculated by: [139]

$$F_p = 0.8510 + 0.1292 \times \left(\frac{P}{600}\right) + 0.0198 \times \left(\frac{P}{600}\right)^2 \tag{C.8}$$

Material factor, $F_m = 2$ for an outer pipe of carbon steel and an inner pipe of stainless steel. Since CEPCI value is 500 for the PCE data in Seider el al. [139], the total module cost of cooler is given by:

$$C_{cool} = F_m F_p (PCE_{cool}) \left(\frac{650}{500}\right) \tag{C.9}$$